



UNIVERSITAT DE  
BARCELONA

## Deposition of environmentally friendly cermets coatings by thermal spray techniques

Fatemeh (Maryam) Bazyaran

**ADVERTIMENT.** La consulta d'aquesta tesi queda condicionada a l'acceptació de les següents condicions d'ús: La difusió d'aquesta tesi per mitjà del servei TDX ([www.tdx.cat](http://www.tdx.cat)) i a través del Dipòsit Digital de la UB ([diposit.ub.edu](http://diposit.ub.edu)) ha estat autoritzada pels titulars dels drets de propietat intel·lectual únicament per a usos privats emmarcats en activitats d'investigació i docència. No s'autoritza la seva reproducció amb finalitats de lucre ni la seva difusió i posada a disposició des d'un lloc aliè al servei TDX ni al Dipòsit Digital de la UB. No s'autoritza la presentació del seu contingut en una finestra o marc aliè a TDX o al Dipòsit Digital de la UB (framing). Aquesta reserva de drets afecta tant al resum de presentació de la tesi com als seus continguts. En la utilització o cita de parts de la tesi és obligat indicar el nom de la persona autora.

**ADVERTENCIA.** La consulta de esta tesis queda condicionada a la aceptación de las siguientes condiciones de uso: La difusión de esta tesis por medio del servicio TDR ([www.tdx.cat](http://www.tdx.cat)) y a través del Repositorio Digital de la UB ([diposit.ub.edu](http://diposit.ub.edu)) ha sido autorizada por los titulares de los derechos de propiedad intelectual únicamente para usos privados enmarcados en actividades de investigación y docencia. No se autoriza su reproducción con finalidades de lucro ni su difusión y puesta a disposición desde un sitio ajeno al servicio TDR o al Repositorio Digital de la UB. No se autoriza la presentación de su contenido en una ventana o marco ajeno a TDR o al Repositorio Digital de la UB (framing). Esta reserva de derechos afecta tanto al resumen de presentación de la tesis como a sus contenidos. En la utilización o cita de partes de la tesis es obligado indicar el nombre de la persona autora.

**WARNING.** On having consulted this thesis you're accepting the following use conditions: Spreading this thesis by the TDX ([www.tdx.cat](http://www.tdx.cat)) service and by the UB Digital Repository ([diposit.ub.edu](http://diposit.ub.edu)) has been authorized by the titular of the intellectual property rights only for private uses placed in investigation and teaching activities. Reproduction with lucrative aims is not authorized nor its spreading and availability from a site foreign to the TDX service or to the UB Digital Repository. Introducing its content in a window or frame foreign to the TDX service or to the UB Digital Repository is not authorized (framing). Those rights affect to the presentation summary of the thesis as well as to its contents. In the using or citation of parts of the thesis it's obliged to indicate the name of the author.

**Fatemeh (Maryam) Bazyaran**

**PhD. Thesis**

# **Deposition of environmentally friendly cermets coatings by thermal spray techniques**

**Fatemeh (Maryam) Bazyaran**

**2018**



**UNIVERSITAT DE  
BARCELONA**

Doctorate program: Engineering and Applied Science

Thesis Title: Deposition of environmentally friendly  
cermets coatings by thermal spray techniques

Fatemeh (Maryam) Bazyan

Thesis Director:

**Dr. Sergi Dosta**

Acting Associate Professor at Barcelona University

**Dra. Irene Garcia Cano**

Associate Professor at Barcelona University

Thesis Tutor:

**Dr. Sergi Dosta**

Acting Associate Professor at Barcelona University

## Index

CHAPTER 0. OBJECTIVES.....	13
CHAPTER 1. INTRODUCTION .....	16
<b>1. GENERAL REVIEW.....</b>	<b>17</b>
1.1. COATING PRODUCTION METHODS.....	19
1.2. THERMAL SPRAY PROCESSES .....	19
<b>2. COLD GAS SPRAY METHOD (CGS) .....</b>	<b>22</b>
2.1. PROCESS PARAMETERS.....	26
2.1.1. PARTICLE VELOCITY.....	26
2.1.2. PARTICLE, GAS AND SUBSTRATE TEMPERATURE .....	29
2.1.3. PARTICLE SIZE AND POWDER MORPHOLOGY .....	29
2.1.4. POWDER FEEDING RATE .....	30
2.1.5. NOZZLE-SUBSTRATE STANDOFF DISTANCE .....	31
2.1.6. SUBSTRATE ROUGHNESS AND THICKNESS .....	31
<b>3. HIGH VELOCITY OXY FUEL PROCESS (HVOF).....</b>	<b>32</b>
3.1. PROCESS PARAMETERS.....	33
3.1.1. FUEL TYPE .....	35
3.1.2. FUEL GAS/O RATIO .....	35
3.1.3. SPRAY DISTANCE .....	35
3.1.4. POWDER FEED RATE .....	36
<b>4. AIR PLASMA SPRAY.....</b>	<b>36</b>
4.1. PROCESS PARAMETERS.....	37
4.1.1. INPUT POWER.....	37
4.1.2. STAND-OFF DISTANCE.....	37
4.1.3. POWDER FEEDING RATE .....	38
<b>5. GREEN CARBIDES .....</b>	<b>38</b>
CHAPTER 2. EXPERIMENTAL PROCEDURE .....	41
<b>1. RAW MATERIALS .....</b>	<b>42</b>
<b>2. STRUCTURAL CHARACTERIZATION.....</b>	<b>42</b>
2.1. MORPHOLOGY .....	42
2.2. PARTICLE SIZE DISTRIBUTION .....	43
2.3. PHASE COMPOSITION .....	43
<b>3. EQUIPMENTS .....</b>	<b>43</b>

3.1.	COLD GAS SPRAY.....	43
3.2.	HIGH VELOCITY OXYFUEL .....	44
3.3.	AIR PLASMA SPRAY.....	45
3.4.	MICRO-HARDNESS .....	46
3.5.	FRACTURE TOUGHNESS .....	47
3.6.	TENSILE STRENGTH .....	48
3.7.	SLIDING WEAR .....	48
3.7.1.	BALL ON DISC TEST.....	48
3.7.2.	RUBBER WHEEL TEST.....	49
CHAPTER 3. RAW MATERIALS CHARACTERIZATION .....		50
<b>1.</b>	<b>SUBSTRATES.....</b>	<b>51</b>
1.1.	LOW-CARBON STEEL.....	51
1.2.	AL7075-T6 .....	51
<b>2.</b>	<b>SPRAYING POWDERS.....</b>	<b>52</b>
2.1.	TiC BASED-GREEN MATRIX.....	52
2.1.1.	Ti-20%TiC .....	52
2.1.2.	Ti-50%TiC .....	53
2.1.3.	Ti-65%TiC .....	53
2.1.4.	TiC-FeCrAlTi .....	55
2.2.	SiC BASED-GREEN MATRIX .....	57
2.2.1.	Ti-SiC .....	57
2.3.	WC BASED-GREEN MATRIX.....	58
2.3.1.	Ti-WC (400 HV) .....	58
2.3.2.	THERMALLY PRE-TREATED Ti-WC (650 HV) .....	59
2.3.3.	THERMALLY PRE-TREATED Ti-WC (1500 HV).....	60
2.3.4.	Ti-WC RICHER IN CARBIDE PHASE.....	60
CHAPTER 4. RESULTS AND DISCUSSION .....		63
4.1.	COATINGS CHARACTERIZATION & PERFORMANCE.....	64
<b>1.</b>	<b>CHARACTERIZATION OF TiC BASED-GREEN MATRIX COATINGS.....</b>	<b>65</b>
1.1.	By CGS.....	65
1.1.1.	MICROSTRUCTURAL PROPERTIES .....	65
1.1.2.	ADHESION TEST .....	72
1.1.3.	WEAR TEST .....	74
1.1.4.	FRACTURE TOUGHNESS.....	78

1.2.	By HVOF .....	78
1.2.1.	MICROSTRUCTURAL PROPERTIES .....	79
1.2.2.	ADHESION TEST .....	82
1.2.3.	FRACTURE TOUGHNESS.....	82
1.2.4.	WEAR TEST .....	82
<b>2.</b>	<b>CHARACTERIZATION OF SiC BASED-GREEN MATRIX COATINGS .....</b>	<b>83</b>
2.1.	By CGS.....	83
2.1.1.	MICROSTRUCTURAL PROPERTIES .....	83
2.2.	By HVOF .....	89
2.2.1.	MICROSTRUCTURAL PROPERTIES .....	90
2.2.2.	ADHESION TEST .....	93
2.2.3.	FRACTURE TOUGHNESS.....	94
2.2.4.	WEAR TEST .....	94
<b>3.</b>	<b>CHARACTERIZATION OF WC BASED-GREEN MATRIX COATINGS.....</b>	<b>95</b>
3.1.	By CGS.....	95
3.1.1.	MICROSTRUCTURAL PROPERTIES .....	96
3.1.2.	FRACTURE TOUGHNESS.....	96
3.1.3.	WEAR TEST .....	97
3.2.	By HVOF .....	101
3.2.1.	MICROSTRUCTURAL PROPERTIES .....	102
3.2.2.	FRACTURE TOUGHNESS.....	105
3.2.3.	WEAR TEST .....	105
3.3.	By APS.....	106
3.3.1.	MICROSTRUCTURAL PROPERTIES .....	107
4.2.	GLOBAL COMPARISON BETWEEN COATINGS .....	111
4.2.1.	GLOBAL TREND FOR TiC SYSTEM .....	113
4.2.2.	GLOBAL TREND FOR SiC SYSTEM.....	114
4.2.3.	GLOBAL TREND FOR WC SYSTEM .....	115
CHAPTER 5. CONCLUSION .....		117
CHAPTER 6. BIBLIOGRAPHY .....		120
CAPÍTULO 7. EL RESUMEN.....		128
1.	OBJETIVOS.....	129
2.	INTRODUCCIÓN.....	129
3.	PROCEDIMIENTOS EXPERIMENTALES .....	132

4.	MATERIAS PRIMAS .....	135
5.	RECUBRIMIENTOS OBTENIDOS .....	136
6.	DISCUSIÓN Y CONCLUSIÓN .....	138

## LIST OF TABLES

Table 1: Properties and chemical composition of 0.20wt%C low-carbon steel

Table 2: Percentage chemical composition of Al7075-T6

Table 3: Microstructural properties of obtained coatings from Ti-20%TiC under different spraying condition

Table 4: Microstructural properties of obtained coatings from Ti-50%TiC under different spraying condition

Table 5: Microstructural properties of obtained coatings from Ti-65%TiC under different spraying condition

Table 6: Splats formation conditions

Table 7: microstructural properties of obtained coatings from Ti-65%TiC under different spraying conditions by CGS

Table 8: Adhesion values of obtained coatings from different Ti-TiC powders

Table 9: Coefficient friction and lost volume comparison for different coatings

Table 10: Comparing Propylene and Hydrogen flame

Table 11: Microstructural properties of obtained coatings from TiC-FeCrAlTi by HVOF

Table 12: Tensile strength of obtained coatings from TiC-FeCrAlTi by HVOF and using Hydrogen and Propylene as fuel gases

Table 13: Lost volume, coefficient friction and wear rate of obtained coating from TiC-FeCrAlTi by HVOF and using Propylene as fuel gas

Table 14: Microstructural characterization of obtained coatings from Ti-SiC by CGS method

Table 15: microstructural properties of Ti-SiC coating by CGS before and after Heat treatment

Table 16: microstructural properties of optimum produced coatings from Ti-SiC by HVOF and using H<sub>2</sub> and Propylene as fuel gases at SOD 225 mm



Table 17: Tensile strength values of produced coating from Ti-SiC onto C St. substrate by HVOF and using Propylene as fuel gas

Table 18: Lost volume and coefficient friction of obtained coating from Ti-SiC by HVOF and using Propylene as fuel gas

Table 19: Microstructural properties of optimum coatings by CGS for Ti-WC (400 HV) system

Table 20: Microstructural properties of coating related to Ti-WC (400 HV) before and after HT

Table 21: microstructural properties of Ti-WC coatings by HVOF and using H<sub>2</sub>

Table 22: microstructural properties of produced coating from Ti-WC (400 HV) by HVOF and using Propylene

Table 23: Microstructural properties of produced coatings of Ti-WC system by APS

Table 24: microstructural comparison of optimum coating of each powder by different thermal spraying techniques

Table 25: Abrasive wear resistance and fracture toughness comparison of optimum coatings

## LIST OF FIGURES

Figure 1: Thermal spray coating scheme

Figure 2: Thermal spray processes [2]

Figure 3: cold gas spray system

Figure 4: particle velocity vs. temperature graphic [12]

Figure 5: "Window of deposition" Impact velocity vs deposition efficiency for a constant impact temperature [18]

Figure 6: The influence of particle velocity onto the quality and deposition efficiency of the coating [18]

Figure 7: particle impact velocity vs particle impact temperature

Figure 8: HVOF process scheme.

Figure 9: Schematic of APS system

Figure 10: Schematic of KINETIC 4000 system and spray gun

Figure 11: HVOF equipment

Figure 12: Plasma technik A-3000 with F4 torch

Figure 13: Vickers micro-indentation equipment

Figure 14: Vickers hardness calculation ( $F$ = Load in kgf,  $d$  = Arithmetic mean of the two diagonals,  $d_1$  and  $d_2$  in mm, HV = Vickers hardness)

Figure 15: adhesion test specimen and the three rupture possibilities

Figure 16: Ball on disc scheme and wear track

Figure 17: Rubber wheel scheme

Figure 18: SEM study of Ti-20%TiC (a) Free surface at 350x (b) 2000x and (c) Cross section at 1500x

Figure 19: SEM study of Ti-50%TiC (a) Free surface at 750x (b) 2000x and (c) Cross section at 1250x

Figure 20: SEM study of Ti-65%TiC (a) Free surface at 750x (b) 2000x and (c) Cross section at 2500x

Figure 21: XRD study of Ti-TiC with different percentage of TiC phase

Figure 22: LS study of Ti-20%TiC, Ti-50%TiC and Ti-65%TiC

Figure 23: SEM study of TiC-FeCrAlTi (a) Free surface at 1000x (b) 4000x and (c) Cross section at 4000x

Figure 24: Laser scattering study of TiC-FeCrAlTi

Figure 25: XRD study of TiC-FeCrAlTi

Figure 26: SEM study of Ti-SiC (a) Free surface at 750x (b) 2000x and (c) Cross section at 4000x

Figure 27: LS study of Ti-SiC

Figure 28: XRD study of Ti-SiC

Figure 29: SEM study of Ti-WC (a) Free surface at 1250x (b) 4000x and (c) Cross section at 3500x

Figure 30: LS study of Ti-WC

Figure 31: SEM study of Ti-WC (650HV) (a) Free surface at 800x (b) 8000x and (c) Cross section at 4000x

Figure 32: LS study of Ti-WC (650HV)

Figure 33: SEM study of Ti-WC (1500HV) (a) Free surface at 2000x (b) 8000x and (c) Cross section at 6000x

Figure 34: LS study of Ti-WC (1500HV)

Figure 35: SEM study of Ti-WC (richer in WC) (a) Free surface at 1000x (b) 4000x and (c) Cross section at 4000x

Figure 36: LS study of Ti-WC (richer in WC)

Figure 37: XRD comparison of Ti-WC (400HV), Ti-WC (650HV), Ti-WC (1500HV) and Ti-WC (richer in WC) [60]

Figure 38: SEM Cross section micrograph of a) Ti-20%TiC, C St. b) Ti-50%TiC, C St. and c) Ti-65%TiC coatings onto the C St.

Figure 39: SEM cross section micrograph of splats at 4500x magnification

Figure 40: SEM Free Surface micrograph of splats at 4000x magnification

Figure 41: impact velocity and temperature vs. spraying parameters

Figure 42: SEM cross section micrograph of obtained coatings from Ti-65%TiC at different spraying conditions

Figure 43: Phase composition comparison of powder and coating by XRD test.

Figure 44: Elemental mapping of Ti-65%TiC coating (#3) by CGS

Figure 45: Cohesive failure after tensile strength test

Figure 46: Wear rate comparison of different coatings of Ti-TiC cermet

Figure 47: BOD samples after test done a) Ti-20%TiC, b) Ti-50%TiC and c) Ti-65%TiC

Figure 48: Wear track in BOD to calculate the lost volume

Figure 49: 3D topography comparison by confocal microscope for obtained coating from a) Ti-20%TiC and b) Ti-65%TiC

Figure 50: SEM micrograph of wear track for coating of Ti-65%TiC at different magnifications

Figure 51: EDS mapping study of coating related to Ti-65%TiC after ball on disc test

Figure 52: SEM cross section micrograph of optimal coating related to TiC-FeCrAlTi at SOD 225 mm using a) H<sub>2</sub> b) Propylene as fuel gases

Figure 53: XRD study of TiC-FeCrAlTi coating by HVOF

Figure 54: Elemental mapping of TiC-FeCrAlTi coating by HVOF and using Propylene as fuel gas

Figure 55: SEM cross section micrograph and XRD of produced coatings of Ti-SiC by CGS onto C St.

Figure 56: Elemental mapping of Ti-SiC coating by CGS

Figure 57: SEM cross section of obtained coating related to Ti-SiC onto C steel + Ti bond coat by CGS.

Figure 58: XRD study of obtained coating related to Ti-SiC by CGS after HT

Figure 59: SEM cross section micrograph of obtained coating related to Ti-SiC onto C steel + Ti bond coat by CGS a) Before HT b) After HT

Figure 60: EDS study of Ti-SiC coating by CGS after HT

Figure 61: Elemental Mapping of Ti-SiC coating by CGS after HT

Figure 62: Elemental Mapping comparison of Ti-SiC coating by CGS a) before and b) after HT

Figure 63: SEM cross section micrograph of produced coatings of Ti-SiC by HVOF onto C St. using a) H<sub>2</sub> b) Propylene as fuel gases

Figure 64: XRD phase composition of obtained coating related to Ti-SiC powder by HVOF and using a) H<sub>2</sub> b) Propylene as fuel gas

Figure 65: Electron microprobe result for Ti-SiC coating by HVOF and using Propylene

Figure 66: Microstructural comparison of Ti-SiC coating by a) HVOF b) CGS

Figure 67: Abrasive wear rate comparison of optimum obtained coatings of Ti-SiC by different spraying techniques

Figure 68: SEM cross section of obtained coatings by CGS method Ti-WC on a) C Steel substrate b) Al substrate

Figure 69: Abrasive wear comparison of coatings related to Ti-WC (400 HV) and Ti-SiC by CGS technique

Figure 70: SEM cross section of obtained coating related to Ti-WC (400 HV) onto C steel + Ti bond coat by CGS.

Figure 71: XRD study of produced coating related to Ti-WC (400 HV) after HT

Figure 72: Elemental Mapping of Ti-WC coating by CGS before HT

Figure 73: Elemental Mapping of Ti-WC coating by CGS after HT

Figure 74: Elemental Mapping comparison of Ti-WC coating by CGS a) before and b) after HT

Figure 75: SEM cross section study of produced coatings related to Ti-WC system by HVOF and using H<sub>2</sub> as fuel gas a) Ti-WC (400 HV) (3<sup>rd</sup> trial) b) Ti-WC (650 HV) (1<sup>st</sup> trial)

Figure 76: SEM cross section micrograph of sample related to Ti-WC (1500 HV) by HVOF and H<sub>2</sub> as fuel gas

Figure 77: SEM cross section study of produced coatings related to Ti-WC (400 HV) system by HVOF and using Propylene as fuel gas (6<sup>th</sup> trial)

Figure 78: Abrasive wear comparison of optimum coatings related to Ti-WC (400 HV) and Ti-WC (650 HV) by different techniques

Figure 79: SEM cross section study of produced coatings related to Ti-WC (650 HV) by APS a) 1<sup>st</sup> trial b) 2<sup>nd</sup> trial c) 3<sup>rd</sup> trial

Figure 80: SEM cross section study of produced coatings related to Ti-WC (1500 HV) by APS a) 1<sup>st</sup> trial b) 2<sup>nd</sup> trial c) 3<sup>rd</sup> trial

Figure 81: XRD phase composition of produced coatings by APS a) Ti-WC (650 HV) b) Ti-WC (1500 HV)

## **ACKNOWLEDGEMNT**

This thesis wouldn't be done without guidance and expertness of Dr. Sergi Dosta, the director of my thesis. I would like to thank him for all the information and supports that he provided me by during these three years of PhD. I would want to express my full appreciation to Professor Jose Maria Guilemany and Thermal spray center of Barcelona (CPT) for these three years of funding and giving me the chance of being one of the members of this research group. Special thanks also go to the Generalitat de Catalunya for the financial support of project 2014SGR1558. I also want to thank Dra. Irene Gracia Cano, the director of CPT and the tutor of this PhD. thesis, Dr. Horacio canals, Dr. Joan Ramon and Mr. Rajab Ali Seraj for sharing with me their knowledge in thermal spray processes. Also I feel obliged to thank all my colleagues in thermal spray center of Barcelona that helped me in all these three years.

## CHAPTER 0. OBJECTIVES



Firstly, the main objective of this research work was to produce environmentally friendly cermets coatings, Ni and Co free matrix, alternative to conventional WC-Co, by thermal spray processes. WC-Co cermets has always been one of the most on demand coatings in anti-wear and anti-corrosion applications in industry but environmental problems caused by heavy metals matrix (Co and Ni) force the redesign of many conventional processes. These elements are not harmful in their fundamental state, but processing generates changes in oxidation states that make them carcinogenic and mutagenic. For this reason, this research has focused on either replacing the existing processes or use raw materials that are less harmful.

Therefore depositing the green carbides cermets onto the different substrates by conventional or novel (CGS) techniques are the main motivation points of this thesis. No one has previously successfully deposited such material by CGS or HVOF method with the same properties as the conventional WC-Co which was also one of the main motivation points. In this work we could produce Ti-TiC coatings with different percentage of Carbide phase by CGS, TiC-based with FeCrAlTi metal matrix by HVOF method, SiC-based cermets with Ti metal matrix by both CGS and HVOF technique and WC-based cermet with Ti metal matrix by CGS, HVOF and APS techniques. For this reason the main objectives of this Thesis entitled "Deposition of green carbide cermets coatings by thermal spray techniques".

## **Schedule**

This work has been written according to the different obtained coating with their corresponding characterization and properties. The introduction was presented in chapter 1, the experimental procedure for characterization and analysis of the powders and the obtained coatings was described in chapter 2. Chapter 3 introduced the raw materials and obtained coatings characterization and performance and global comparison between produced coatings was described in chapter 4. Chapter 5 was included the conclusions of the present study and finally chapter 6 was the bibliography.

## CHAPTER 1. INTRODUCTION

## **1. GENERAL REVIEW**

Protection the surface of the materials against any external damaging factor has been studied in surface engineering. One of the most common technologies to achieve this goal is cost-effective, high quality thermal spray processes.

Thermal spraying techniques are coating processes in which melted (or heated) materials are sprayed onto a surface [1]. The "feedstock" (coating precursor) is heated by electrical (plasma or arc) or chemical means (combustion flame). Properties and microstructure of the sprayed coatings depend on the occurring phenomena during the particle flight [2].

Thermal spraying can provide thick coatings (approx. thickness range is 20 micrometers to several mm, depending on the process and feedstock), over a large area at high deposition rate as compared to other coating processes such as electroplating, physical and chemical vapor deposition. Coating materials available for thermal spraying include metals, alloys, ceramics, plastics and composites. They are fed in powder or wire form, heated to a molten or semi-molten state and accelerated towards substrates in the form of micrometer-size particles. Combustion or electrical arc discharge is usually used as the source of energy for thermal spraying. Resulting coatings are made by the accumulation of numerous sprayed particles. The surface may not heat up significantly, allowing the coating of flammable substances [3].

Coating quality is usually assessed by measuring its porosity, oxide content, macro and micro-hardness, bond strength and surface roughness. Generally, the coating quality increases with increasing particle velocities.

Several variations of thermal spraying are distinguished [4]:

- Plasma spraying
- Detonation spraying
- Wire arc spraying
- Flame spraying
- High velocity oxy-fuel coating spraying (HVOF)

- High velocity air fuel (HVOF)
- Warm spraying
- Cold spraying

In spite of the advantages of thermal spray techniques, there are some drawbacks that limit using those conventional techniques. The main ones are [2]:

- Oxidation of metallic feedstock
- Chemical modification at flight of sprayed particles, like decarburization, oxidation or reduction.
- Particles in liquid state can evaporate and reduce their size.
- Increase of tensile stresses.
- Substrate microstructure modification due to heat and impact.

Whilst thermal spray is widely used in many applications, it uses thermal energy to melt or soften the feedstock. This can cause thermal degradation and partial oxidation of the coating material which may be undesirable. For metallic materials that are very prone to oxidation, thermal spray needs to be conducted under protected atmosphere or a vacuum, introducing extra cost. The heat input of thermal spray processes introduces residual stress into the coatings, which can limit the thicknesses that can be attained. Furthermore, the thermal balance has to be carefully managed through part cooling and gun manipulation to avoid excessive internal stresses and, in the case of thermally sensitive substrates, potential substrate degradation. These existing limitations in thermal spray processes has promoted the development of spraying techniques where low costs and high deposition efficiencies, are essential when a coating technique is chosen, in industries increasingly specialized and demanding development material costs reduction, decrease in surface treatments (pre- and post-spraying), possibility of increasing the life cycle of the equipment, reduction of problems associated with material melting (oxidation, corrosion, tensile stresses, microstructure change), have made of cold gas spray (CGS) an efficient, clean and cost competitive technique.

The main objective of CGS technology, as well as thermal spray techniques, is producing the coating to improve material's surface for the desirable application [2].

### 1.1. Coating production methods

Melting processes are one of the most common processes in producing the surface coating in industry

One of the subcategories of melting processes in producing the surface coating is thermal spray processes.

### 1.2. Thermal spray processes

Thermal spraying is a group of coating processes in which finely divided metallic or nonmetallic materials is deposited in a molten or semi-molten condition to form a coating. The coating material may be in the form of powder, ceramic-rod, wire, or molten materials. In this method the particles or droplets accelerate to speed range of 50 to 1000 m/s. Particles with high temperature and high speed impact the substrate surface which results a high deformation in particles that is called splats. A continuous particles impact onto the substrate surface, solidify and produce the coating layers. After impact, particles cool down at very high rates to form a uniform, very fine-grained, polycrystalline coatings or deposits [5]. Figure 1 shows the schematic of Thermal spray coating.

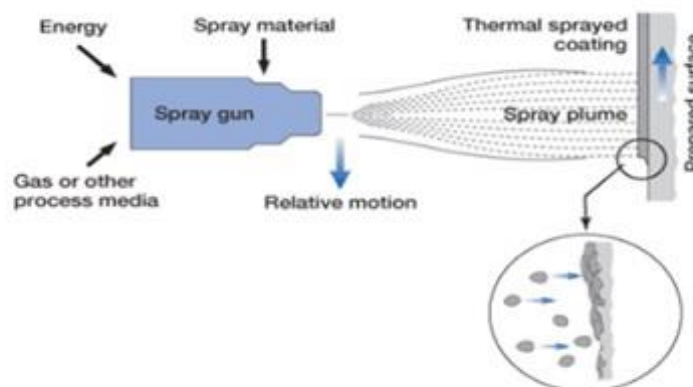


Figure 1: Thermal spray coating scheme

Benefits of thermal spraying compared to other coating processes are many, and include [2]:

- Versatility with respect to the coating material, which can be metal, cermet, ceramic and polymer, in the form of powder, rod or wire. There is a comprehensive choice of coating materials to meet the needs of a wide variety of applications, in particular protection from wear and corrosion damage.
- Coatings of metal, cermet, ceramic and plastic can be applied to any substrate that will not degrade from the heat of the impinging particles or gas jets.
- The coating is formed with minimal heating of the substrate and the coating does not need to fuse with the substrate to form a bond. Substrate temperature seldom exceeds 300°C. As a consequence, coatings can be applied to components with little or no pre- or post-heat treatment and component distortion is minimal. The coatings can also be applied to thermal sensitive substrates such as low melting point metals and plastics.
- Thick coatings, typically up to 10 mm, can be applied and often at high deposition rates. This means that thermal spraying can also be used for component reclamation and spray forming. Parts can be rebuilt quickly and at low cost, usually at a fraction of the replacement price.
- Thermal spraying has the capacity to form barrier and functional coatings on a wide range of substrates.

Figure 2 shows the three major categories of thermal spray processes. Each process develops certain specific properties in the coatings such as bond strength, porosity, oxides and hardness.

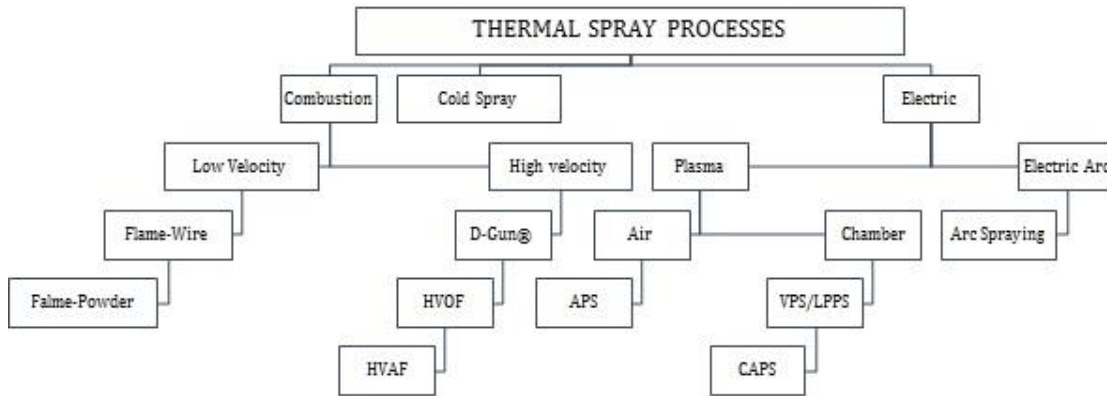


Figure 2: Thermal spray processes [2]

The most common applications of thermal spray coatings are [2]:

- Wear resistant coatings
- Corrosion resistant coatings
- Thermal insulation coatings
- Abradable and abrasive coatings
- Electrically conductive coatings
- Electromagnetic shielding
- Electrically resistive or insulating coatings
- Electrochemical active coatings
- Heat transfer improvement
- Dimensional restoration coatings
- Medical coatings
- Polymer coatings

Among the different thermal spray techniques, cold gas spray (CGS) is increasingly gaining importance compared to conventionally sprayed coatings. This technique is a recently emerging process being expected to deposit temperature-sensitive materials because it usually doesn't involve the use of a high-temperature heat source. Owing to its relatively low deposition temperature, the decarburization and detrimental phase inherently occurring in conventional thermal spraying techniques can be minimized or even avoided [6-7]. In this technique so many factors have to be considered in order to achieve optimized material deposition and properties. In cold spray process, deposition velocity influences the degree of



material deformation, whilst most materials can be easily deposited at relatively low deposition velocity (<700 m/s). Some advantages of this method are [8]:

- High thermal and electrical conductivity of coatings;
- High density and hardness of coatings;
- High homogeneity of coatings;
- Low shrinking;
- Possibility to spray micro-sized particles (5–10  $\mu\text{m}$ );
- Possibility to spray nanomaterials and amorphous materials;
- Short stand-off distance;
- Minimum surface preparation;
- Low energy consumption;
- Possibility to obtain complex shapes and internal surfaces;
- High productivity due to high power feed rate;
- High deposition rates and efficiencies;
- Possibility to collect and reuse 100% of particles;
- No toxic wastes;
- No combustion;
- Increased operational safety due to the absence of high temperature gas jets and radiation

## **2. COLD GAS SPRAY METHOD (CGS)**

Cold gas spray (CGS) is a solid-state spraying technique that produces coating by exposing a powder, with a certain size distribution, to a high-pressure gas stream (Nitrogen or Helium). These particles acquire high kinetic energy, thus allowing Cold spray is a solid-state deposition process in which small powder particles (in the range of 5 to 50  $\mu\text{m}$ ) are accelerated to velocities in the order of 500 to 1200m/s in a supersonic jet of compressed gas onto a substrate where the powder particles deform and bond together rapidly building up a thick layer of deposited materials [9].

The metal powder particles are fed centrally, by a separate gas stream typically introduced into the high-pressure side of a de Laval converging-diverging nozzle where a preheated gas (usually air, He, N<sub>2</sub>, or mixture

depending on the deposition material and gas temperature) in the range of 300-800°C is compressed and will expand to supersonic velocities while decreasing in pressure and temperature. Such velocities can be reached due to the changes of geometry and Mach inside the nozzle. It has to be noted that the gas is heated not to heat or soften spray particles, but instead to achieve higher sonic flow velocities, which ultimately result in higher particle impact velocities. Since the contact time of the injected particles with the hot gas is short and the gas cools as it expands, it is considered that the particles temperature remains below its melting temperature. The term “cold spray” has been used to describe this process due to the gas stream’s exiting temperature (-100 to 100°C). The fact that this is a solid-state process will allow for a uniform, thick, porosity and oxide free coating and usually maintaining the same proprieties as those of the bulk material. Unlike the conventional deposition techniques, which require both kinetic (particle velocity) and thermal (temperature) energy in order to promote coating formation onto a substrate, the cold spray process simply uses the kinetic energy of the powder particles for the coating formation. The kinetic energy of the impinging particles is sufficient to produce plastic deformation and high interfacial pressures. Furthermore, because cold spray is a low-temperature process, i.e., does not use thermal energy, the obtained coatings are less porous, and present less oxidation and higher hardness. A wide variety of materials such as pure metals, metallic alloys, polymers and composites onto various substrate materials obtaining very high coating deposition rates, can be obtained using this novel deposition process [9]. Figure 3 shows the schematic of cold gas spray system.

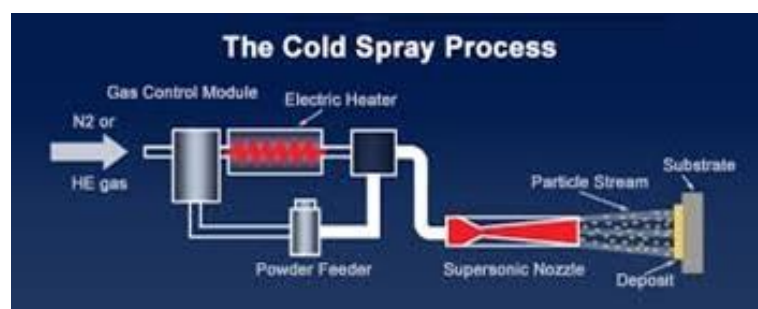


Figure 3: cold gas spray system

The distinguishing feature of the cold spray process compared with conventional thermal spray processes is its ability to produce coatings with high-velocity rather than high-temperature particle jet. Although the process gas is preheated to temperatures in the range of 30 to 1000°C to compensate for the adiabatic cooling during expansion, the particle temperature remains below 200°C. Consequently, the deleterious effects of high-temperature oxidation, grain-growth evaporation, melting, recrystallization, tensile residual stresses, de-bonding, gas release, and other concerns associated with thermal spray methods employing a liquefaction step are minimized or eliminated [10].

Figure 4 compares the particle velocity and gas temperature ranges of cold spray and other thermal spray processes. In the cold spray process, the gas and particle temperatures are much lower and the gas and particle velocity are much higher than in other thermal spray processes. There typically are four regions of particle/substrate interactions that can be defined by particle velocity. In the first region, the particle velocity ( $V_p$ ) is too low for a given coating/substrate combination to form a coating, and the feedstock particles are reflected from or bounce off of the surface and do not form a contiguous coating or deposit. When the particles impinge at moderate velocities, solid particle erosion of the substrate surface occurs, but no coating is deposited. When the particles reach a critical velocity ( $V_{crit}$ ), the particles begin to plastically deform, adhere to the substrate, and form a coating. The critical velocity varies with particle and substrate material. As  $V_p$  increases, the particles undergo more deformation, typically leading to higher coating densities. At very high velocities, the solid particles start to erode the surface of the substrate. When this occurs, the particle velocity is called the erosion velocity ( $V_{erosion}$ ) [11].

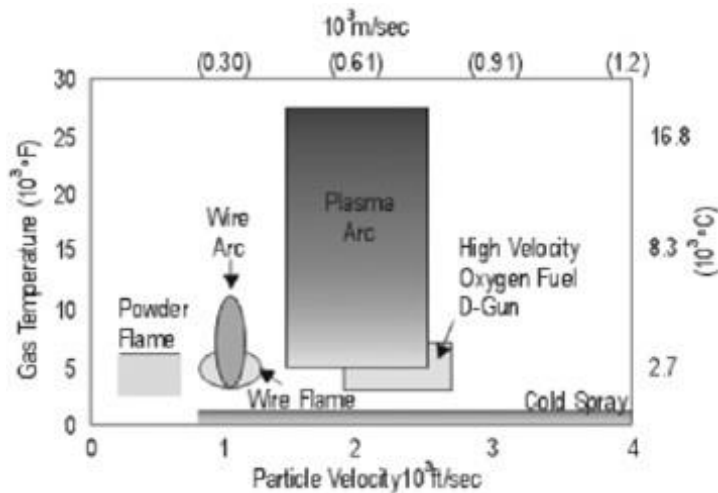


Figure 4: particle velocity vs. temperature graphic [12]

The main advantages of this process are [13-14]:

- Low porosity and low oxide content coatings are obtained.
- Lower jet temperatures prevent decarburization and high impact velocities produce a relatively pore-free coating.
- High density, phase purity and homogeneous microstructure of cold spray coatings promote exceptional corrosion characteristics.
- Ability to deposit a wide range of materials with a stable molten phase.
- Ability to deposit on a wide range of substrates, even to temperature-sensitive materials: thermal energy in a single droplet is quite limited therefore avoiding thermal contraction.
- Very high deposition rates (the material is deposited as 10-100  $\mu\text{m}$  molten droplets).

The main applications of cold gas spray are:

- Applications in aerospace, defense, automotive and electronics industries.
- High-performance applications such as electrical-thermal conductivity, high-temperature oxidation protection and corrosion resistance and also electronic applications;

- Automotive industry in copper coatings as current-carrying thick films, zinc coatings for selective galvanizing to protect weld spots, production and repair of rapid tooling and thermal layers;
- Aerospace industry in oxidation-resistant coatings, high-thermal conductivity coatings for thermal management, and production and repair of critical components and parts.

## 2.1. PROCESS PARAMETERS

The cold gas process will be influenced by several parameters (critical velocity of particles, gas and substrate temperature, powder size, etc.). Controlling these parameters will allow understanding the nature of the cold gas spray phenomenon and control the basic coating properties. One of the most important characteristics of the process is the deposition efficiency, which is defined as the ratio of the mass gain of the substrate during its exposure to the flow with the proper set of parameters and the decrease/consume in powder mass in the feeder during the same time. The relative deposition efficiency, RDE, is used to estimate the weight gains of coatings of several samples, through measuring its weights before and after deposition [15-16].

### 2.1.1. PARTICLE VELOCITY

The particle velocity prior to impact is one of the most important parameters in the cold spray process. The first particle impacting onto the substrate increase the reactivity of the surface due to the creation of a high concentration of dislocations and the elimination of impurities which can decrease the contact surface between particles and substrate. Understanding the adhesion mechanisms of particles to the substrate surface can be explained by impact critical velocity which the particle velocity has to exceed in order to successfully obtain a coating. The Critical velocity depends on sprayed materials and is a key factor for spray techniques based on the impact of solid particles. When the particle velocity is low, the particle rebounds on the surface upon impact. As the velocity increases, the particle starts to erode the substrate surface resulting in a weight loss of the

substrate materials. When the velocity reaches its characteristic value, the particle starts to adhere on the surface (critical velocity). If the particle velocity further increases, hypervelocity impact phenomena start to show up with noticeable jet formation and significant weight loss. The velocity distribution was combined with the measured deposition efficiency and the particle size distribution, to give the size and velocity of the largest particle that would bond successfully to the substrate [17]. Erosion can also appear when the particle velocity is too high thus exceeding the deposition efficiency saturation point and causing a large-impact dynamics phenomenon. Brittle materials would cause erosion for any velocity at temperatures below their melting point. Figure 5 shows the window of deposition and correlation between the impact velocity and deposition efficiency at the constant impact temperature.

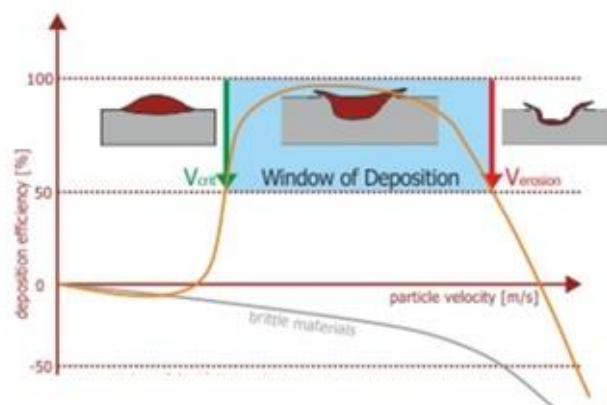


Figure 5: "Window of deposition" Impact velocity vs deposition efficiency for a constant impact temperature [18]

Figure above shows that is important to have a narrow distribution window of particle size due to the effects of erosion/adhesion because as explained before when a particle doesn't reach its critical velocity it will impact the surface of substrate and bounce back eroding the surface so reducing the deposition efficiency of the process as well. There are three types of impact between the particles and the surface of the substrate [18]:

1. The coating particle has reached the minimum impact velocity which is needed to excite a bonding mechanism with the engineering part.

This so called "critical velocity" influences the coating material properties.

2. Since the impact velocity is higher than the critical velocity, the deformation and bonding quality of the particles increase.
3. When the impact velocity is too high ("erosion velocity"), more material is eroded than added. No coating is produced.
4. In order to excite dense and well-formed coatings, the impact velocity of the particles should be between the critical and the erosion velocity.

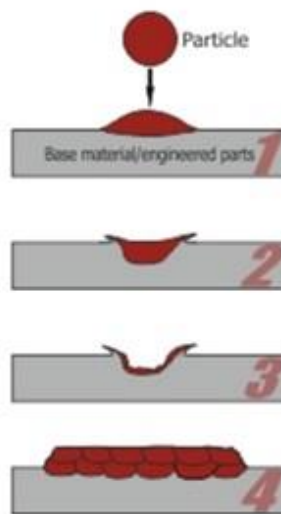


Figure 6: The influence of particle velocity onto the quality and deposition efficiency of the coating [18]

As it is shown in figure 6, when particle velocity is higher than the critical one, the deposition efficiency increases with increasing the impact velocity. A further increase of velocity leads to an increase in deposition efficiency until it reaches the saturation level of almost 100% deposition efficiency. After reaching this limit the deposition efficiency will decrease with an increase in particle velocity large-impact dynamics phenomenon. At the velocity where deposition efficiency is 0%, erosion velocity is defined—being usually two to three times higher than critical velocity [18].

### 2.1.2. PARTICLE, GAS AND SUBSTRATE TEMPERATURE

Particle, gas and substrate temperature can affect the impact velocity of the particles. The temperature of these three parameters has a significant influence on deposition efficiency as well. Therefore increasing the initial temperature of particles and the substrate can effectively improve the coating quality.

Increasing the gas temperature will result higher particle velocity and lower critical velocity values. It means that increasing the gas temperature is not to heat the particles temperature but to increase the gas velocity. It is also remarkable that the particle and substrate temperature will affect the physical and mechanical properties of the particle at the substrate. Particles with higher temperature need less kinetic energy to heat particle surface areas by plastic deformation, therefore increasing the particle temperature should allow one to decrease the particle velocity necessary to achieve the same deposition efficiency for the coating. Moreover an increase in particle temperature improves the particle-particle adhesion. Figure 7 presents how critical velocity varies with temperature [19].

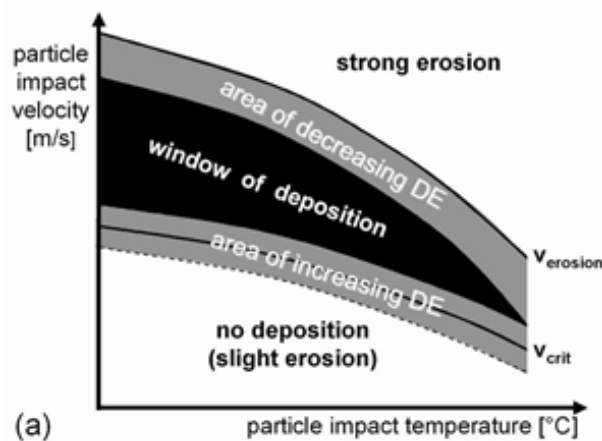


Figure 7: particle impact velocity vs particle impact temperature

### 2.1.3. Particle size and powder morphology

For powders with a smaller particle size distribution a higher particle velocity is expected. Consequently, a smaller particle size will result higher particle impact velocity because a lower gas/particle temperature is required which this low temperature can avoid producing the oxide phases and



therefore coating quality will be increased significantly. Though smaller-sized particles upon a low particle impact velocity are either unable to adhere or are loosely adhered and may be subsequently removed by the gas pressure jet during the subsequent gun pass. In addition, smaller-sized particles decelerate more than larger-sized particles after traveling through the bow shock and are more susceptible to deviation by bow shock even at high particle impact velocities [20]. Since one is relying on the coupling of the high-velocity gas stream to accelerate the particles, the particle morphology will determine the deposition efficiency. Long aspect shapes do not present a large cross-sectional area to promote drag effects. This type of particle geometry will tend to orientate into a direction that will present a reduced cross-section perpendicular to the gas flow reducing the drag coupling and consequently the final particle velocity. The particle density is another factor to consider. Particles with a high density, such as tungsten, will accelerate more slowly than particles with a lower density such as aluminum. The very-high-density materials may also require higher velocity powder carrier gas flows, such as those provided by helium, to maintain particle suspension in the gas flow for the journey to the nozzle [18].

#### 2.1.4. Powder feeding rate

The cold spray process is capable of creating dense and thick coatings on any substrates. Varying the mass flow rate at which the feedstock particles are fed into the carrier gas stream can change the thickness of the coating. Increasing the powder feed rate increases the thickness of the coating linearly until a maximum powder mass flow rate is reached for which there are too many particles impacting the surface of the substrate, resulting in excessive residual stresses causing the coating to peel. It was shown that the peeling was not a result of flow saturation but, instead, of excessive particle bombardment per unit area of the substrate. By increasing the travel speed of the substrate or elevating the propellant gas temperature, this can be overcome, and once again well-bonded dense coatings are achieved. Increasing the propellant gas temperature creates thicker coatings with higher coating adhesion when compared with identical non-heated coatings.

It is also possible to increase the powder mass flow rate to create thick coatings when the gas is heated and to not observe the peeling of the coating [21].

#### 2.1.5. Nozzle-substrate standoff distance

The nozzle-substrate standoff distance has also an influence on the cold spray deposition process. The bow shock formed at the impingement zone plays a critical role in the Cold Spray process; not only does it reduce the velocity of the gas, but also that of the entrained particles. Therefore at small standoff distances, when the strength of the bow shock is high, deposition performance is reduced. While at large standoff distances, when the bow shock has disappeared, deposition can continue unhindered. Deposition efficiency was shown to be strongly dependent on standoff distance as a result of the bow shock and the gas-particle relative velocity outside of the nozzle. Three distinct standoff regions were identified that affect deposition performance: 1) the small standoff region, where the presence of the bow shock adversely affects deposition performance, and is limited by the length of the nozzle's supersonic potential core; 2) the medium standoff region, where the bow shock has disappeared and, if the gas velocity remains above the particle velocity (positive drag force), the deposition efficiency continues to increase; and 3) the large standoff region, where the gas velocity has fallen below the particle velocity (negative drag force), and the particles begin to decelerate. For optimal deposition performance, the standoff distance should be set within Region 2 [22].

#### 2.1.6. Substrate roughness and thickness

The substrate surface roughness is shown to have an effect on the mass deposited and the deposition efficiency of only the first few layers of deposited material, but not on subsequent layers resulting from coating build up. A high surface roughness provides a larger substrate surface area onto which hard particles can impact and adhere. Ploughing of the hard particles into the soft substrate seems to be favorable for the initial deposition process. These factors all contribute to the small increase in mass deposited and the deposition efficiency observed on the high-roughness substrates. The

different grit types do not have any noticeable effect on the coating structure. The experimental results show that cold spray can be successfully used to produce coatings on thin parts without causing significant and apparent damage to the substrate. It is also shown, however, that the thrust of the supersonic jet is mostly susceptible to causing damage to the substrate as opposed to particle impingement, and therefore substrate thickness limitations should be considered. The substrate thickness was shown to have no noticeable effect on the deposition efficiency or the resulting coating structure [23].

### **3. HIGH VELOCITY OXY FUEL PROCESS (HVOF)**

High Velocity Oxygen Fuel (HVOF) coating is a thermal spray coating process used to improve or restore a component's surface properties or dimensions, thus extending equipment life by significantly increasing erosion and wear resistance, and corrosion protection. Molten or semi-molten materials are sprayed onto the surface by means of the high temperature, high velocity gas stream, producing a dense spray coating which can be ground to a very high surface finish. The utilization of the HVOF coating technique allows the application of coating materials such as metals, alloys and ceramics to produce a coating of exceptional hardness, outstanding adhesion to the substrate material, and providing substantial wear resistance and corrosion protection [24]. This thermal projection by high speed is based on combustion: the one of a fuel that is generally propene, propylene, natural gas, hydrogen or kerosene, with oxygen or air, as a supporter of combustion. Consequently, gases expand towards the outside, which generates a beam supersonic that accelerates particles. Reached temperatures ( $T_{max}$ , flame is 2860°C) by particles in the supersonic beam are, generally, minors whom in the case of plasma projection (in addition, time of residence and the thermal interchange also are smaller). But the speed is maximized, gas speeds of 1370 m.s<sup>-1</sup> using nitrogen like carrying dust gas, giving denser coverings. The size of the dust of projection used in HVOF is in a rank of 5 - 45 um and volumes oscillate between 20-80 g/min. Frequently used distances of projection vary between 150-400 mm.

Some of the strong points of this technique are the microstructural uniformity and, product of the time of residence and the temperature of the beam, the diminished degradation of particles by the temperatures reached. On the other hand, comparatively with other techniques of thermal spray, it displays the adjustment to [25]:

- A greater margin of material bases.
- Limitless size of the pieces to cover
- Diversity of materials
- Portable equipment
  
- Low costs of application and installation
- Optimization of parameters (that influence much in the properties of the coverings)
- Faster process
- Possibility of greater thicknesses
- Minor volume of remainders.

These improvements give HVOF too many applications like:

- Wear resistance Sliding, Abrasive, Erosion, etc.
- Chemical resistance
- High Temperature applications

Figure 8 displays the schematic of HVOF process.

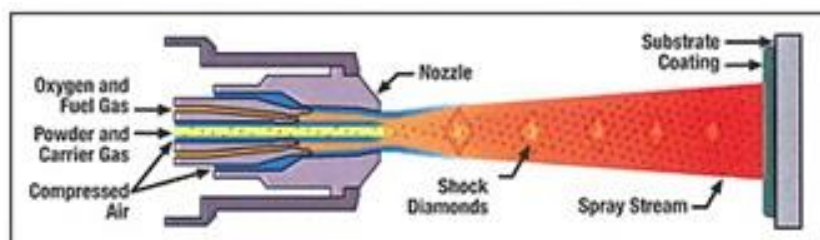


Figure 8: HVOF process scheme.

### 3.1. PROCESS PARAMETERS

HVOF spraying is a very complex process, which has a large variety of variables affecting the deposit formation and hence coating properties. These variables include hardware characteristics (e.g., nozzle geometry and

spraying distance) and process parameters, e.g., fuel gas, gas flow density, and powder feedstock. In the spray process, the powder particles experience very high speed combined with fast heating up to its melting point or above. This high temperature may cause evaporation of the powder or some components of it, dissolution, and phase transformations. Due to this complex nature of HVOF technique, the control and optimization of the process in order to achieve coating with desired properties is a highly challenging task. There are different ways of optimizing and analyzing the thermal spray processes and deposit formation. These include statistical methods such as Taguchi and design of experiments (DoE), numerical modeling and simulation, and FE methodology. In the Taguchi method, for example, the test matrix can be significantly reduced and the relative importance between variables can be determined sufficiently. The result in Taguchi is dependent on the design and selection of variables and their levels and the result may therefore be misleading. Determining the importance and weight of a large number of variables is very difficult with the HVOF process. This applies to different modeling procedures as well. Good coating quality with suitable properties and required performance for specific applications is the goal in producing thermal spray coatings. In order to reach this goal, a deeper understanding of the spray process as a whole is needed. Starting material, spray process and particle-substrate interactions all affect the formation of coating with different microstructure and hence the coating properties and eventually the coating performance. Use of submicron and nanostructured powders sets demands for the coating process in order to maintain the fine-scaled structures and enhance the coating properties. For better control of thermal spraying, different sensing devices have been developed during the last decade. These diagnostic tools have enabled better investigation and measuring of the spray process, and helped to understand the impact of different process variables on in-flight particle state (flux, temperature and velocity) [17].

### 3.1.1. Fuel type

Selection of fuel gas depends upon economics, coating material and desired coating properties. Hydrogen fuel gas is used when processing oxygen sensitive materials. Propylene should be used when high heat input is necessary. High melting, oxide based ceramics can only be sprayed by the HVOF process when acetylene fuel gas is used [25].

### 3.1.2. Fuel gas/O ratio

The influence of oxygen-rich flame is resulting in higher temperature and lower velocity. When fuel-rich flame is used, the temperature decreases (as the flame energy decreases), and particle velocity increases. Kinetic and thermal energy transferred to the particles is dependent on the flame energy (enthalpy of the used fuel, fuel density, and ratio of fuel to oxygen). Higher energy levels of the flame yield higher kinetic and thermal energies to the particles. Increment of airflow to the flame decreases the temperature and increases the particle velocity slightly by increasing the drag force to the particles and shortening of their dwell time. Changes in fuel-oxygen mixture cause stronger effect. Feed rate plays also a role on the kinetic and thermal energy. The oxide content of the coatings is predominantly determined by the in-flight reactions. Therefore the fuel-rich conditions produce coatings with less oxidation. Higher particle speeds reduce particle overheating, thus preventing the oxidation and decarburization of carbides [25]. On the other hand, higher particle temperature leads to slightly higher oxide content.

### 3.1.3. Spray distance

The distance between the spraying gun and the substrate is termed as spraying distance or standoff distance (SOD). SOD influences the velocity of the particles and the length of time that particles are exposed to the high velocity spray, thus influencing the degree of particle melting. A longer SOD may cause a reduction in the velocity of the droplets during spraying due to the frictional forces from the ambient environment. A shorter SOD would indicate the substrate experiences more of the heating effects from the high velocity spray. Thus, SOD affects the substrate temperature and also the coating properties deteriorate with increasing spraying distance [26].

### 3.1.4. Powder feed rate

Powder feed rate has the direct influence on coating's thickness. As the feeding rate increases, the thickness increases linearly, though over increasing the feed rate can have the negative effect on coating deposition, because with increasing the feeding rate, too many particles impact the surface and can due to the peeling effect [27].

## 4. AIR PLASMA SPRAY

The Plasma Spray Process is basically the spraying of molten or heat softened material onto a surface to provide a coating. Material in the form of powder is injected into a very high temperature plasma flame, where it is rapidly heated and accelerated to a high velocity. The hot material impacts on the substrate surface and rapidly cools forming a coating. This plasma spray process carried out correctly is called a "cold process" (relative to the substrate material being coated) as the substrate temperature can be kept low during processing avoiding damage, metallurgical changes and distortion to the substrate material. Figure 9 demonstrates the schematic of plasma spray method [28].

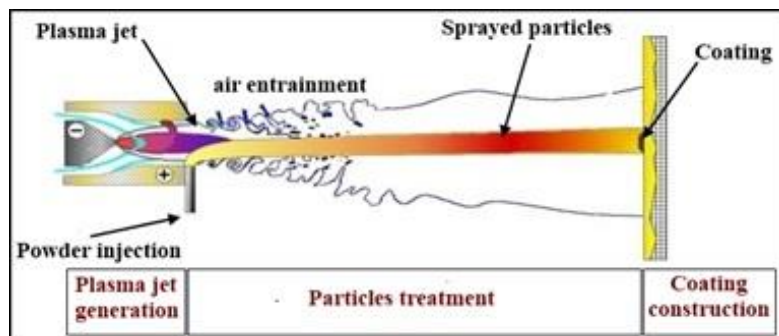


Figure 9: Schematic of APS system

Plasma spraying has the advantage that it can spray very high melting point materials such as refractory metals like tungsten and ceramics like zirconia unlike combustion processes. Plasma sprayed coatings are generally much denser, stronger and cleaner than the other thermal spray processes with the exception of HVOF, HVOF and cold spray processes. Plasma spray coatings probably account for the widest range of thermal spray coatings and

applications and make this process the most versatile. Disadvantages of the plasma spray process are relative high cost and complexity of process [29].

#### 4.1. PROCESS PARAMETERS

Spraying parameters such as input power, stand-off distance and powder feed rate can influence the microstructure and the mechanical properties of the coating by affecting the thermal energy and kinetic energy of particles. If thermal energy over increases the particles tend to be vaporized than impacting the substrate surface. Though, low thermal energy of particles can avoid them from being molted.

##### 4.1.1. Input power

The spraying power is an important parameter which can affect the quality of the coating, since it has an influence on impact temperature and velocity of particles. It can also affect the porosity of coating; it has an inversely proportional relationship with the porosity of coating. Low input power can cause poor adhesion and incomplete melting of powders since more complete particle melting can result in lower porosity because when the particles impact the substrate surface or the formed coating, they are not able to develop completely to form the coating then the pores and cracks will be formed due to the splat solidifying the splats. Though increasing the power level above 25 kW can decrease the deposition efficiency of coating [30].

##### 4.1.2. Stand-off distance

The stand-off distance can affect the porosity of coating as well as the input power but unlike input power, it has a directly proportional relationship with the porosity. As the spraying distance decreases, the crystalline phase of the coatings increases because of the increase in the particle temperature at the moment of impact. At lower spraying distance, the particles which impact the substrate are semi or fully melted and as a result the crystalline phase increases because the solidification rate gradually decreases as the coating thickness increases. The stand-off distance can also control the cohesion between the splats because it affects the temperature and velocity of impact particles. Therefore, a shorter SOD



can cause better cohesion between the formed splats. As spraying distance increases, the particles have more time to react with the air inside the flame, which as a result oxide phases can be formed in coating [30].

#### 4.1.3. Powder feeding rate

Feeding rate can affect the impact velocity and temperature as well as the other spraying factors. An increase in powder feeding rate can cause rough coating and incomplete melting of the powders. When the powder feed rate value is low, the splats poorly flatten and spread out on the substrate surface and as a result pores and cracks can be formed at the boundaries of splats. Though when the powder feed rate is extremely low, most of particles are fully melted and dense coating can be produced. Increasing the feeding rate above the specific value can also cause developing the cracks and pores in coating [30].

### 5. GREEN CARBIDES

The Mono-carbides of groups IV, V, and VI metals show remarkable properties, such as high hardness, wear resistance, and melting points [31-35]. When such a transition that metal carbide phases are cemented in a relatively ductile matrix happens; a combination of high abrasion resistance and toughness are achieved [33, 34]. Titanium carbide based cermets were first announced commercially in 1930 [36, 37] as the first carbide tools for high-speed cutting of tool steels. Although WC-Co coatings have been produced successfully in many cases, such as wear resistant materials but their high densities prevent their use in applications that command reduction in weight. Instead lightweight carbides based on Ti can be used to improve and modify the tribological properties of aerospace structural materials [38]. Titanium carbide based cermet materials also show agreement for low-weight, high-strength wear resistant applications at low and high temperatures. Their use as lightweight protective coatings is being studied in aerospace, transportation vehicles, and industrial mechanical equipment, where low mass and/or low inertia designs are required [38]. In the applications, light alloys of aluminum and titanium show high strength, high stiffness at low weight, corrosion protection, and fatigue resistance. Despite

their promise, however, these base materials are restricted by their low wear resistance. Hence, surface protecting coatings are needed. Due to the inhomogeneous nature of the TiC-metal matrix coatings and the limited temperature capabilities of the base materials, coating processes such as plasma spray can offer the materials flexibility and processing capabilities necessary to provide such coatings. Metal-bonded titanium carbide coatings produced by plasma spraying can thus be a cost effective alternative to enhance and modify the tribomechanical properties of primary aerospace structural materials. Titanium carbide cermet coatings also offer substantial weight savings in such applications by virtue of their reduced density and increased elastic moduli. The properties of titanium carbide and titanium carbide based cermets, processed by conventional powder metallurgy routes or by vapor deposition processes, have been reported [39, 40]. Thermally sprayed coatings of WC-Co have been widely advanced for tribological applications [41-44]. WC-Co has been used as the primary wear-resistant coating material due to its high hardness, acceptable oxidation-corrosion behavior, and excellent compatibility with many iron based substrate materials. Its choice as a protective coating for lightweight structures is not considered optimal for many of the lightweight materials being considered in aerospace and other transportation vehicles. The high density of such coatings ( $\sim 13.5 \text{ g/cm}^3$ ) makes them heavier than necessary and may compromise some lightweight structural designs. Alternatively, the high relative cost of WC-Co (U.S. \$500/m<sup>2</sup> for WC/Co as compared to \$125/m<sup>2</sup> for Ti-TiC for as-coated 250  $\mu\text{m}$  thick coatings assuming 65% coating efficiency) is also a disadvantage to other, less dense wear-resistant coatings such as TiC based hard metals, which are less than 25% the weight and, thus, 25% the cost of WC-Co coatings. Other potential advantages anticipated in using such materials in thermal spray processes were recently reviewed [45, 46]. Although thermal spraying of materials such as NiCr-TiC has been reported to be very successful [47, 48], the substrates used for such coatings have almost always been steel. The application of such coatings on light metal substrates has probably been limited in the thermal spraying industry because of the high temperature effects associated with most spray

processes. A majority of light alloys, unlike steel, have low melting points, which prohibits their use by this industry. Moreover, recently conventional Co- and Ni-based cermet carbides have considered as allergic cermets and are labelled as suspect carcinogenic agents which can cause inhalation toxicity problems. Therefore replacing Ti, Ti alloys (TiCr) and Fe alloys (FeCrAl) are less hazardous and more environmentally friendly alternative to Ni- and Co-based cermets and present some safety and health issues [49].

## CHAPTER 2. EXPERIMENTAL PROCEDURE

## **1. RAW MATERIALS**

In this research work different feedstock powders from Ti-TiC with different percentage of carbide phase (20, 50, 65 and 80%), Ti-SiC, various types of Ti-WC (400HV, 650HV, 1500HV and the one richer in WC) and TiC-Fe alloys with different morphologies were provided by MBN Co. of Italy and sprayed onto the different substrates (Al and C Steel) by different thermal spray techniques (CGS, HVOF and APS). The powders sprayed onto the rectangular (50x20x5 mm<sup>3</sup>) and cylindrical (d=25,4mm; h=35mm) substrates for different purposes. In chapter 3 each powder has been described in details.

## **2. STRUCTURAL CHARACTERIZATION**

There are some parameters for each powder which should take into the account. These parameters include: particle morphology, particle size and particle size distribution, cross section and free surface of powders and phase composition.

### **2.1. Morphology**

Powder morphology is one of the most important characters of each powder which should be obtained before spraying. The complete information of powder from the particle size and particle shape can be found by morphological study of the powder. For this purpose the powders went through the scanning electron microscopy (Phenom ProX desktop scanning electron microscope (SEM)) though for some powders FEI QUANTA 200 SEM has been used to evaluate the morphology of samples. Powder samples were embedded in polymeric matrix, polishing the surface of specimen and performing metallization with Au, in order to enhance surface conductivity. The SEM cross section and free surface images of each powder at different magnification were taken in order to observe the particle shape and particle size.

## 2.2. Particle size distribution

The particle size distribution of the powders was examined by using laser diffraction test (Beckman Coulter LS 13320). The particle size range for powder was measured before spraying test.

## 2.3. Phase composition

The phase composition of powders was obtained through XRD Technique; the X-Ray diffraction test was used to analysis the phase composition and phase quantification of each powder. The used equipment was a SIEMENS D500  $\theta/2\theta$  Bragg-Brentano type using Cu  $K\alpha_{1+2}$  ( $\alpha_1=1,54060$  and  $\alpha_2=1,54443$ ) radiation at 40 Kv and a current of 30 mA. The obtained diffractogram was analyzed by Xpert analysis software to identify the phase composition and the quantity of each phase by comparison with the database of the program. For some powders it has been used different XRD system, A Siemens D5005 X-ray diffractometer with a Co- $K\alpha$  radiation  $\lambda$  of 1.79 Å. All XRD data were collected using a  $\theta$ -2 $\theta$  geometry mode, recording the diffraction intensity in the range of 2 $\theta$  between 20-130 degrees and operating at 40 kV and 40mA, with a step of 0.020° and a step time of 1s. The Difrac®Plus Eva software version 2.0 was used to identify the crystalline peaks, by comparison with the International Center for Diffraction Data (ICDD) database and Joint Committee on Powder Diffraction Standards (JCPDS) files.

# 3. EQUIPMENTS

## 3.1. COLD GAS SPRAY

In this research work three different techniques, CGS, HVOF and APS were used to obtain the coatings. The first method was Cold Gas Spray technique. Several powders were sprayed onto the different substrates by using this technique. In this method different parameters like gas pressure, gas temperature and stand of distance for each powder were applied in order to improve the microstructure of obtained coatings like porosity and deposition efficiency. The cold gas spray system with a commercial KINETICS® 4000 (CGT GmbH, Germany) spray gun with a maximum operating pressure of 4

MPa and temperature of 800 °C was employed and it used nitrogen as the process gas. The equipment consists of:

- Control panel
- Powder supply
- Gas dosing system
- Feeding powder
- Spray gun

Besides, KINETICS® 4000 has the possibility of using a pre-chamber of 120mm in length connected to the nozzle of the spray gun where the feedstock powders are heated up for a longer time. The spraying powders were fed into the gun and heated and accelerated through a De-laval nozzle and reached the Max supersonic speed. Figure 10 shows a scheme of the KINETIC 4000 system and also the spray gun.



**Equipment:** KINETIC® 4000/34kW (Cold Gas Technology, Ampfing, Germany)

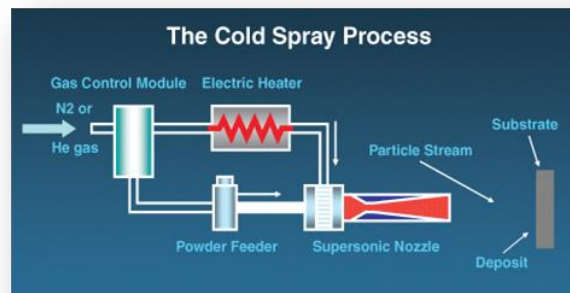


Figure 10: Schematic of KINETIC 4000 system and spray gun

### 3.2. HIGH VELOCITY OXYFUEL

The second method in this research work was high velocity oxy fuel. The HVOF equipment used was a Sulzer (Winterthur, Switzerland) DJH with two different heads: DJH 2700 for propylene and DJH 2600 for hydrogen. Consequently, gases expand towards the outside, which generates a beam

supersonic that accelerates particles. Reached temperatures ( $T_{\max}$ . flame is  $2860^{\circ}\text{C}$ ) by particles in the supersonic beam are, generally, minors whom in the case of plasma projection (in addition, time of residence and the thermal interchange also are smaller). But the speed is maximized, gas speeds of  $1370\text{ m}\cdot\text{s}^{-1}$  using nitrogen like carrying dust gas, giving denser coverings. The size of the dust of projection used in HVOF is in a rank of  $5 - 45\text{ }\mu\text{m}$  and volumes oscillate between  $20\text{-}80\text{ g}/\text{min}$ . Frequently used distances of projection vary between  $150\text{-}400\text{ mm}$ . Figure 11 presents the used HVOF equipment in this research work:

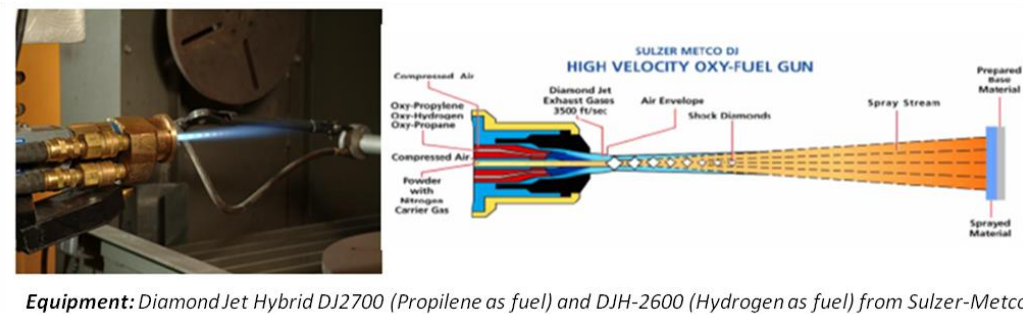


Figure 11: HVOF equipment

### 3.3. AIR PLASMA SPRAY

The third used technique in this research work to obtain coatings was conventional APS (Atmospheric Plasma Spray). The APS equipment was Plasma technik A-3000 with F4 Torch. Plasma temperatures in the powder heating region range from about  $6000$  to  $15,000\text{ }^{\circ}\text{C}$  ( $11,000$  to  $27,000\text{ }^{\circ}\text{F}$ ), significantly above the melting point of any known material. To generate the plasma, an inert gas—typically argon or an argon-hydrogen mixture is superheated by a dc arc. Powder feedstock is introduced via an inert carrier gas and is radially accelerated toward the substrate by the plasma jet. Provisions for cooling or regulating the spray rate may be required to maintain substrate temperatures in the  $95$  to  $205\text{ }^{\circ}\text{C}$  range. Figure 12 shows the APS equipment used in this research work:



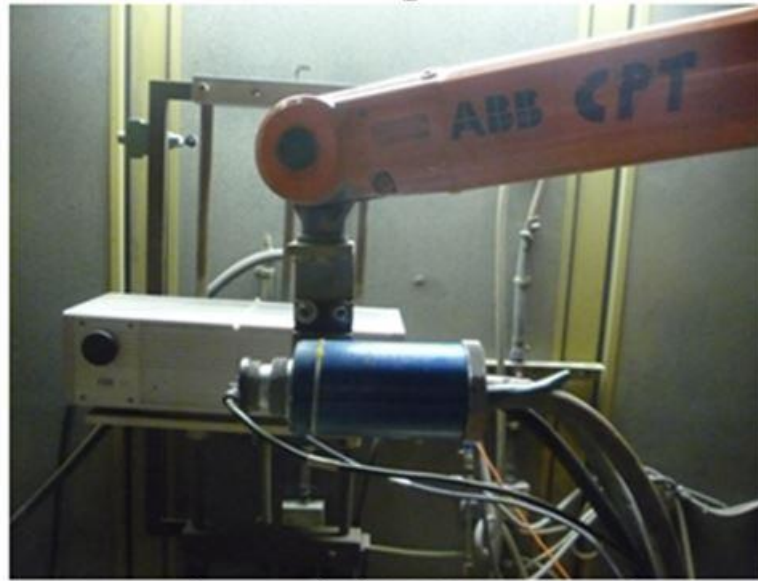


Figure 12: Plasma technik A-3000 with F4 torch

### 3.4. MICRO-HARDNESS

This parameter has been evaluated by means of a Matsuzawa MTX- $\alpha$  Vickers equipment according to the ASTM E384-99 standard. [50] The load of 200 gf to 300 gf was applied to produce the pyramid-shaped footprint Vickers indentation and 10 measurements were made along the coating and an average was measured. Figure 13 shows the Vickers micro-indentation equipment used in this research work and figure 14 shows the hardness calculation: [51]



Figure 13: Vickers micro-indentation equipment

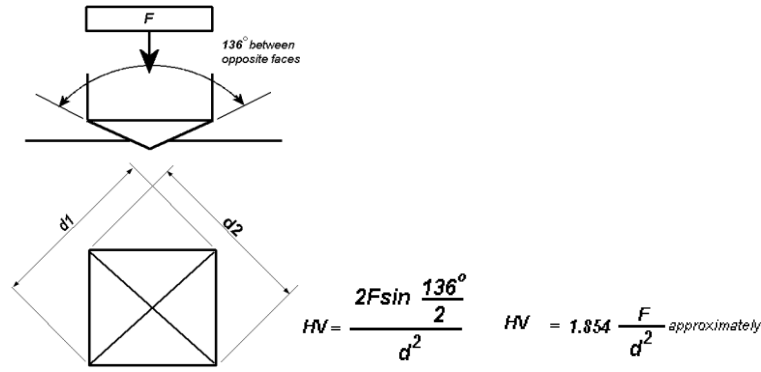


Figure 14: Vickers hardness calculation ( $F$ = Load in kgf,  $d$  = Arithmetic mean of the two diagonals,  $d_1$  and  $d_2$  in mm, HV = Vickers hardness)

### 3.5. FRACTURE TOUGHNESS

The fracture toughness of optimum coatings by both CGS and HVOF techniques was tested to measure the impact of formation of brittle phases in HVOF and increasing the ductility in CGS sprayed coatings. To study the fracture toughness as a function of material microstructure the Vickers indentation technique was used. The elastic modulus was estimated using a *Knoop* indentation technique by performing 10 *Knoop* indentations at a load of 9.80N. Crack model used for predicting the fracture toughness was half-penny (Eq. 1) and in order to measure the fracture toughness Vickers indentations at 9,80 N were performed on polished coating cross-sections, and its diagonals and crack lengths measured using an optical microscope. An average of 10 indentations was made and the total crack length was estimated by using Equation 1, where  $2d_{||}$  and  $2d_{\perp}$  are the parallel and perpendicular Vickers diagonals to the coating surface produced in the indentation, and  $a_l$  and  $a_r$  are the left and right crack lengths; to determine the fracture toughness Equation 2 was used, where  $H_v$  and  $E$  are the Vickers hardness and elastic modulus, respectively:

$$c = (2d_{||} + 2d_{\perp})/4 + (a_l + a_r)/2 \quad (\text{Eq. 1})$$

$$Kc = 0.0711 (H_v d^{1/2}) [E/H_v]^{2/5} [c/d]^{-3/2} \quad (\text{Eq. 2})$$

This equation is only valid for a Half-Penny crack regime that occurs when  $c/d \geq 2.5$  where  $d$  is the Vickers half-diagonal.

### 3.6. TENSILE STRENGTH

Coating adhesion has been evaluated following the ASTM C-633 standard with SERVOSIS ME-402/10 equipment. This test consists of gluing a cylindrical coated sample with a resin to an uncoated grit blasted sample. There are 3 different failures after the test is done. It can fail in the glue, between the coating layers or the rupture can happen at the interface of coating-substrate. Figure 15 shows the adhesion test specimen and the three rupture possibilities.

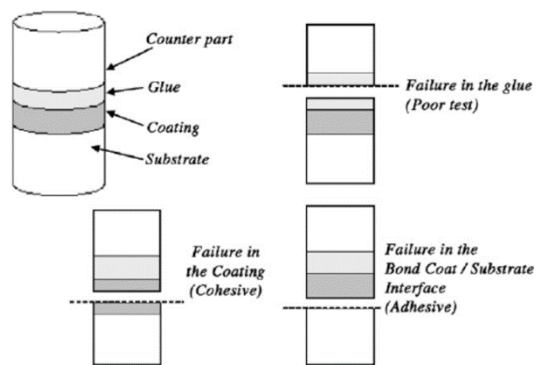


Figure 15: adhesion test specimen and the three rupture possibilities

### 3.7. SLIDING WEAR

#### 3.7.1. BALL ON DISC TEST

This test under ASTM G99-03 standard allows the evaluation of the coefficient friction of the polished coating and moreover after the test is done the lost volume can be obtained using the confocal microscope by measuring the wear track. Figure 16 below shows the ball on disc scheme and the wear track.

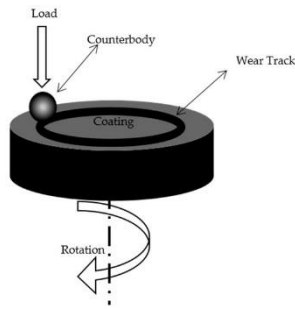


Figure 16: Ball on disc scheme and wear track

### 3.7.2. RUBBER WHEEL TEST

The abrasive wear test was evaluated using rubber wheel equipment following the ASTM G65-00 standard. Dry sand rubber wheel abrasion test is one of the most widely used abrasion testing method. The abrasive, for example dry sand, is fed between the specimen and the rotating rubber wheel which was shown in Figure 17. Abrasive wear occurs when hard particles are compressed with normal pressure against the surface of a metal, causing material removal. The test allows comparison of wear-resistant materials by their volume loss in cubic millimeters, with materials of higher wear resistance showing lower volume loss.

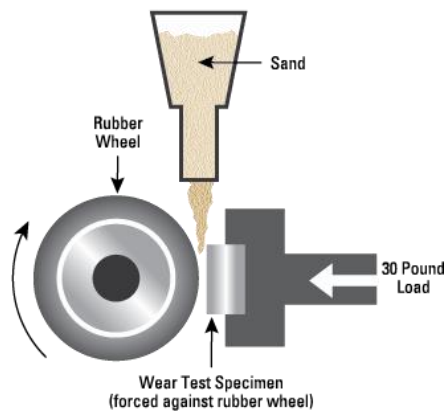


Figure 17: Rubber wheel scheme

## CHAPTER 3. RAW MATERIALS CHARACTERIZATION

## 1. SUBSTRATES

In this Thesis special focus was given to coatings obtained onto low carbon steel and aluminum alloy, Al7075-T6 substrates. Rectangular substrates with (100x20x5 mm) dimension and cylindrical (d=25,4mm; h=35mm) substrates for different purposes, were prepared first by grinding the surface in order to eliminate surface oxidation and later sand grit blasting to create roughness on the surface and increase the adhesion between substrate and coating.

### 1.1. Low-carbon steel

Low carbon steel alloys contain up to 0.30wt%C. Low carbon steel alloys are relatively soft and weak but have excellent ductility and toughness, they are machinable and are not expensive to produce. Their applications include automotive industry, I-beams, sheets, pipelines, buildings and bridges. These applications require materials that are usable under a wide variety of conditions; therefore, these products must have adequate strength and excellent mechanical properties, appealing appearance after fabrication, and compatibility with other materials and with various coatings and processes. Table 1 shows some properties and chemical composition of the 0.20wt%C low-carbon steel.

Table 1: Properties and chemical composition of 0.20wt%C low-carbon steel

AISI No.	Tensile Strength (MPa)	Yield Strength (MPa)	Elongation. (%)	Hardness (HV)	Composition (Wt. %)
1020	448,2	330,9	36	143	0,20C 0,45Mn

### 1.2. Al7075-T6

Aluminum and its alloys due to their specific strength are used in a wide range of application. Among Aluminum alloys, 7075 has a superior strength and is used in aircraft industry. The mechanical properties of 7075 alloy are improved by reducing its iron and silicon contents. Al7075-T6 has hardness of  $178 \pm 8$  HV which was obtained by applying a load of 100gf onto the polished surface of the substrate. It has the tensile strength of approximately 510-527 MPa and yield strength of 434-503 MPa. Table 2 shows the chemical composition of Al7075-T6.

Table 2: Percentage chemical composition of Al7075-T6

Zn	Mg	Cu	Cr	Fe	Si	Mn	Ti	Al
5.59	2.63	1.52	0.24	0.21	0.07	0.06	0.02	89.66

## 2. SPRAYING POWDERS

### 2.1. TiC based-green matrix

TiC-based cermets currently attract much attention and are widely used in the cutting and forming applications due to high hot hardness, strength, chemical stability and excellent wear and oxidation resistance [52-54]. The different chemical composition of binders can create superior properties [55, 56]. The metal binders used in TiC-based cermets are alloys of metallic elements (Fe, FeCrAl, TiCr and Ti).

#### 2.1.1. Ti-20%TiC

Ti-20%TiC powder was synthesized by High Energy Ball Milling process. This method permits production of composite powders suitable for application in thermal spray processes. Hard phase materials like carbides are incorporated into various metallic matrices including light weight alloys based on Titanium and Aluminum. This mechanical alloying process is simple and efficient to produce fine powders but with the contamination issue. TiC and Ti were used as starting materials. Powder mixture later mixed with ethanol was sealed in with WC-Co hard metal balls (8 and 12 mm in diameter and 50-50 in weight percentage, respectively) in a glove box containing inert atmosphere of Ar. The ball to powder weight ratio is controlled to be 15:1. The milling process was carried on a high energy ball mill with the selected rotation velocity of 250 rpm. After 10 h of milling, the powder was taken from the vial and dried at room temperature in Ar [57, 58]. Figure 18(a) and 18(b) show SEM Free surface and 18(c) shows SEM Cross section of the Ti-20%TiC powder at different magnification respectively.

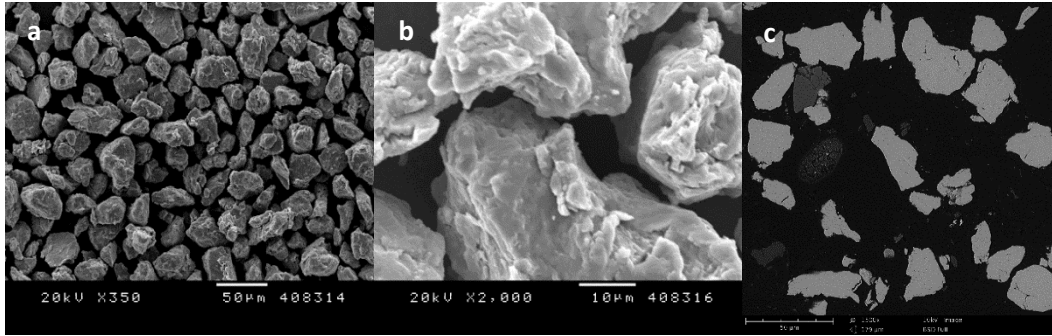


Figure 18: SEM study of Ti-20%TiC (a) Free surface at 350x (b) 2000x and (c) Cross section at 1500x

### 2.1.2. Ti-50%TiC

Ti-50%TiC is another cermet with higher percentage of Carbide phase designing for spray by CGS technique. This cermet like Ti-20%TiC was synthesized by High Energy Ball Milling process which was explained before. Figures 19(a) and 19(b) show SEM Free surface and 19(c) shows SEM Cross section images of Ti-50%TiC powder at different magnification.

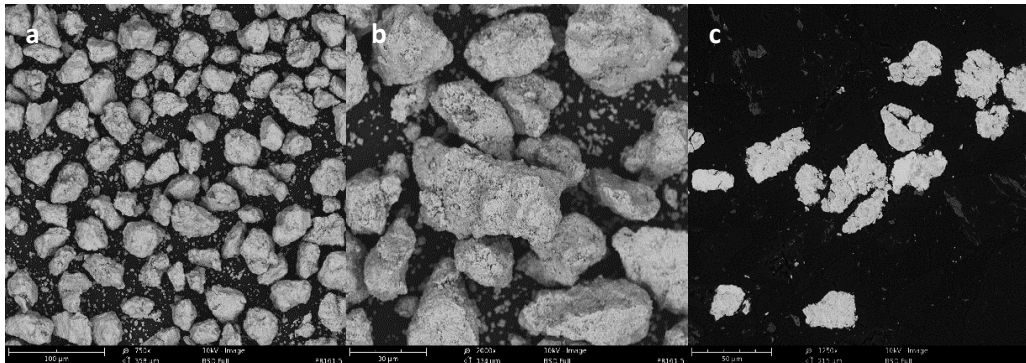


Figure 19: SEM study of Ti-50%TiC (a) Free surface at 750x (b) 2000x and (c) Cross section at 1250x

### 2.1.3. Ti-65%TiC

Ti-65%TiC is another cermet with higher percentage of Carbide phase designing for spray by CGS technique. This cermet like Ti-50%TiC was synthesized by High Energy Ball Milling process which was explained before. Figures 20(a) and 20(b) show SEM Free surface and 20(c) shows SEM Cross section images of the Ti-65%TiC powder at different magnification. It can be



observed that the carbon (the darker phase) has been distributed in Ti (lighter phase) matrix.

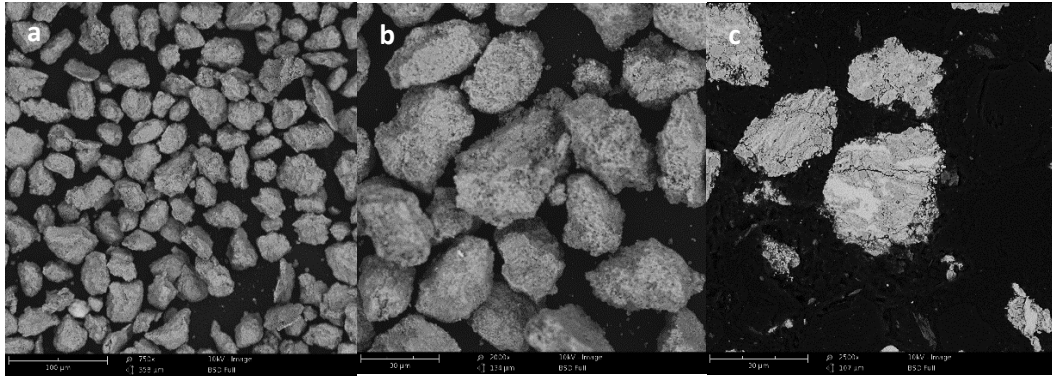


Figure 20: SEM study of Ti-65%TiC (a) Free surface at 750x (b) 2000x and (c) Cross section at 2500x

The XRD comparison of Ti-TiC with different percentage of TiC is shown at below graph (Figure 21). From the XRD graph can be found that by increasing TiC phase from 20 to 65% the normalized intensity of TiC has been increased.

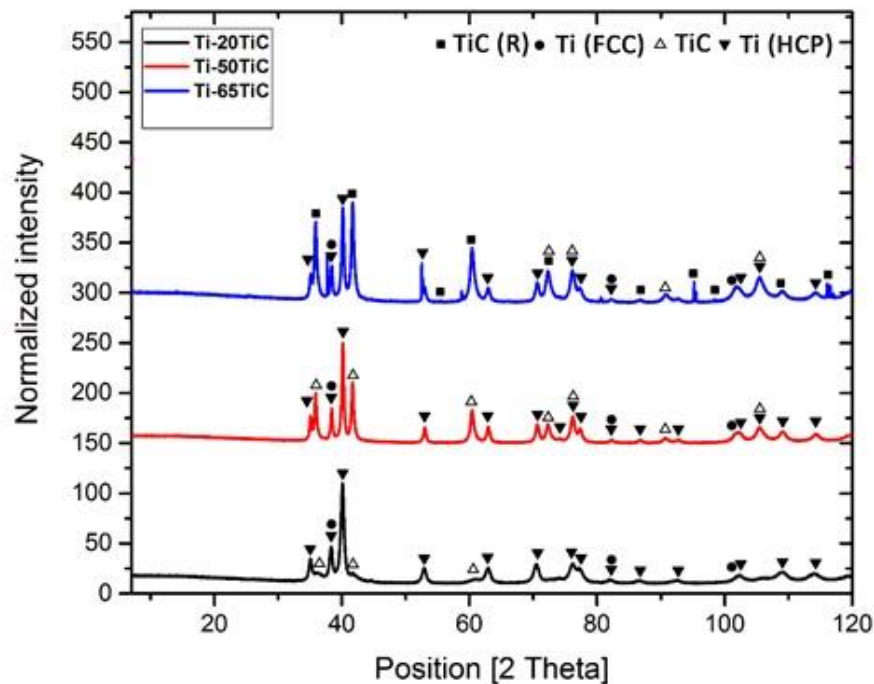


Figure 21: XRD study of Ti-TiC with different percentage of TiC phase

The differential volume (%) vs particle diameter (um) of Ti-TiC powders was studied and shown at graphs 22(a) to 22(d) for Ti-20%TiC, Ti-50%TiC and Ti-65%TiC respectively.

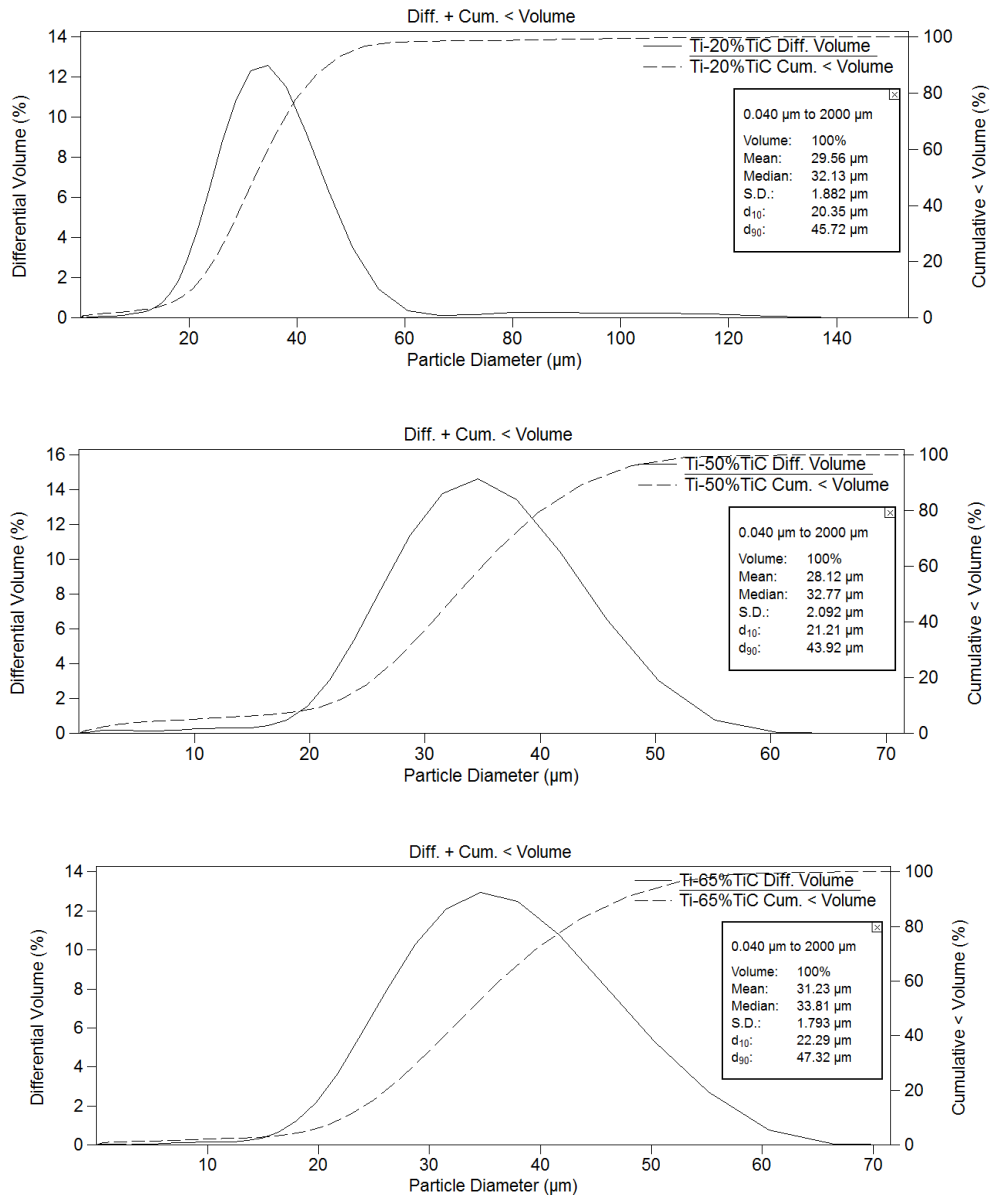


Figure 22: LS study of Ti-20%TiC, Ti-50%TiC and Ti-65%TiC

#### 2.1.4. TiC-FeCrAlTi

TiC-FeCrAlTi (75-25 v/v) is another green cermet produced for some spraying tests by HVOF technique. As it is mentioned before the metal binders can be varied but among all Fe-based alloys are the most commonly used metallic materials, because of low costs, good fracture toughness and non-toxic nature comparison with other binders like Ni and Co. [59] Figure 23(a) and 23(b) show SEM Free surface and 23(c) shows SEM Cross section images of TiC-FeCrAlTi powder and figures 24 and 25 show LS and XRD study of this powder respectively.

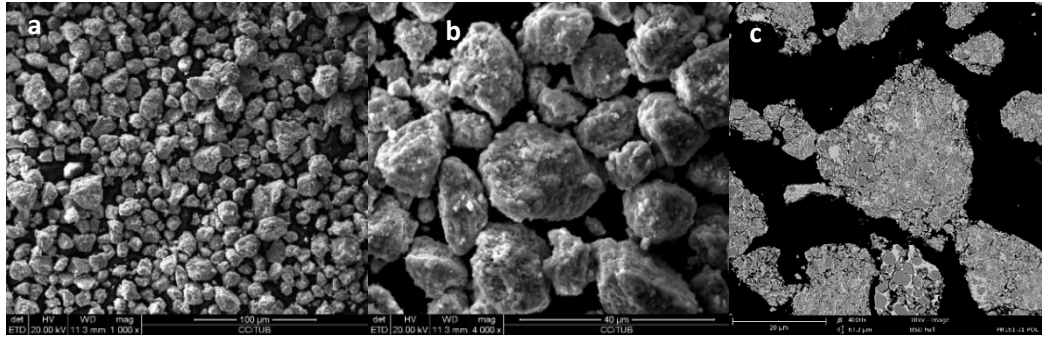


Figure 23: SEM study of TiC-FeCrAlTi (a) Free surface at 1000x (b) 4000x and (c) Cross section at 4000x

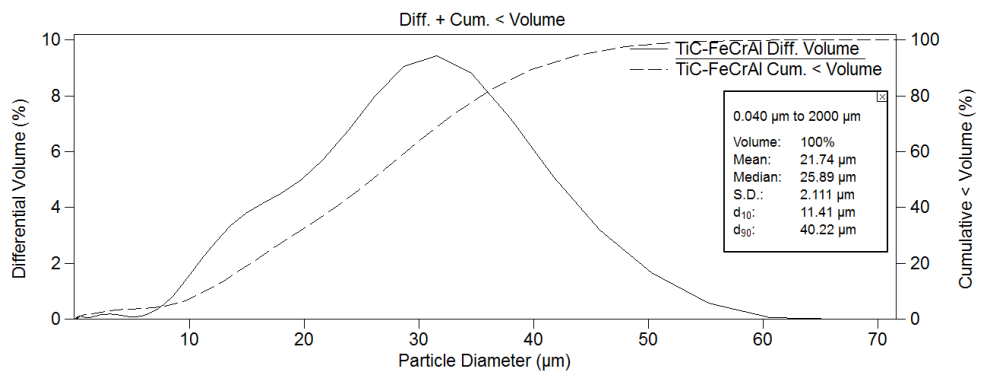


Figure 24: Laser scattering study of TiC-FeCrAlTi

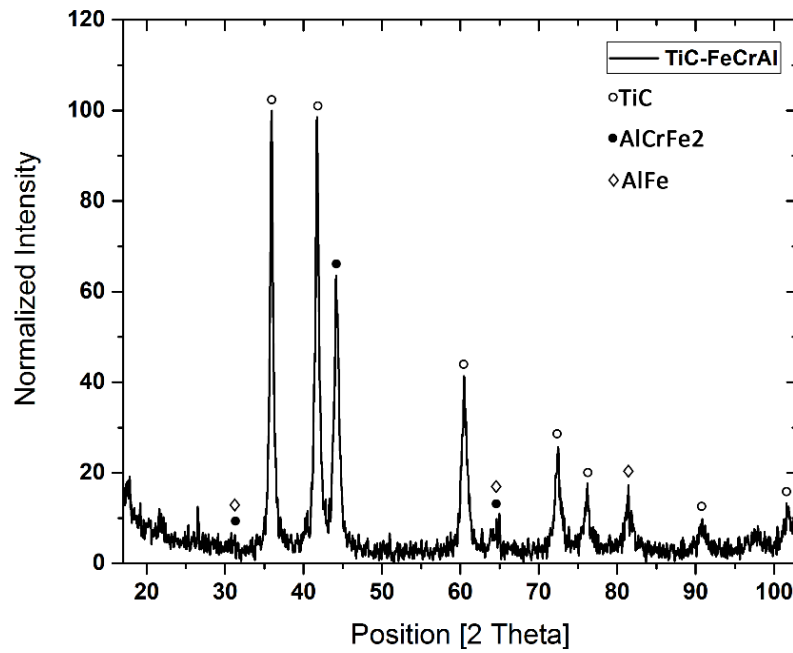


Figure 25: XRD study of TiC-FeCrAlTi [60]

## 2.2. SiC based-green matrix

### 2.2.1. Ti-SiC

Ti-SiC (50-50 v/v) is a light weight cermet in compare to WC-Co, this powder has been developed for some spraying tests with HVOF and CGS techniques. The expected hardness of produced coating is 1000HV. Figures 26(a) and 26(b) show the SEM Free surface and 26(c) shows SEM Cross section images of Ti-SiC powder.

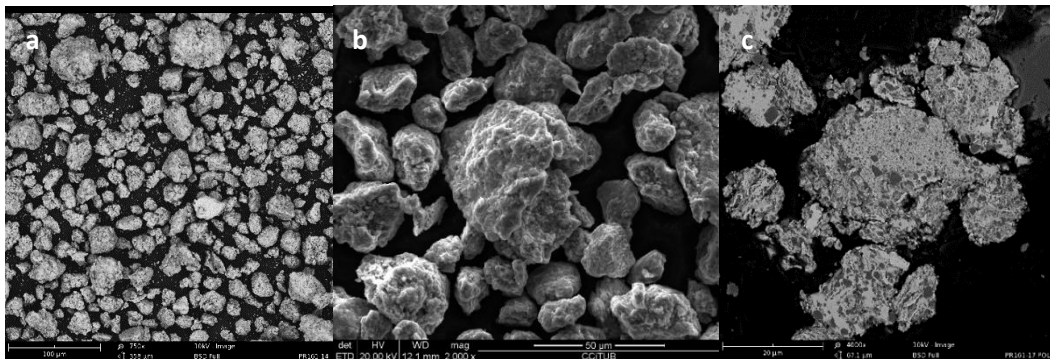


Figure 26: SEM study of Ti-SiC (a) Free surface at 750x (b) 2000x and (c) Cross section at 4000x

The LS study of this powder and XRD graph were shown at below graphs. (Figure 27 and 28)

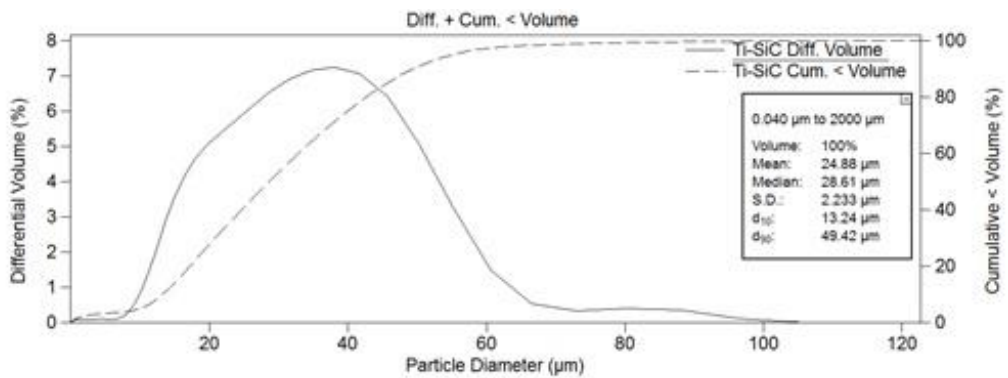


Figure 27: LS study of Ti-SiC

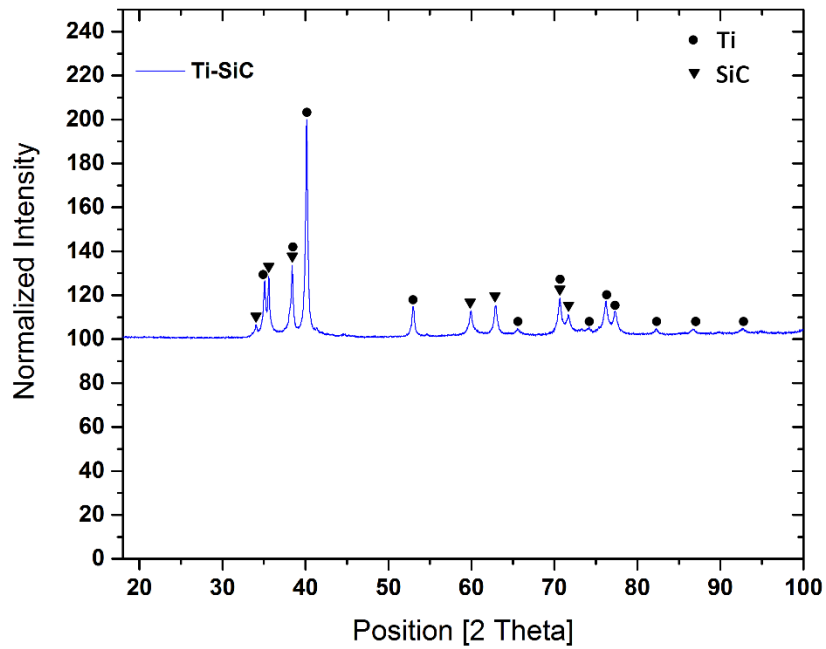


Figure 28: XRD study of Ti-SiC [60]

### 2.3. WC based-green matrix

#### 2.3.1. Ti-WC (400 HV)

Ti-WC (50-50 v/v) is another Co free wear resistant cermet which has been developed for spraying by both HVOF and CGS techniques. The expected properties of the coating are thickness of about 1mm and the hardness of as-sprayed coating up to 800 HV and 1100-1500HV after the heat treatment (HT). Figures 29(a) and 29(b) show SEM free surface and 29(c) shows SEM cross section of this powder. LS study of this powder was shown at figure 30.

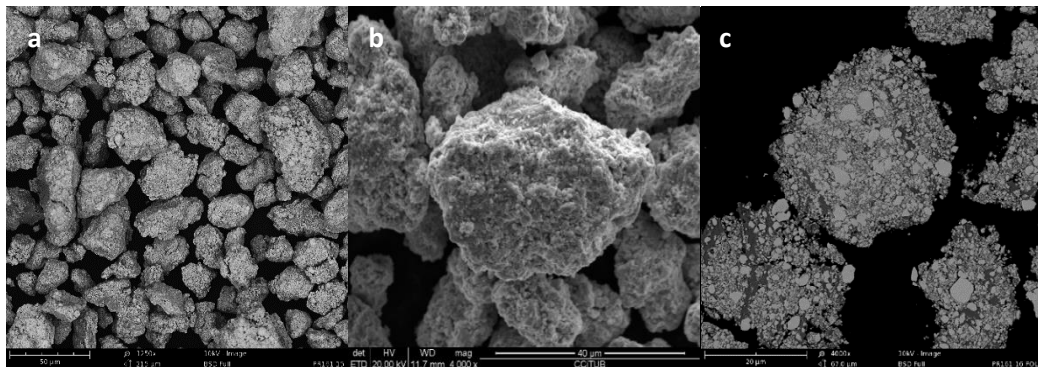


Figure 29: SEM study of Ti-WC (a) Free surface at 1250x (b) 4000x and (c) Cross section at 3500x

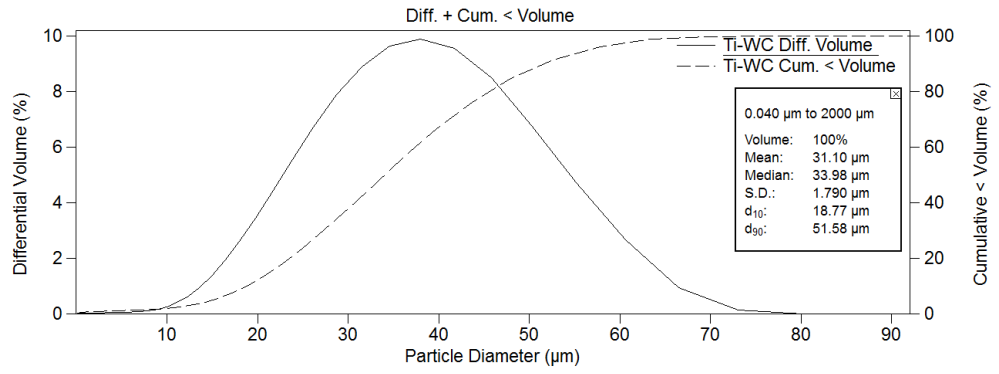


Figure 30: LS study of Ti-WC

### 2.3.2. Thermally pre-treated Ti-WC (650 HV)

Thermally pre-treated Ti-WC is another cermet provided by MBN with hardness of 650HV. This powder has been developed for spraying tests by HVOF and APS techniques. Figures 31(a) and 31(b) show SEM free surface and 31(c) shows SEM cross section study of this powder. LS study of this powder was shown at figure 32.

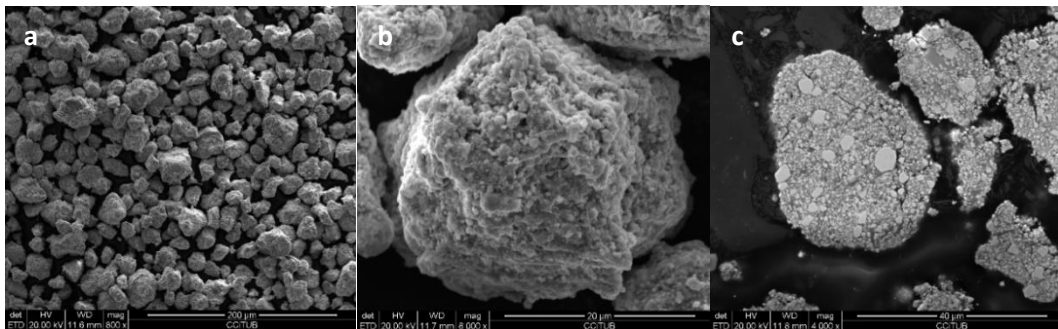


Figure 31: SEM study of Ti-WC (650HV) (a) Free surface at 800x (b) 8000x and (c) Cross section at 4000x

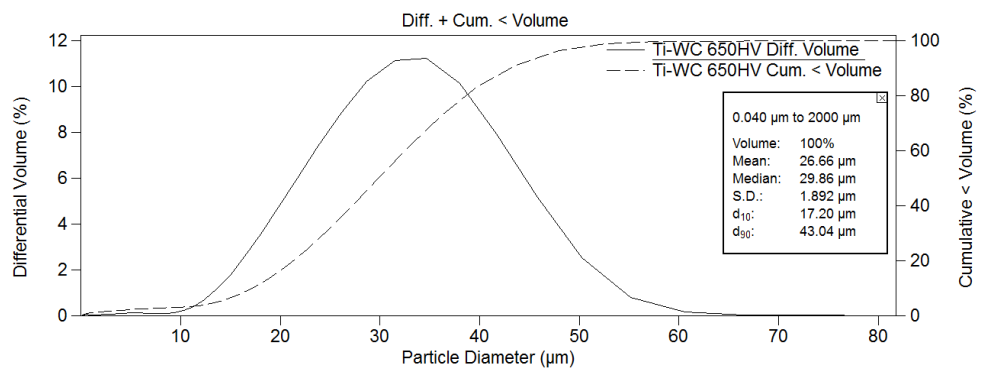


Figure 32: LS study of Ti-WC (650HV)

### 2.3.3. Thermally pre-treated Ti-WC (1500 HV)

Harder version of thermally pre-treated Ti-WC with hardness of 1500HV has been developed for spraying tests by HVOF, APS and CGS techniques. The expected hardness of the coating is a range between 1000 and 1500HV for as-sprayed sample. Figures 33(a) and 33(b) show SEM free surface, 33(c) shows SEM cross section and figure 34 shows the LS study of this powder.

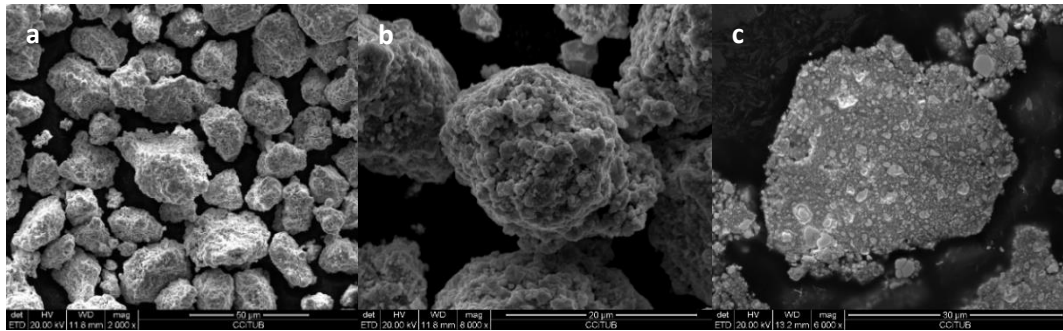


Figure 33: SEM study of Ti-WC (1500HV) (a) Free surface at 2000x (b) 8000x and (c) Cross section at 6000x

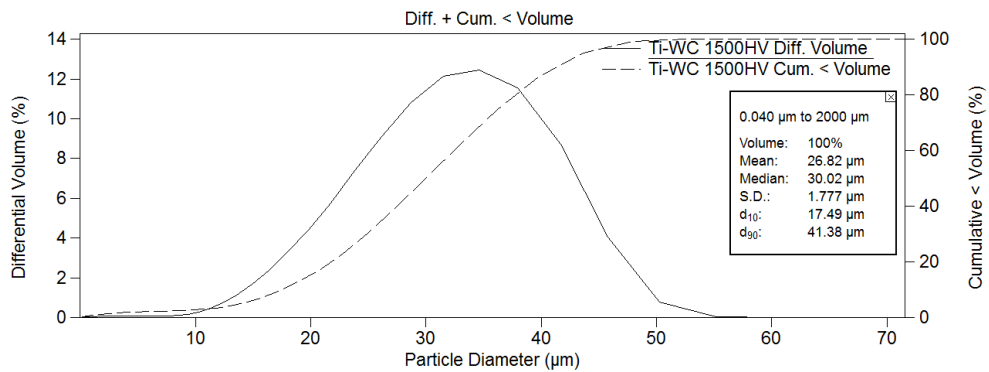


Figure 34: LS study of Ti-WC (1500HV)

### 2.3.4. Ti-WC richer in carbide phase

Ti-WC (45-55 v/v) richer in WC is another cermets provided by MBN for spraying tests by HVOF and CGS techniques and the potential hardness is near 1000HV for as-sprayed sample. Figures 35(a) and 35(b) show SEM free surface and 35(c) shows SEM cross section and figure 36 shows the LS study of this powder.

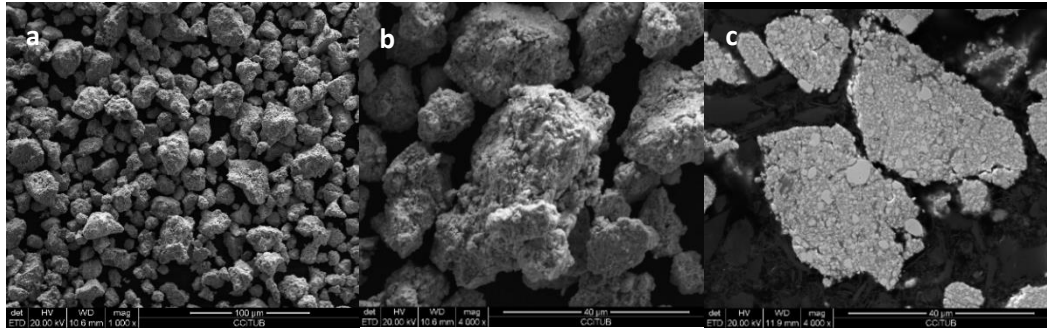


Figure 35: SEM study of Ti-WC (richer in WC) (a) Free surface at 1000x (b) 4000x and (c) Cross section at 4000x

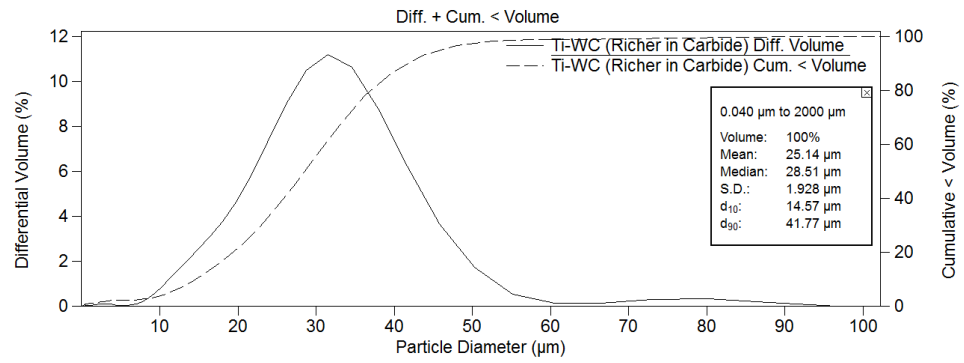


Figure 36: LS study of Ti-WC (richer in WC)

The XRD comparison of these four WC based carbides has been studied and shown at figure 37.



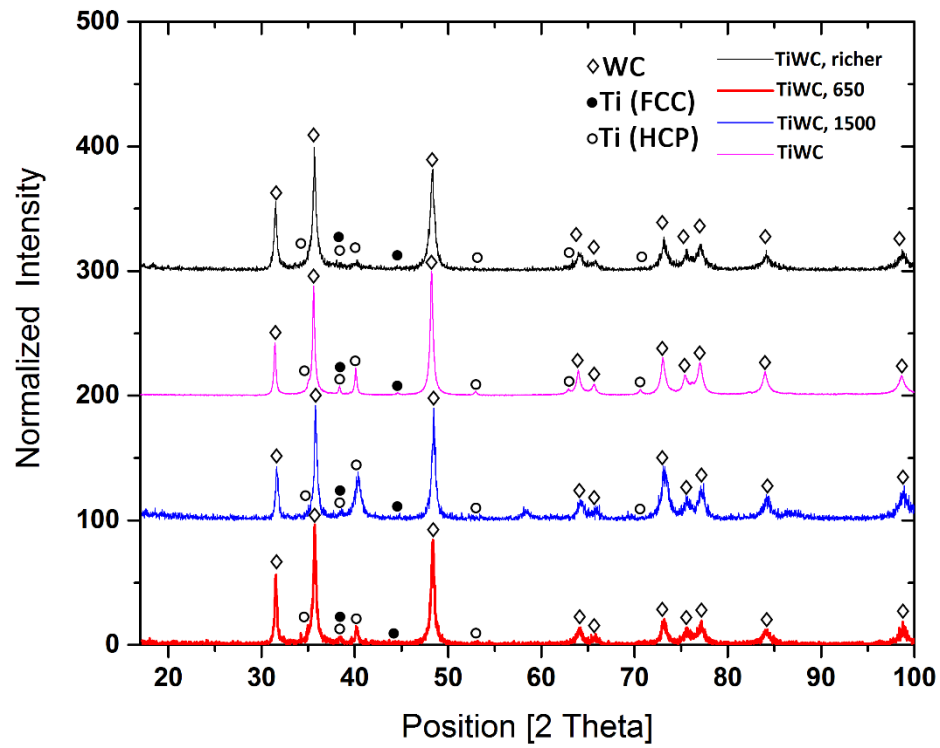


Figure 37: XRD comparison of Ti-WC (400HV), Ti-WC (650HV), Ti-WC (1500HV) and Ti-WC (richer in WC) [60]

## CHAPTER 4. RESULTS AND DISCUSSION

## 4.1. COATINGS CHARACTERIZATION & PERFORMANCE

# 1. Characterization of TiC based-green matrix coatings

## 1.1. By CGS

After characterization of each individual powder, they were sprayed onto different substrates by different techniques. The optimization of spraying parameters depends on the final application. In the case of CGS technique, previous experience of the thermal spray center (CPT) with similar nature spraying powders was considered. Ti-TiC with different amount of hard TiC phase was sprayed under pressure of 4 MPa and Temperature of 800°C, at different SOD onto the carbon steel and Al substrates.

### 1.1.1. Microstructural properties

Initial properties of obtained coatings including thickness, hardness and porosity at optimal condition (previous trials) are shown as follow:

Table 3: Microstructural properties of obtained coatings from Ti-20%TiC

Powder	Ti-20%TiC	Ti-20%TiC	Ti-20%TiC	Ti-20%TiC
Substrate	Al	Al	C St.	C St.
Distance (mm)	40	20	40	20
Thickness (um)	460±27	426±29	605±26	583±29
Hardness (HV)	429±28	406±48	408±68	401±55
Porosity (%)	3,6±0,03	3,8±0,04	3,9±0,02	6,4±0,03

Table 4: Microstructural properties of obtained coatings from Ti-50%TiC

Powder	Ti-50%TiC	Ti-50%TiC	Ti-50%TiC	Ti-50%TiC
Substrate	Al	Al	C St.	C St.
Distance (mm)	40	20	40	20
Thickness (um)	456±17	416±21	453±19	447±22
Hardness (HV)	472±32	437±50	470±55	431±70
Porosity (%)	0,36±0,02	0,38±0,03	0,37±0,01	0,42±0,01

Table 5: Microstructural properties of obtained coatings from Ti-65%TiC

Powder	Ti-65%TiC	Ti-65%TiC	Ti-65%TiC	Ti-65%TiC
Substrate	Al	Al	C St.	C St.
Distance (mm)	40	20	40	20
Thickness (um)	187±26	177±39	175±40	158±34
Hardness (HV)	366±50	306±55	455±44	421±37
Porosity (%)	0,29±0,01	0,48±0,02	0,28±0,02	0,34±0,01

As it can be observed from the above results of microstructural characterization of produced coatings for each powder, obtained coatings onto carbon steel substrates showed better hardness than Al substrates because Al substrate is softer than carbon steel and the strain hardening onto the carbon steel substrate is higher. For all the powders higher thickness was happened at SOD 40 mm which can be explained by formation of bow shock that has been also explained in first chapter [22]. At small standoff distances (20 mm), the strength of the bow shock is high and as a result deposition performance is reduced. At medium standoff distance (40 mm) the bow shock has disappeared and the gas velocity remains above the particle velocity and as a result the deposition efficiency increases and finally at large standoff distance (more than 40 mm) the gas velocity is lower than the particle velocity and the deposition efficiency started to decrease, for optimal performance the standoff distance must be set at medium region (40 mm) [22]. Even though, decreasing of bow shock can be explained because of decreasing the particle size and as a result decreasing the density. It can be also found from properties of produced coatings for all three Ti-TiC powders that by increasing the SOD from 20 to 40, hardness has been increased too which can be related to the decreasing the porosity of produced coatings by increasing the amount of carbide phase which can be observed in SEM micrographs of coatings.

Figure 38(a) to 38(c) show the SEM cross section micrograph of optimal coatings for each powder onto carbon steel substrates:

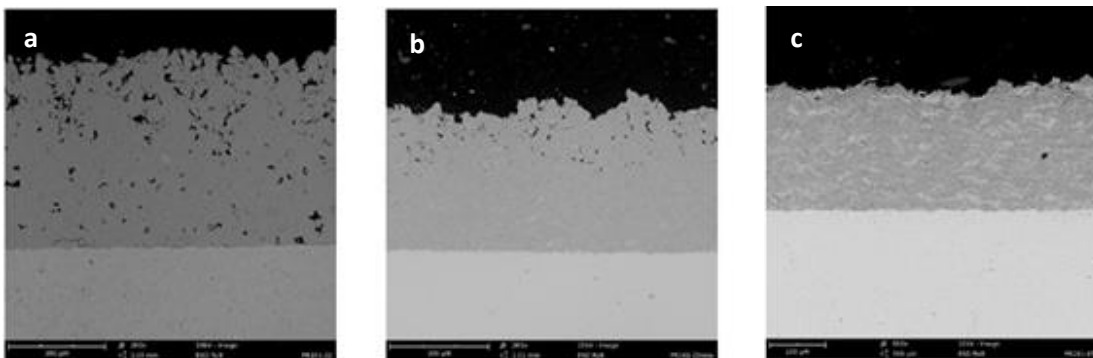



Figure 38: SEM Cross section micrograph of a) Ti-20%TiC, C St. b) Ti-50%TiC, C St. and c) Ti-65%TiC coatings onto the C St.

From the above SEM cross section micrographs of coatings can be concluded by increasing the percentage of carbide phase from 20% to 65% there has been a decrease in the porosity of coatings which can be related to the increasing of hammering effect of the new coating particles. By increasing the amount of hard carbide phase, the hammering effect of new particles increases the denseness of the coating. We expected higher value of hardness from Ti-65%TiC coating than Ti-50%TiC which it was not fulfilled with the optimum condition of previous trial, therefore Ti-65%TiC was needed to be further optimized. For this reason firstly the splat formation under different spraying condition was studied and later Ti-65%TiC was sprayed onto Carbon steel substrate considering different spraying condition and keeping the SOD constant, which is shown at below table.

Table 6: splats formation conditions

Splat Number	Gas Pressure	Gas Temperature
#1	Low	Increasing 
#2	Medium	
#3	Medium	
#4	Medium	
#5	High	

Though for spraying trials with temperature above 800°C and the pressure above 4MPa an impact cold gas spray system 5/11 with impact gun 5/11 with maximum operating temperature of 1100°C and maximum operating pressure of 5 MPa was employed. Figure bellows shows the SEM cross section and free surface micrographs of splats at different spraying conditions:

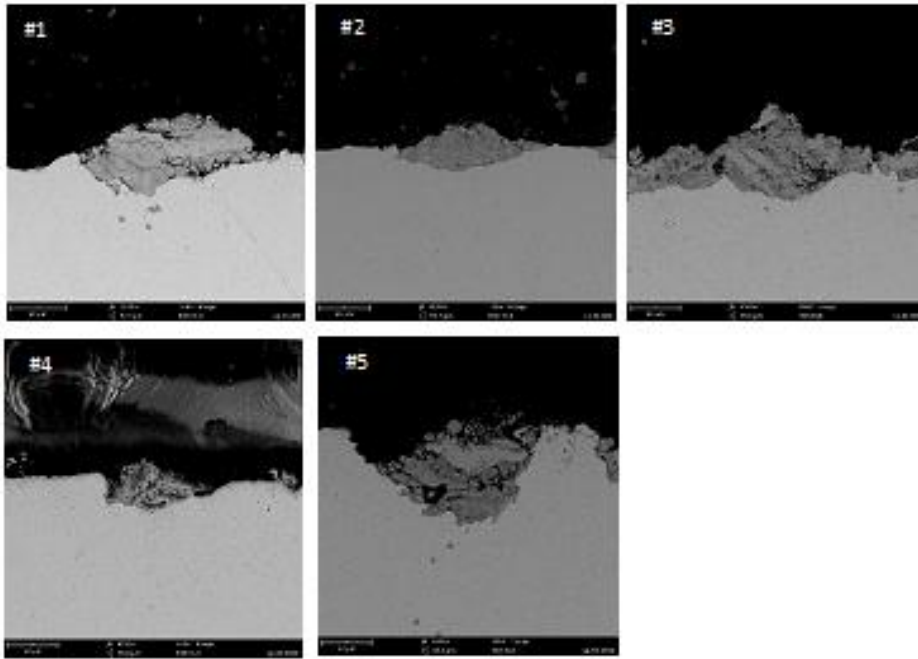


Figure 39: SEM cross section micrograph of splats at 4500x magnification

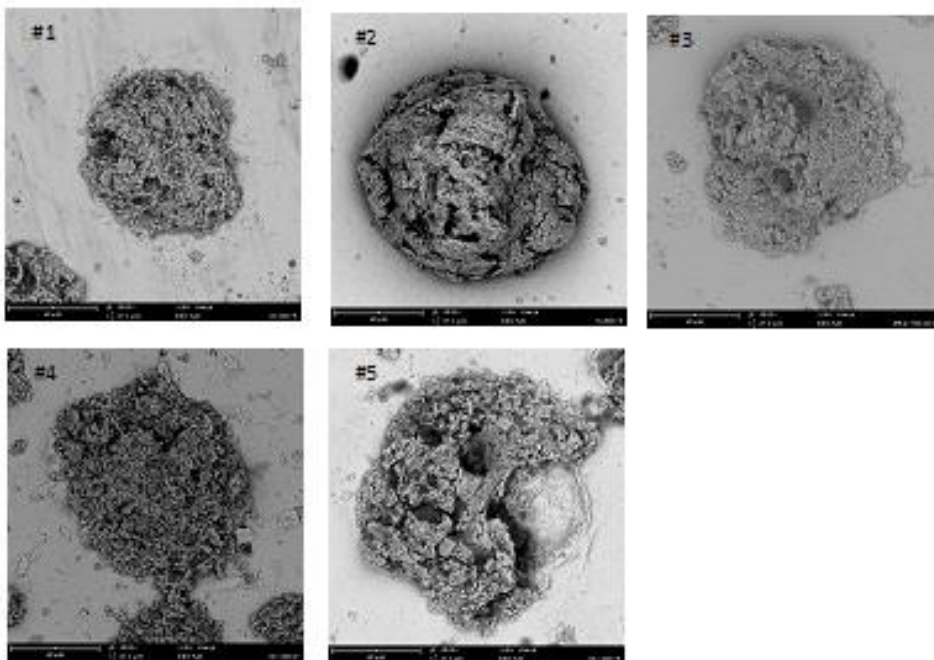


Figure 40: SEM Free Surface micrograph of splats at 4000x magnification

From the SEM cross section and free surface study of each splat which were shown in Figures and respectively can be developed that by increasing the gas pressure from #1 to #2 a significant difference in particle deposition onto the surface has been observed but there was no notable difference between the image #2 and #3 which it means that by keeping the pressure constant

and increasing the temperature, the difference might be appear in microstructural properties not in splat formation, in splats #2 and #3 the deformation of particles and the deposition efficiency were improved however by increasing the temperature to the max and increasing the pressure, visible cracks in deposited particles, weak bonding in central area of splats-substrate interface, less penetration and less plastic deformation have been observed. For better understanding the splat formation and optimizing the best condition, the average of impact velocity and temperature of particles were calculated using a computational model which is shown in below figure:

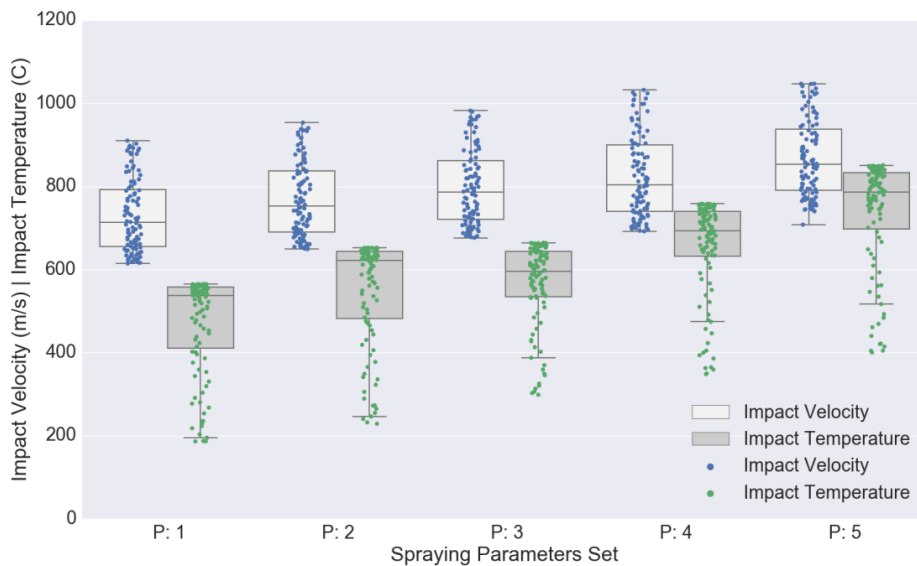


Figure 41: impact velocity and temperature vs. spraying parameters

In above boxplots the impact velocity and temperature for the particles were presented. The impact velocity and temperature of 100 particles (representing the particle size distribution of the powder material) were calculated for each spraying condition. The boxplot is a method used to visualize statistical populations without making assumptions of their actual statistical distribution; the data was grouped within quartiles indicating the degree of dispersion and skewness of the data. As it was shown in Figure above as the process temperature has been increased the particles impact velocity and temperature have been increased gradually within a 600-1100



m/s range. The effect of the process temperature was depicted in the transition from conditions #2 to #3 where the particles impact temperature was maintained within the same range but was more concentrated in the upper boxplot's quartiles. A more significant transition happened at the spraying condition #4 where the particles impact temperature was substantially increased to a 500-750°C range. At the spraying condition #5 the particles velocity of the larger particles (generally located at the lower quartile of the boxplot) was notably increased due to the higher total pressure and temperature of the process. Spraying pressure and temperature both had the direct relation with the impact velocity of particles though increasing the pressure affected the impact velocity of particles more than the temperature. As it will be shown later, the deposition has been decreased at higher gas pressures and temperatures; therefore excessive particle velocities may result erosion and avoiding a proper deposition process. After studying the splat formation, the powder was sprayed onto the carbon steel substrate at different spraying conditions. After producing the coatings the SEM cross section micrographs of coatings were obtained which are shown at figure below:

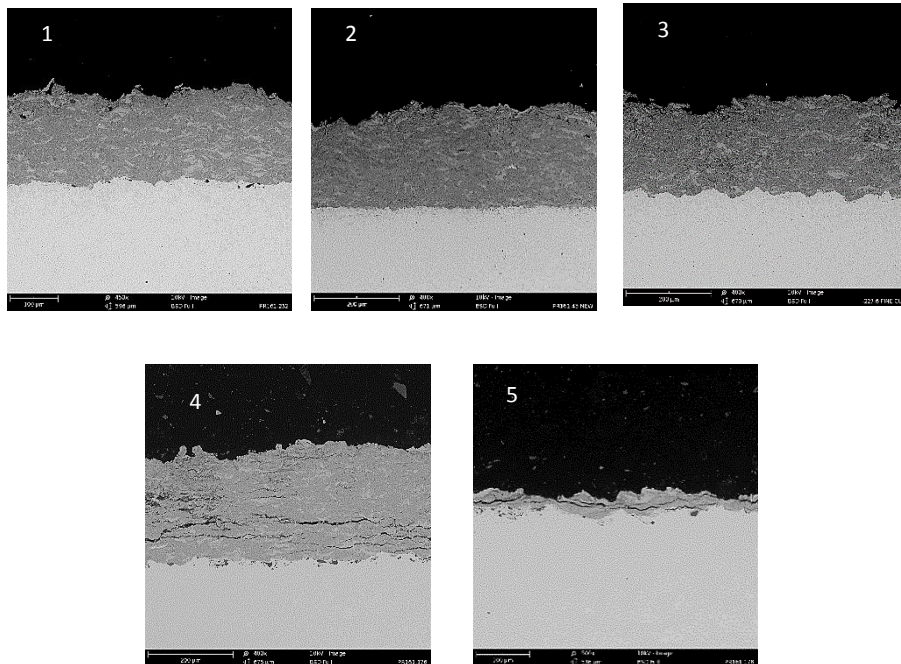


Figure 42: SEM cross section micrograph of obtained coatings from Ti-65%TiC at different spraying conditions

To evaluate the optimal coating, hardness and thickness was considered as initial properties of coatings. According to the results shown at table below, obtained coating at condition #3 was the hardest and had quite high thickness which can be related to the greater plastic deformation of particles.

Table 7: microstructural properties of obtained coatings from Ti-65%TiC under different spraying conditions by CGS

Trial #	Thickness (um)	Hardness (HV)
#1	172±17	407±93
#2	175±40	455±44
#3	192±15	546±38
#4	247±16	518±12
#5	No Deposition	No Deposition

For the optimum coating (#3) the XRD comparison of coating and initial powder has been obtained and the element mapping of coating has been taken to observe the microstructure of coating and the formed phases in coating:

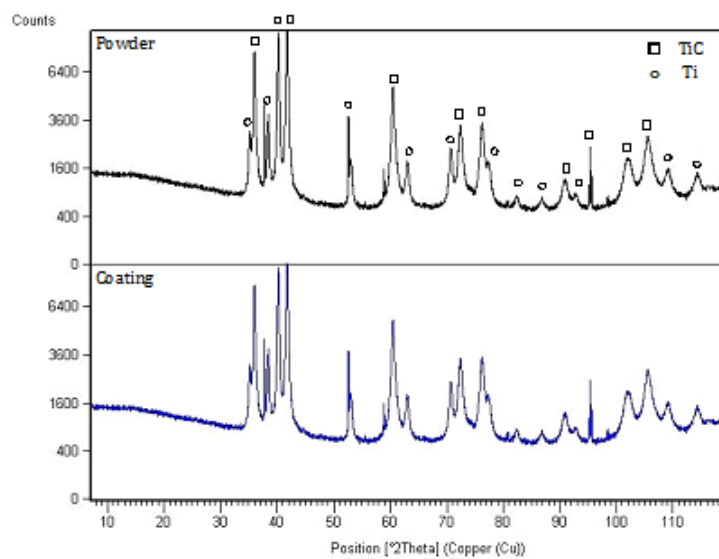


Figure 43: Phase composition comparison of initial powder and coating by XRD test.

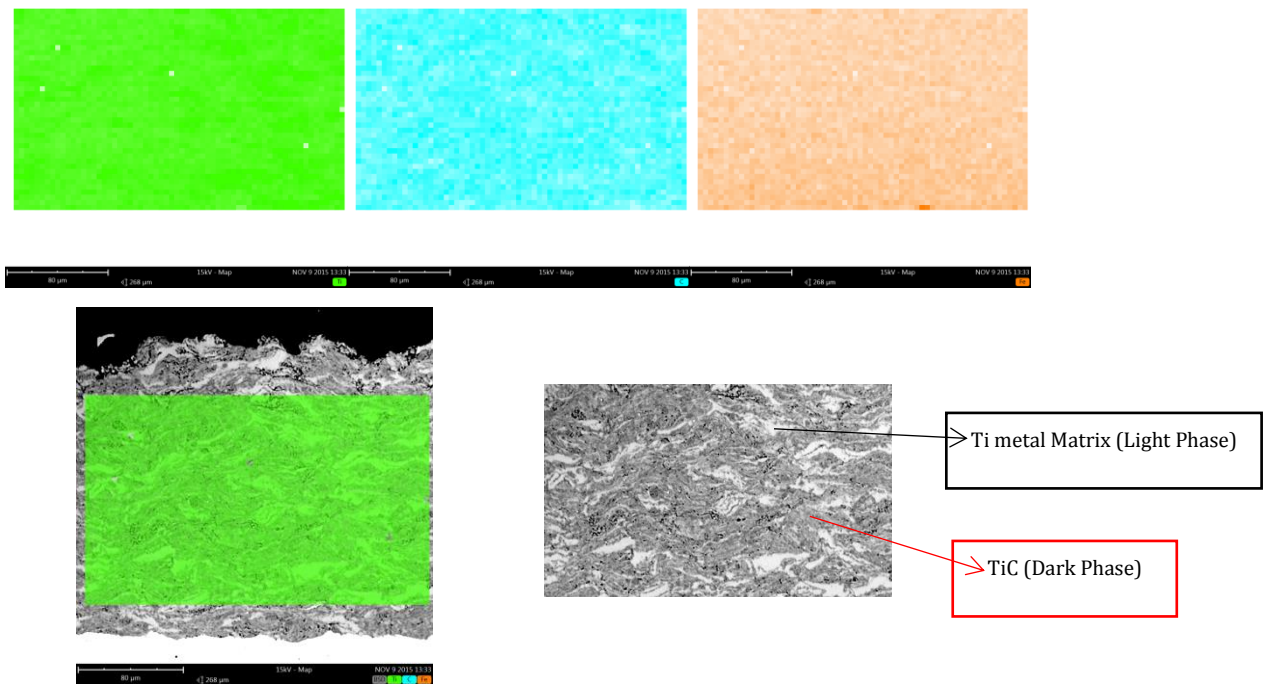


Figure 44: Elemental mapping of Ti-65%TiC coating (#3) by CGS

XRD comparison graph shows that there were no changes in phase composition of powder during the cold gas spray process and the composition of initial powder and coating were the same as it was expected from CGS process. Also as it can be seen in higher magnification SEM micrograph of coating and the result of Elemental mapping, TiC (dark phase) has been distributed in Ti matrix (light phase) homogenously and there is no trace of Oxygen or any other composition in coating.

### 1.1.2. Adhesion test

As it has been explained in chapter 2, the tensile strength of coating has been evaluated following the ASTM C-633 standard with SERVOSIS ME-402/10 equipment. For each powder 3 cylindrical samples were prepared and tensile strength test was done. The adhesion values of obtained coatings from Ti-20%TiC, Ti-50%TiC and Ti-65%TiC (#2 and #3) powders are shown at below table.

Table 8: Adhesion values of obtained coatings from different Ti-TiC powders

Powder	Ti-20%TiC	Ti-50%TiC	Ti-65%TiC (#2)	Ti-65%TiC (#3)
Adhesion value (MPa)	21±1,5	23±1,2	25±2,2	29±1,4

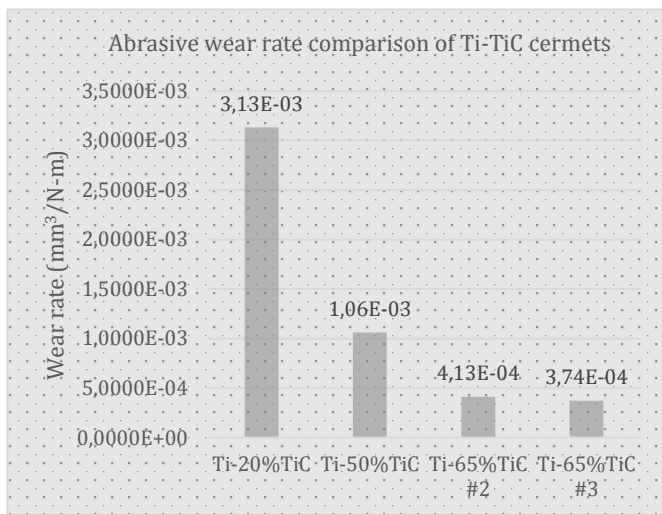
As it can be observed from the above results, tensile strength of the coatings has been increased by increasing the amount of carbide phase. When powder impact the substrate, powder with higher amount of hard phase deforms the substrate more and immerge the substrate deeper and as a result stronger mechanical bonding between the coating and substrate will be happened which consequently causes higher adhesion strength between the coating and the substrate also because of higher amount of hard carbide phase, the hammer effect increases and the porosity decreases. Also because of better microstructural properties of produced coating under condition #4 than #3, the tensile strength of coating has been slightly improved. Figure 46 shows that the failure for all the coatings has been happened between the coating's layers, therefore the rupture would be cohesive. Normally in cold spraying, a certain degree of ductility of the particles and hardness of the substrate are needed to obtain sufficient localized plastic deformation to build up a dense coating. This and the adiabatic shear instabilities resulting from high strain rate deformation upon impact are the phenomena believed to play a major role in particle/substrate bonding - influenced by spraying conditions and powder characteristics - during cold spraying. This was the main reason why Ti-65%TiC performed better under tensile tests than other TiC cermets with lower amount of ductile metal phase. [17]



Figure 45: Cohesive failure after tensile strength test

### 1.1.3. Wear test

Two different wear tests were applied; abrasive wear Rubber wheel and sliding wear Ball on disc test. As it has been mentioned in chapter 2 the abrasive wear test was evaluated according to the ASTM G65-00 standard. Below graph shows the comparison of abrasive wear rate of three powders with different amount of carbide phase. It can be observed that by increasing the percentage of TiC content, the abrasive wear properties have been improved.



Powder	Wear rate (mm³/N.m)
Ti-20%TiC	3,1E-03±7,8E-05
Ti-50%TiC	1,0E-03±4,5E-05
Ti-65%TiC (#2)	4,1E-04±1,4E-05
Ti-65%TiC (#3)	3,7E-04±6,2E-06

Figure 46: Wear rate comparison of different coatings of Ti-TiC cermet

It can be understood from the above values, by increasing the amount of carbide phase and decreasing ductile Ti binder because of higher value of hardness of obtained coating, the coating has shown the better wear resistance against the abrasive wheel. The wear rate difference between coating #2 and #3 can be also explained because of higher temperature of coating #3. By increasing the temperature the plastic deformation of Ti ductile metal increases, though at lower temperature the remained non-deformed TiC particles in the coating are higher and during the wear test, they can be detached from the coating and play the abrasive particles role and as a result increase the wear rate. Another wear test was BOD which was done under ASTM G99-03 standard which allowed the evaluation of the coefficient friction and the lost volume. Figure 48 shows the BOD samples after the test which presents the difference between three different coatings

of Ti-TiC powders. Also table 9 shows the comparison of coefficient friction of 4 different coatings and also lost volume which has been evaluated using the confocal microscope.

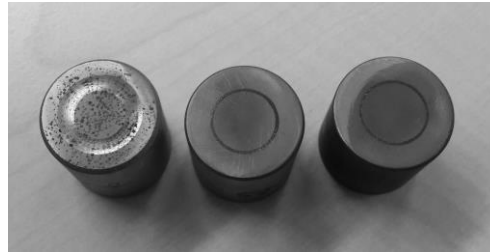


Figure 47: BOD samples after test done a) Ti-20%TiC, b) Ti-50%TiC and c) Ti-65%TiC

Table 9: Coefficient friction and lost volume comparison for different coatings

Powder	Lost Volume (mm <sup>3</sup> )	Coefficient Friction
Ti-20%TiC	21,00±3,050	0,64±0,010
Ti-50%TiC	0,06±0,003	0,48±0,015
Ti-65%TiC (#2)	0,03±0,001	0,45±0,011
Ti-65%TiC (#3)	0,024±0,002	0,36±0,010

From the BOD results can be found that by increasing the percentage of carbide phase the lost volume has been decreased and consequently the coefficient friction has been decreased. Lower lost volume of coating at higher amount of carbide phase can be related to the higher hardness of obtained coating by decreasing the ductile Ti binder. Also for obtained coating related to Ti-65%TiC (#2) there has been a decrease in lost volume and coefficient friction in compare to #3 which can be explained by greater coating in order to lower porosity and higher hardness under condition #3. Figure 48 shows the wear track in order to calculate the lost volume which is as below formula:

$$\underline{\text{Lost volume (mm}^3\text{)} = \text{Wear track's area (mm}^2\text{)} \times \text{the ball's track's perimeter (2}\pi R \text{ (mm))}}$$

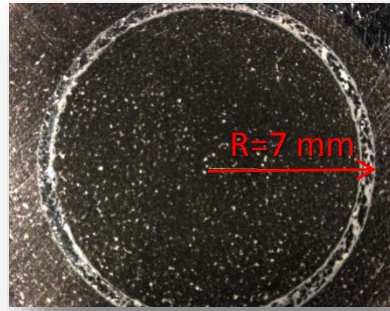


Figure 48: Wear track in BOD to calculate the lost volume

Below graph (Figure 49) shows the 3D topography comparison of two different coatings by using confocal microscope after BOD to evaluate the lost volume for Ti-20%TiC and Ti-65%TiC:

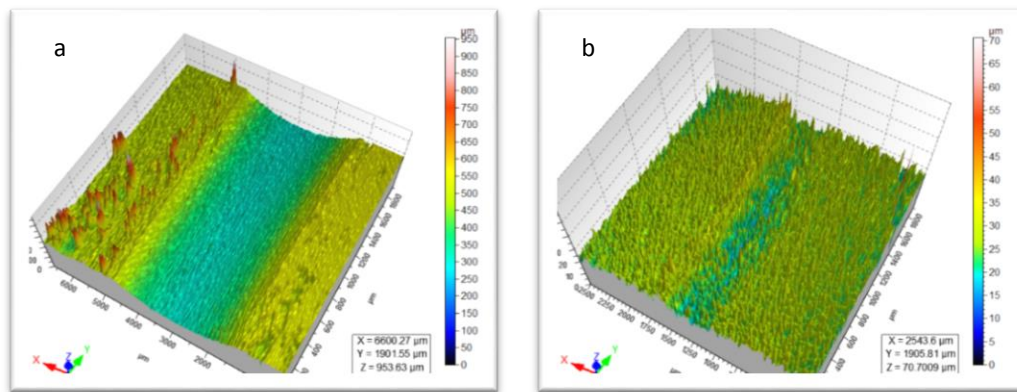


Figure 49: 3D topography comparison by confocal microscope for obtained coating from a) Ti-20%TiC and b) Ti-65%TiC

It can be observed that wear track is wider for lower amount of carbide phase and as a result the lost volume had higher value. Below image shows the SEM micrograph of wear track of Ti-65%TiC Coating at different magnifications.

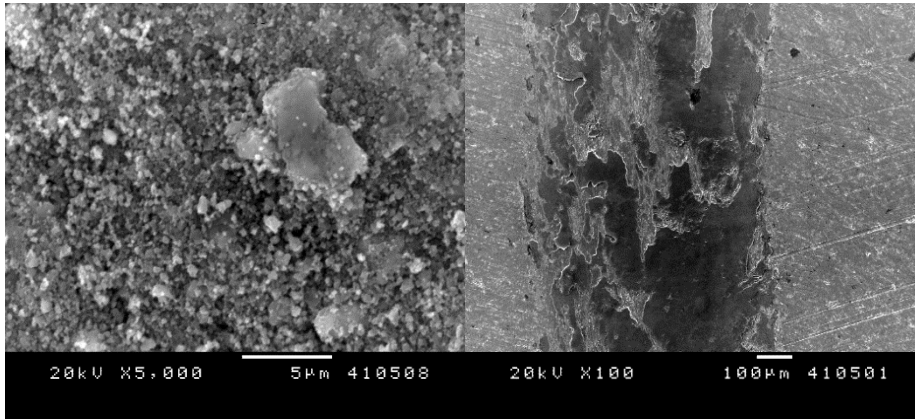


Figure 50: SEM micrograph of wear track for coating of Ti-65%TiC at different magnifications

The EDS mapping study of wear track for dark and light areas has been done to analyze the elements which are shown at below figure.

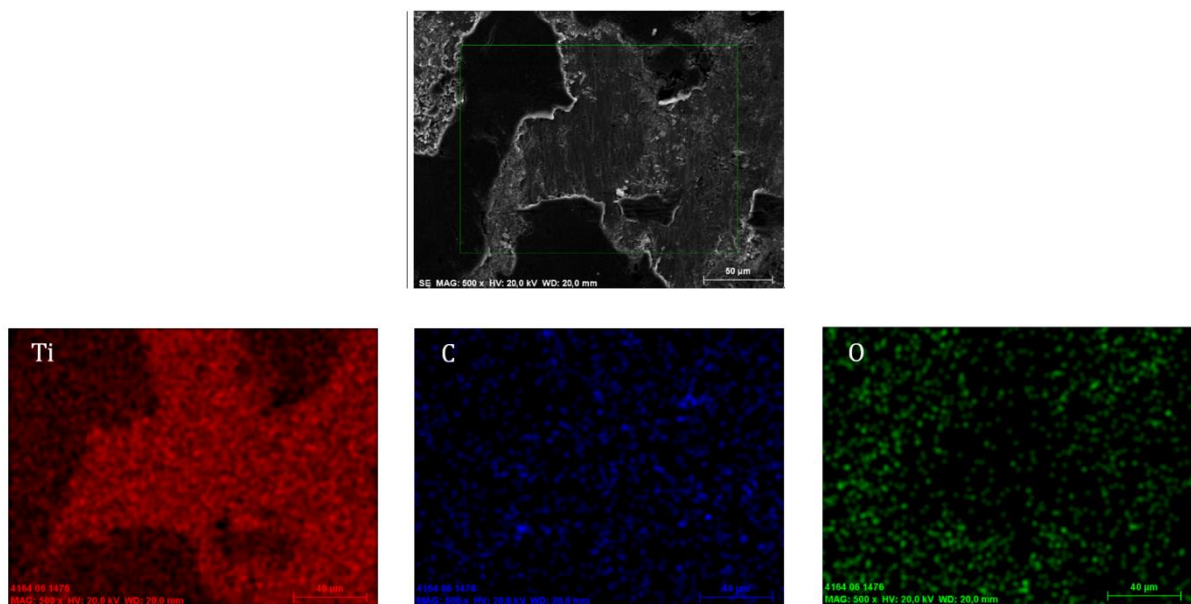


Figure 51: EDS mapping study of coating related to Ti-65%TiC after ball on disc test

EDS mapping study shows the more presence of oxygen in the dark zone than the light zone unlike more presence of Titanium in light zone than dark zone and quite uniform distribution of Carbon in both zones. This observation is attributable to the debris pulled off during the test and the high temperatures reached.



### 1.1.4. Fracture toughness

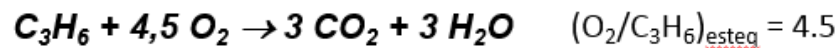
The fracture toughness of optimum coatings by both CGS and HVOF techniques was tested to measure the impact of formation of brittle phases in HVOF and increasing the ductility in CGS sprayed coatings. To study the fracture toughness as a function of material microstructure the Knob indentation technique was used (Chapter 2). For optimum coating of Ti-TiC system which was related coating to Ti-65%TiC at condition #3, the fracture toughness value of  $2,4 \pm 0,3 \text{ MPa}\cdot\sqrt{m}$  was obtained.

### 1.2. By HVOF

TiC-FeCrAlTi is another TiC-based cermet designed for spraying by HVOF technique. Before discussing the obtained results, consideration when comparing a Propylene and Hydrogen flame has been discussed as following table:

Table 10: Comparing Propylene and Hydrogen flame

#### **Considerations when comparing a propylene and hydrogen flame**



Fuel gas	Max flame T (°C)	Heat of combustion (MJ/m <sup>3</sup> )	O <sub>2</sub> /fuel ratio		
			Max flame T	Neutral flame (stoichiometry)	HVOF application
Propane	2828	93.2	4.5	5	3.0-8.0
Propylene	2896	87.6	3.7	4.5	3.5-7.0
Hydrogen	2856	10.8	0.42	0.5	0.3-0.6
Ethylene	2924	59.5	2.4	3.0	2.0-5.0
Acetylene	3160	56.4	1.5	2.5	1.3-4.0
Kerosene	2760	37.3 MJ/l	2.9	3.4	2.8-4.8

Max Temperature of H<sub>2</sub> flame happens when O<sub>2</sub>/H<sub>2</sub>=0.42 (Standard) and Max Temperature of Propylene flame happens when O<sub>2</sub>/Propylene=3.7 (Standard). Heat transfer of Hydrogen flame is bigger than Propylene flame, so powder particles will be melted easily in the H<sub>2</sub> flame. Considering that hydrogen pressure is larger than propylene pressure, it is expected that the

deposits will be less porous by using hydrogen as there will be a much effective densification. With a higher velocity, the particles impact the substrate leaving fewer voids at the inter splat boundaries. If  $O_2$ /fuel gas ( $H_2$ , Propylene) is lower than stoichiometric value therefore there is excess gas to cool down the particles and as a result particles arrive cooler. When Total gas volume increases the velocity of particles increases too.  $H_2$  flame is less oxidant than Propylene flame but Heat transfer in  $H_2$  flame is higher than Propylene therefore it may observe higher oxidation in the hydrogen flame than propylene because of larger melting. When Flame temperature increases, Velocity of particles decreases, Porosity decreases and as a result Crack decreases. When Air increases, Velocity of particles increases and as a result Porosity increases. Small particles accelerate initially fast and decelerate fast too and their cooling rates are higher. Also due to their higher surface/volume ratio they will be more easily oxidized than the larger ones. After characterization of powder, it was sprayed onto the Carbon steel substrates by HVOF technique using both Hydrogen and Propylene as fuel gases. The spraying parameters were considered according to the optimal condition for WC-Co. For this powder three samples with three different standoff distances (220, 225 and 250) were done. At first trial this powder was sprayed onto the steel substrate by using  $H_2$  and considering the standard condition of cermets where the ratio of  $O_2/H_2$  was 0.44 (less than the stoichiometric value). The second trial was done by using propylene as fuel gas and considering the standard condition of cermets which the ratio of fuel gases  $O_2/Propylene=4.08$  (less than the stoichiometric value).

### 1.2.1. Microstructural properties

After obtaining thick and dense coatings, the samples went through the microstructural characterization to select the optimal coating in terms of hardness value. Figure 51 (a) and (b) show the SEM cross section micrograph of optimal coating at SOD 225 mm (optimum) by using Hydrogen and Propylene as fuel gases respectively:

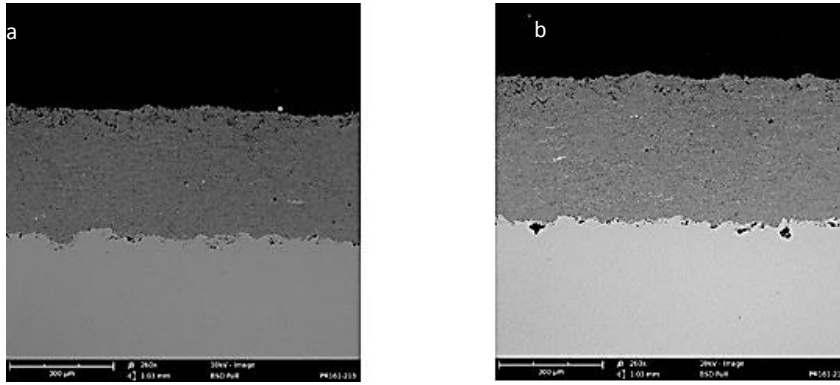


Figure 52: SEM cross section micrograph of optimal coating related to TiC-FeCrAlTi at SOD 225 mm using (a) H<sub>2</sub> (b) Propylene as fuel gases

The microstructural characterization of optimal coating has been shown in table 11.

Table 11: Microstructural properties of coatings from TiC-FeCrAlTi by HVOF

Powder	TiC-FeCrAlTi	TiC-FeCrAlTi
Substrate	C St.	C St.
Fuel gas	Hydrogen	Propylene
Distance (mm)	225	225
Hardness (HV)	954±54	962±95
Thickness (μm)	353±11	359±6
Porosity (%)	<0,2	<0,1

From the microstructural characterization of obtained coatings can be understood that there is no significant difference in microstructural properties of produced coatings by using both fuel gases, although a slightly lower hardness and higher porosity of coating related to TiC-FeCrAlTi by Hydrogen than Propylene can be explained because of higher temperature of Hydrogen flame, more decarburization and more formation of oxide phases. For better understanding the phase composition of coating, the XRD analysis on coating was done which has been shown as follow. Also for observing the distribution of the elements in coating, the elemental mapping of coating at higher magnification has been taken. From the below results can be found that TiC in the TiC-FeCrAlTi coating was partially converted into TiO<sub>2</sub>. It was also observed that Fe reacted with Cr and Al and formed Fe-Cr and Fe-Al solid solutions. A partial oxidation of matrix material (FeO) was observed as

well. This powder has been synthesized by mechanical alloying (HEBM) and existence of heterogeneous mixture of alloying elements in the powder particles is a possibility. The dark contrast spherical-like regions are titanium carbide, whereas, the surrounding brighter region is the Fe-Cr matrix.

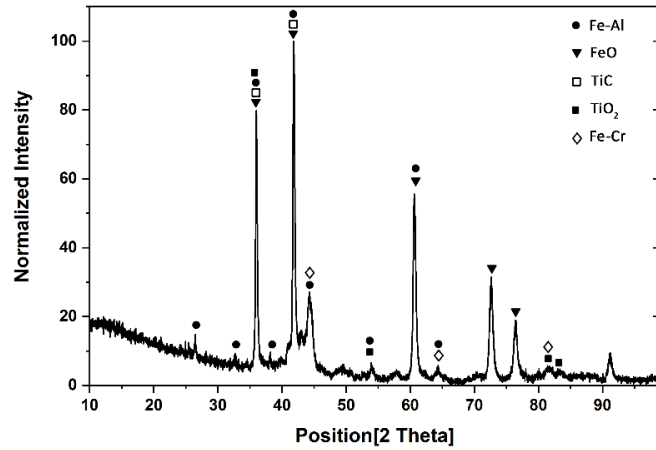


Figure 53: XRD study of TiC-FeCrAlTi coating by HVOF

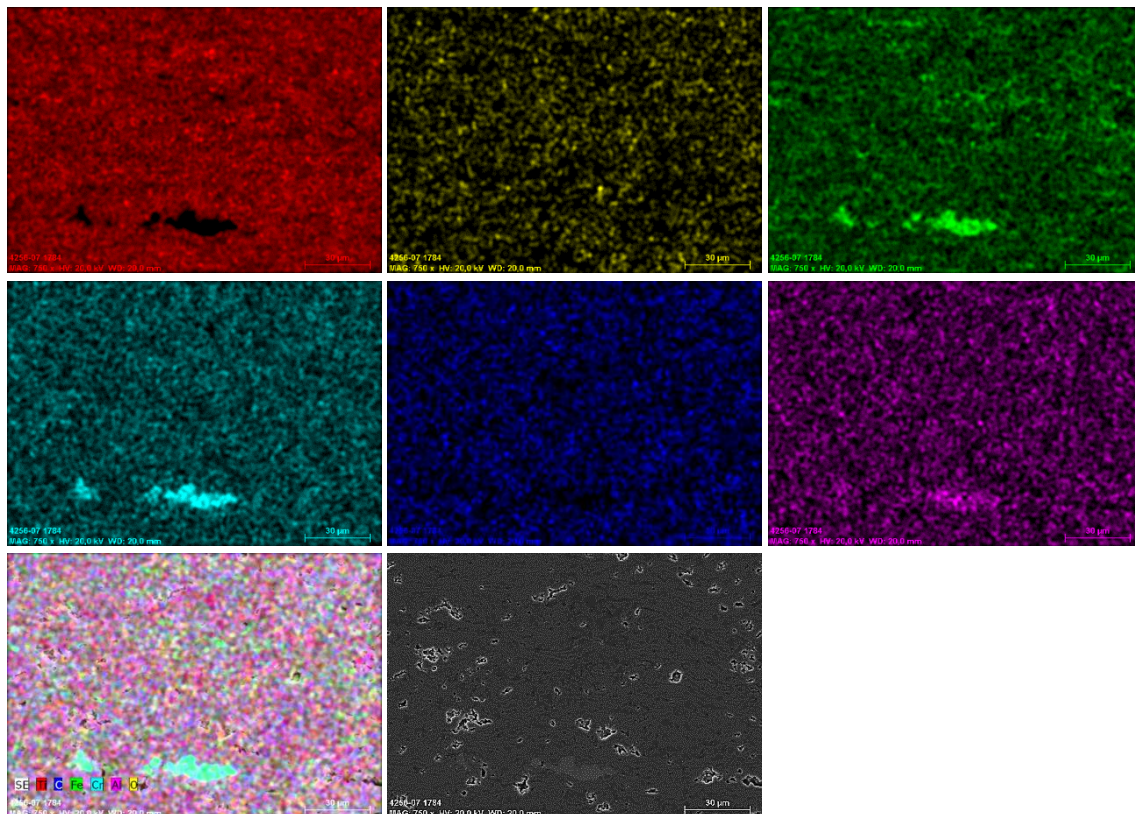


Figure 54: Elemental mapping of TiC-FeCrAlTi coating by HVOF and using Propylene as fuel gas

### 1.2.2. Adhesion test

For the optimal coating obtained from TiC-FeCrAlTi, by HVOF and using Hydrogen and Propylene, three cylindrical samples were prepared and adhesion strength test were applied.

Table 12: Tensile strength of obtained coatings from TiC-FeCrAlTi by HVOF and using Hydrogen and Propylene as fuel gases

Powder (TiC-FeCrAlTi)	Hydrogen	Propylene
Adhesion value (MPa)	70±6	72±4

As it can be observed in above table, tensile strength of TiC-FeCrAlTi coating by using Propylene and Hydrogen was quite the same though the slight difference can be related to the formation of more fragile oxide phases at coating layers and also higher porosity of coating by using Hydrogen as the fuel gas. For this coating the failure happened in the glue.

### 1.2.3. Fracture toughness

For optimum coating of TiC-FeCrAlTi system the fracture toughness value of  $4,1 \pm 0,5 \text{ MPa} \cdot \sqrt{m}$  was obtained. The higher resistance to the abrasive wear of this coating can be also related to its high value of fracture toughness.

### 1.2.4. Wear test

The optimal coating produced from TiC-FeCrAlTi was selected for further test. Three BOD cylindrical samples were sprayed according to the optimal condition by using propylene as fuel gas and the coefficient friction and the lost volume were studied. Rubber wheel test was also done to evaluate the wear rate of coating and further comparison of optimum coating of each system. Table 13 shows the coefficient friction, the lost volume and the wear rate.

Table 13: Lost volume, coefficient friction and wear rate of obtained coating from TiC-FeCrAlTi by HVOF and using Propylene as fuel gas

Powder, technique, gas	Lost volume (mm <sup>3</sup> )	Coefficient friction	Wear rate (mm <sup>3</sup> /N.m)
TiC-FeCrAlTi, HVOF, Propylene	3,0E-03±4,0E-4	0,37±0,04	2,6E-04±1,4E-05

## 2. Characterization of SiC based-green matrix coatings

### 2.1. By CGS

After characterization of Ti-SiC powder, it was sprayed by both HVOF and CGS techniques. First Ti-SiC was sprayed onto C St. substrate by CGS technique using Nitrogen as fuel gas at two different SOD 20 and 40 and considering the optimum condition of previous trial for WC-Co cermet by CGS and after characterization of obtained coatings the optimal SOD was selected.

#### 2.1.1. Microstructural properties

After producing dense and thick coatings related to Ti-SiC, the samples went through the microstructural characterization in order to obtain the optimum coating for further tests. The optimum coating was obtained at SOD 40 mm. Table 14 shows the Initial characterization of obtained coatings from Ti-SiC.

Table 14: Microstructural characterization of obtained coatings from Ti-SiC by CGS method

Powder	Ti-SiC	Ti-SiC
Substrate	C St.	C St.
Gas	N <sub>2</sub>	N <sub>2</sub>
Distance (mm)	20	40
Hardness (HV)	454±44	477±25
Thickness (um)	186±18	195±8
Porosity (%)	0,43±0,01	0,41±0,02

From the above table can be found that obtained Coating from Ti-SiC powder onto C St. at SOD 40 showed slightly higher hardness and thickness than SOD 20 which the reason has been explained in previous system (Ti-TiC system). Figure 52 also shows the SEM cross section micrograph and XRD phase composition of produced coatings at SOD 40 mm for Ti-SiC powder.

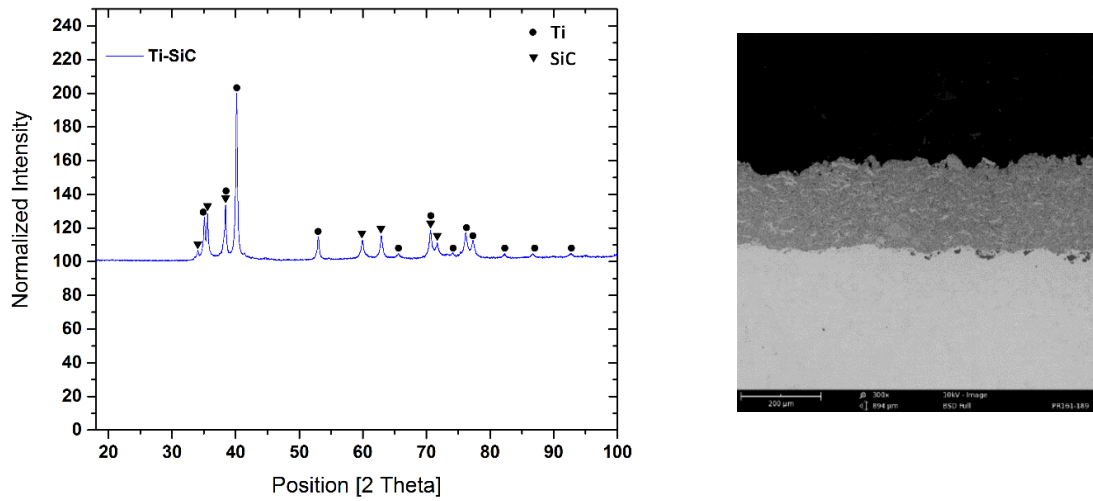


Figure 55: XRD and SEM cross section micrograph of Ti-SiC coatings onto C St.by CGS  
 For this coating the elemental mapping at high magnification was taken which has been shown as follow:

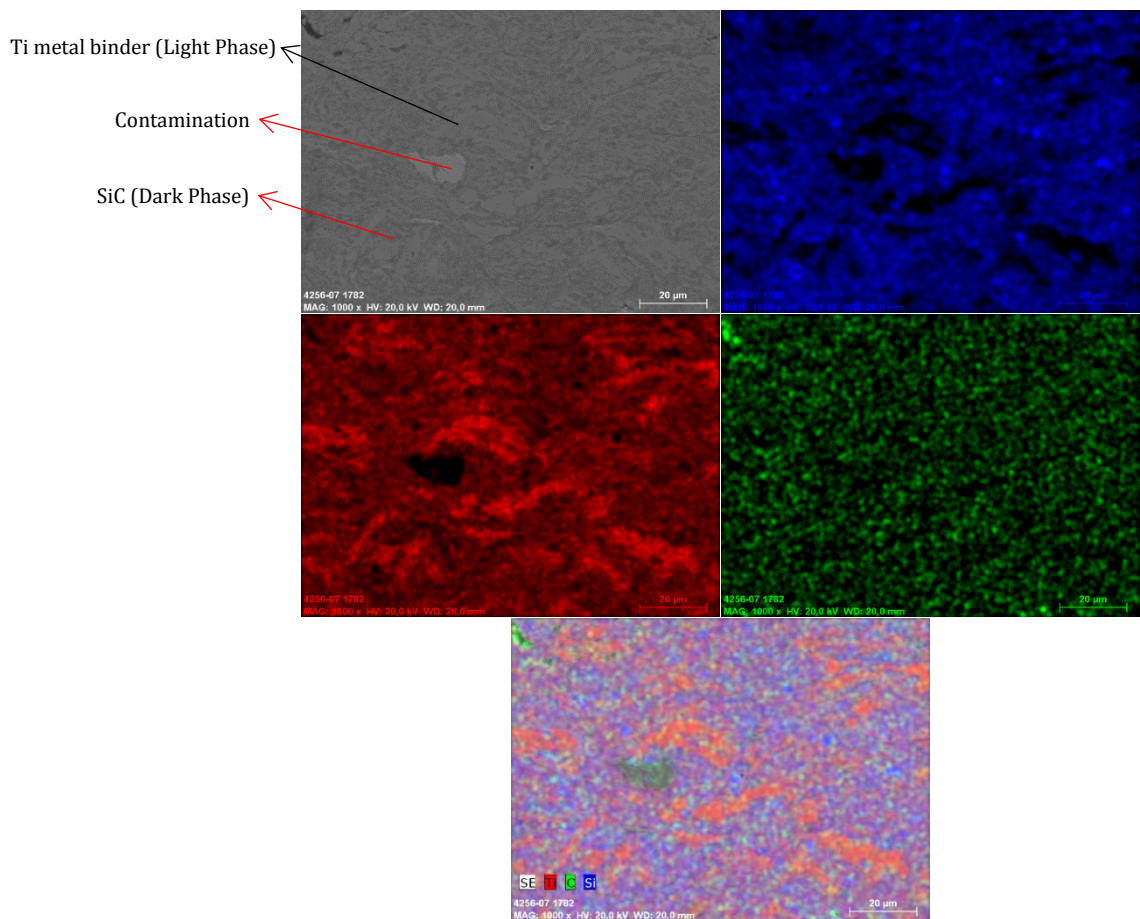


Figure 56: Elemental mapping of Ti-SiC coating by CGS

As it was expected the phase composition of coating and initial powder was remained the same and there was no phase decomposition in produced

coating. Also it can be observed that SiC has been homogeneously distributed among the Ti binder and a dense coating with low porosity has been produced. In order to improve the microstructural properties of obtained coating related to Ti-SiC by CGS, Later the powder was sprayed onto Carbon steel substrate with micro layer of Ti bond coat in order to improve the adhesion strength of coating and substrate and after obtaining the coating, it went through the post heat treatment. Generally, heat treatment of thermal sprayed deposits can release residual stress, decrease the porosity and improve the microstructure and properties of the deposits [61-63]. The microstructure of the cold sprayed Ti-SiC was also significantly changed after annealing at temperature of 750°C. The interfaces between the deposited powder particles tended to disappear and a stronger metallurgical bond was formed. When the annealing temperature was 750°C, the interfaces were almost completely healed. Annealing led to the recrystallization of the deformed grains and remarkable grain growth accompanied by the disappearance of particle interfaces [61–63]. Thus, the bonding of the particles was significantly increased owing to the formation of metallurgical bonding through solid-state diffusion [64]. Below table shows the microstructural properties of coating before and after HT. After characterization of obtained coating after post HT, the hardness of coating was increased from 500 HV to 800 HV.

Table 15: microstructural properties of Ti-SiC coating by CGS before and after Heat treatment

HT*	Powder	Substrate	Hardness	Thickness
Before	Ti-SiC	C Steel+Ti bond coat	508±73 HV	236±28
After	Ti-SiC	C Steel+Ti bond coat	817±82 HV	236±28

\*(HT Temperature: 750°C, HT Isotherm: 60 mins, Ramp: 5 (°C/min), Atmosphere: Vacuum)

Below figure shows the SEM cross section micrograph of produced coating onto Carbon steel substrate with thin layer of Ti bond coat.



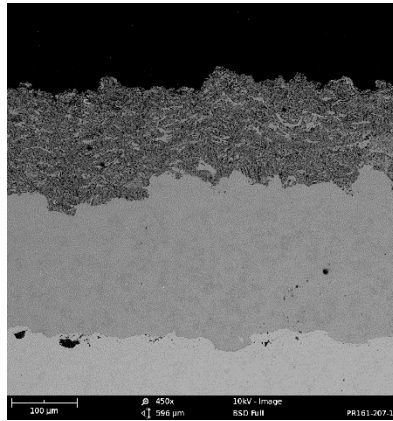


Figure 57: SEM cross section of obtained coating related to Ti-SiC onto C steel + Ti bond coat by CGS.

As it can be observed after post heat treatment the hardness of coating has been increased. In order to explain the increasing of hardness the XRD study of coating was obtained and phase composition was evaluated which has been shown at below figure.

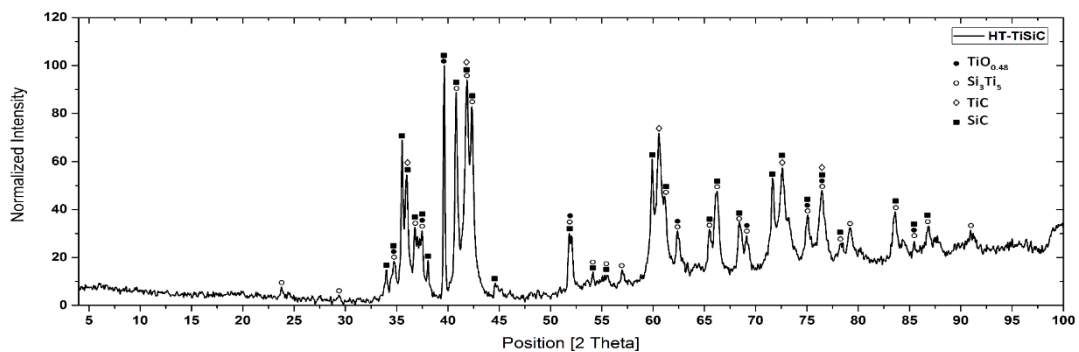


Figure 58: XRD study of obtained coating related to Ti-SiC by CGS after HT

Also for better understanding the formed composition during the annealing process SEM micrograph of coating before and after HT at higher magnification was taken and the Elemental mapping of coating before and after HT was done.

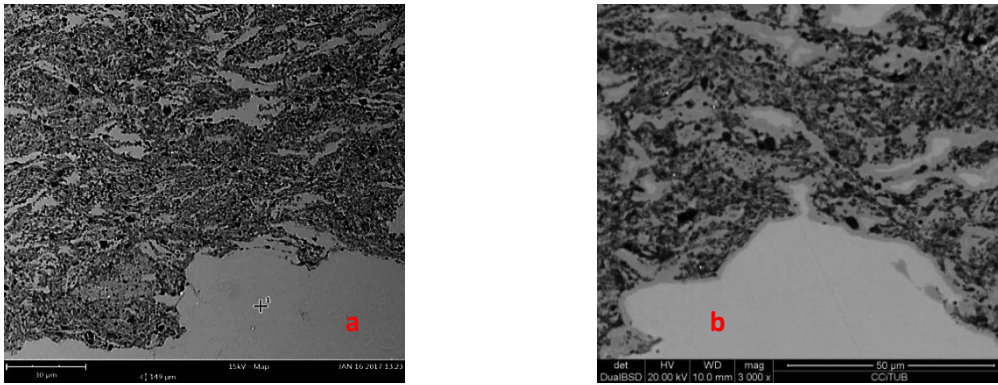


Figure 59: SEM cross section micrograph of obtained coating related to Ti-SiC onto C steel + Ti bond coat by CGS a) Before HT b) After HT

As it can be observed at above images after post HT, a continuous layer has been formed at the interface of coating and Ti bond coat which the EDS analysis has been detected it as an intermetallic alloy of Ti and Si. Before HT there was only two detected phases in the coating, Ti (Light phase) and SiC (Dark phase) but after annealing treatment because of decomposition of SiC, formation of intermetallic alloys, phase dissolution and precipitation of new carbides and formation of oxide phases, different phases have been detected. Below image shows the elemental detection of formed phases in coating after HT by EDS:

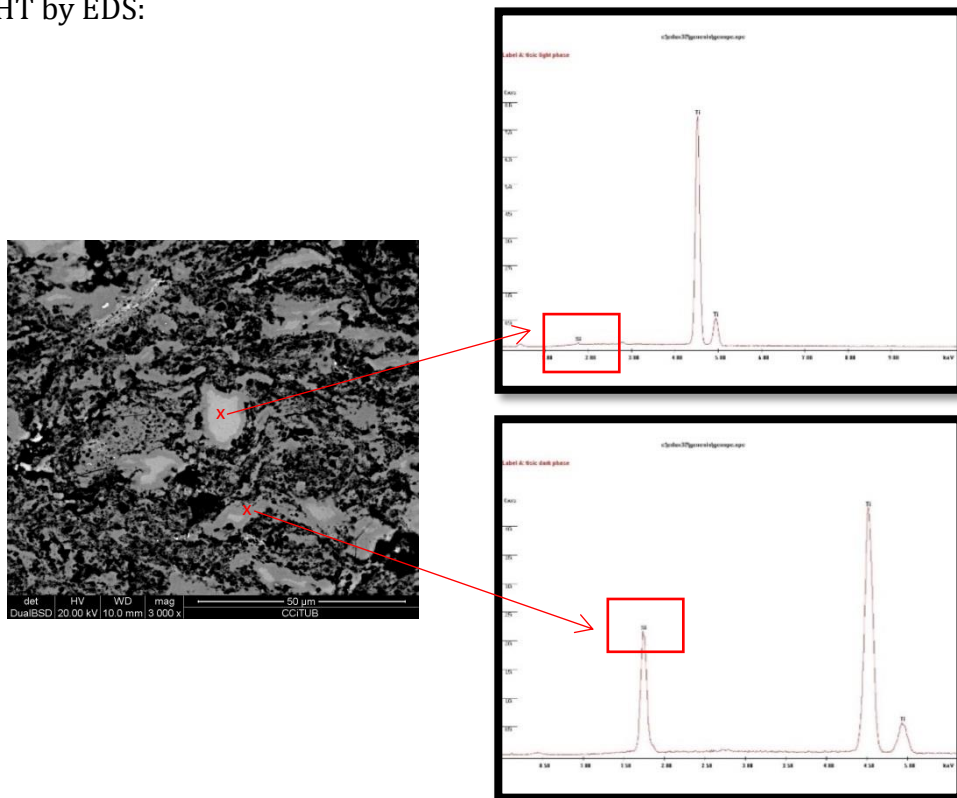


Figure 60: EDS study of Ti-SiC coating by CGS after HT

From the above EDS result could be found that light phase has less amount of Si than dark phase, though both phases are composed of Ti and Si. Also Elemental mapping of coating after HT has been done and shown in below image:

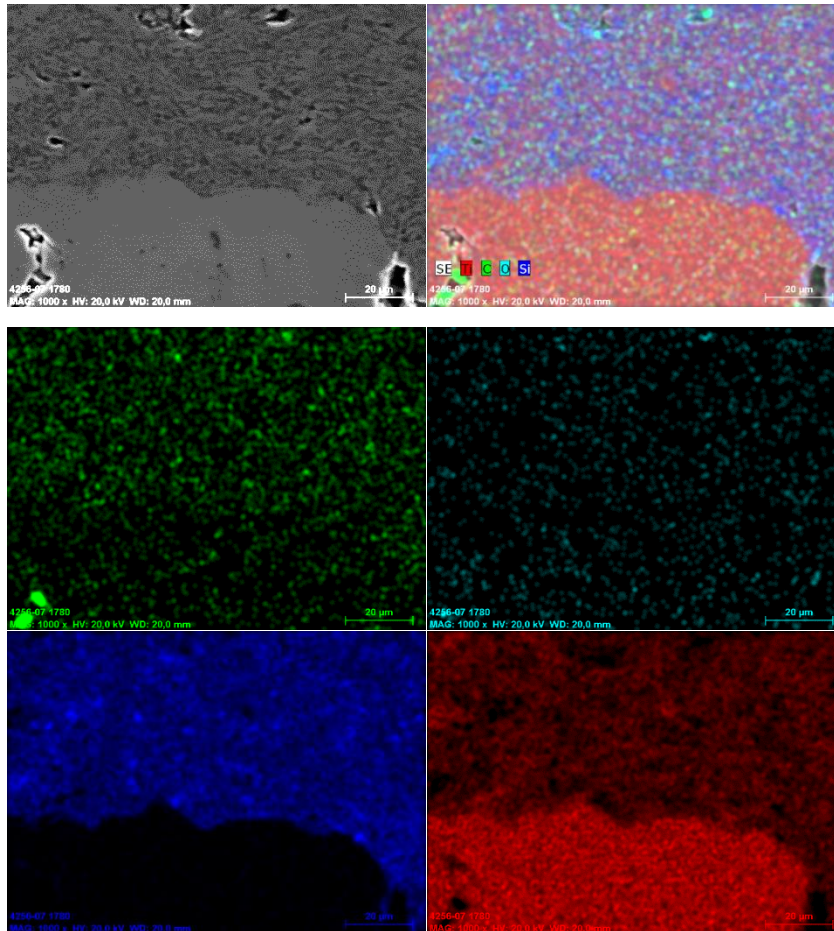


Figure 61: Elemental Mapping of Ti-SiC coating by CGS after HT

As it has been explained at previous paragraphs, sample annealing leads to the formation of intermetallic phases ( $\text{Si}_3\text{Ti}_5$ ) and produces more homogeneous coating structure which can promote less porosity and higher mechanical properties. From the mapping comparison of coating before and after HT (below image) can be perfectly observed the dissolution of SiC phase in Ti matrix and precipitation of TiC in coating and homogenous distribution of formed phases and also less porosity in coating. The higher hardness after post HT is also because of hardening effect of Titanium carbide which has more hardness than Ti metal. Post annealing generally has an effect in

reducing residual stresses caused by the difference in the thermal expansion coefficients between coatings and substrate. In addition, it often promotes the interfacial adhesion due to the inter-diffusion of elements in the coatings and substrate. Annealing dissolves the carbide phases back to the matrix and re-precipitate new carbides again. Despite the higher hardness of coating related to Ti-SiC powder by CGS after the post HT, it didn't meet the expected hardness, and therefore another trial by HVOF in order to improve the microstructural properties of coating was performed.

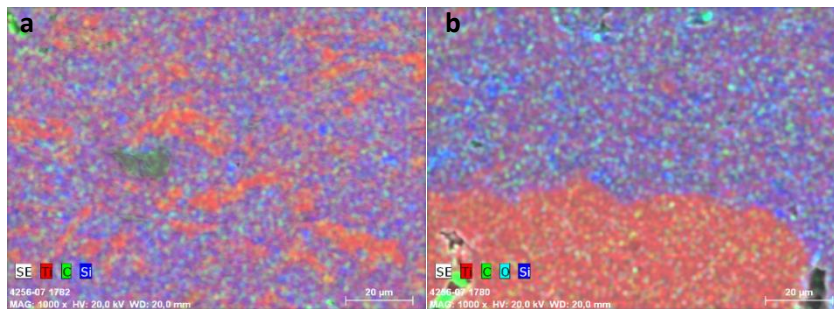


Figure 62: Elemental Mapping comparison of Ti-SiC coating by CGS a) before and b) after HT

## 2.2. By HVOF

For first trial, Ti-SiC was sprayed by HVOF technique and using Hydrogen as the fuel gas. The standard parameters of the cermets carbides were implemented for this trial and the powder was sprayed onto the carbon steel substrates at 3 different distances 200, 225 and 250. With the standard condition considering the ratio of  $O_2/H_2=0,44$  and the spraying temperature less than the max flame. Ti-SiC was also sprayed by HVOF and using propylene as fuel gas in order to observe the difference in properties of obtained coatings by different fuel gases. This trial was done with changing the fuel gas to Propylene considering the standard spraying parameters for carbides. The powder was sprayed onto the Carbon steel substrate and the dense and homogenous coatings with satisfying properties were obtained.

### 2.2.1. Microstructural properties

After characterization of obtained coatings with using different fuel gases, the initial properties of coatings were evaluated which at below table the optimums which were at SOD 225 mm were shown.

Table 16: microstructural properties of optimum produced coatings from Ti-SiC by HVOF and using H<sub>2</sub> and Propylene as fuel gases at SOD 225 mm

Powder	Ti-SiC	Ti-SiC
Substrate	C St.	C St.
Fuel gas	Hydrogen	Propylene
Distance (mm)	225	225
Hardness (HV)	681±58	978±60
Thickness (um)	305±10	302±14
Porosity (%)	0,22	0,12

Below figures show SEM cross section micrograph of obtained coatings from Ti-SiC with different fuel gases.

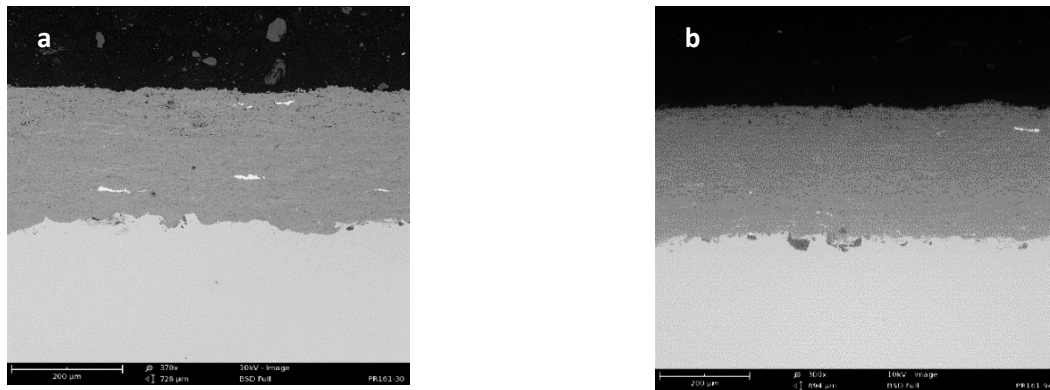


Figure 63: SEM cross section micrograph of optimum produced coatings of Ti-SiC by HVOF onto C St. by using a) H<sub>2</sub> b) Propylene

XRD study of obtained coating related to Ti-SiC by HVOF and using H<sub>2</sub> and Propylene as fuel gases have been done and the results have been shown as below graphs:

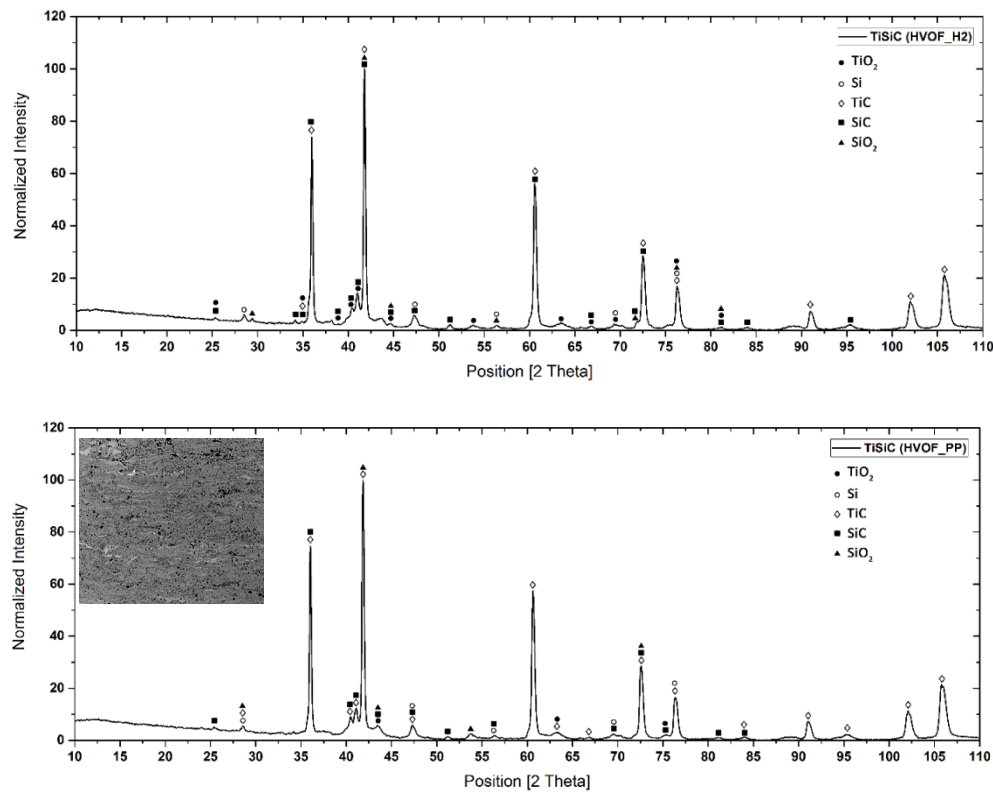


Figure 64: XRD phase composition of obtained coating related to Ti-SiC powder by HVOF and using a) H<sub>2</sub> b) Propylene as fuel gas

Lamellar structure coating related to Ti-SiC by HVOF and using Propylene has significantly higher hardness (1000 HV) than the one produced by using H<sub>2</sub> as fuel gas. As it has been mentioned in previous paragraphs, Hydrogen flame has the higher temperature and the probability of SiC decomposition is higher and more SiC phase (hard phase) is decomposed and the amount of hard SiC phase in coating becomes less and as a result the hardness is decreased. From the XRD study of produced coatings related to Ti-SiC using both H<sub>2</sub> and Propylene could be understood that in both coatings SiO<sub>2</sub> phase was formed but the more peaks related to SiO<sub>2</sub> phase was detected in coating by H<sub>2</sub> than Propylene. SiO<sub>2</sub> has less hardness than SiC and is more brittle therefore more amount of SiO<sub>2</sub> than SiC in formed coating by H<sub>2</sub> caused the lower hardness value. Also SEM study of obtained coatings by H<sub>2</sub> showed more porosity than the one from Propylene therefore showed less hardness value. Also HVOF coating of Ti-SiC presented higher hardness value than CGS mainly because of decomposition of Ti-SiC powder during the process and therefore hardening effect of SiO<sub>2</sub> phase. Besides the higher hardness, HVOF

coating was more brittle (less fracture toughness value which will be explained further) than CGS coating due to the lower content in elemental ductile Ti matrix and the presence of fragile and hard SiO<sub>2</sub> phase formed during the HVOF spraying process. Also to determine the chemical composition and prove the existence of oxygen element in produced coating of Ti-SiC by HVOF and using Propylene as the fuel gas, an electro microprobe analysis was done which has been shown as follow:

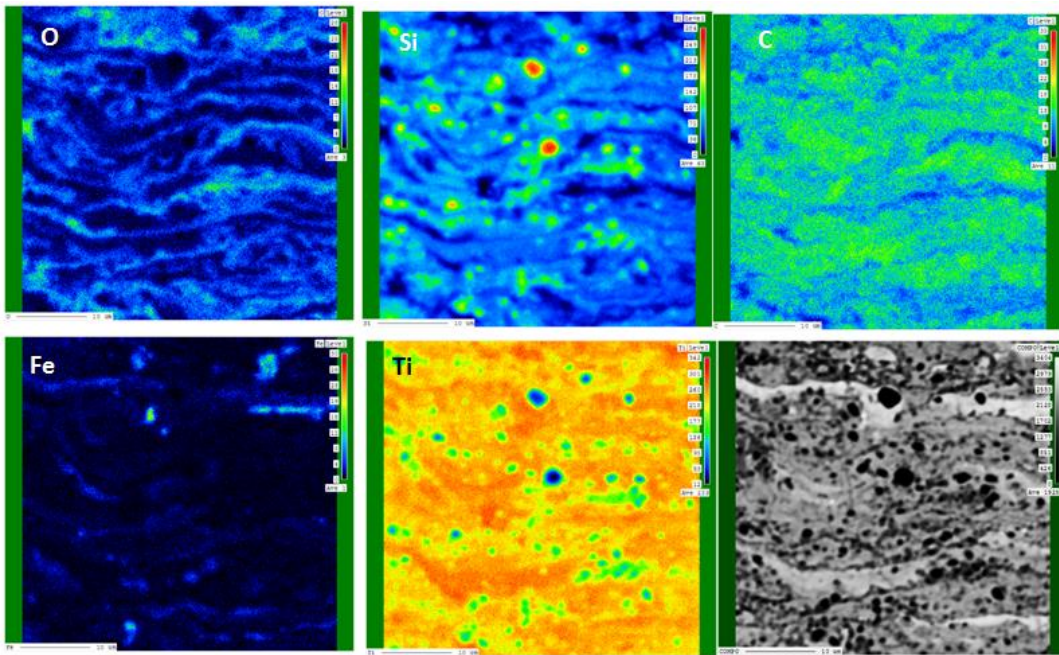


Figure 65: Electron microprobe analysis result for Ti-SiC coating by HVOF and using Propylene

From the above result can be understood that the achieved temperature during this process caused a depletion of the ductile Ti matrix thus forming a more brittle coating as well as bands of dissolution of the SiC into the Ti matrix. There is a hardening of the matrix due to dissolution which is resulting in fewer free carbides in the final coating henceforth a decrease in some mechanical properties such as fracture toughness, as a direct consequence of the formation of hard phases has been observed. Below images show the lamellar grain structure of coating by HVOF against produced coating by CGS.

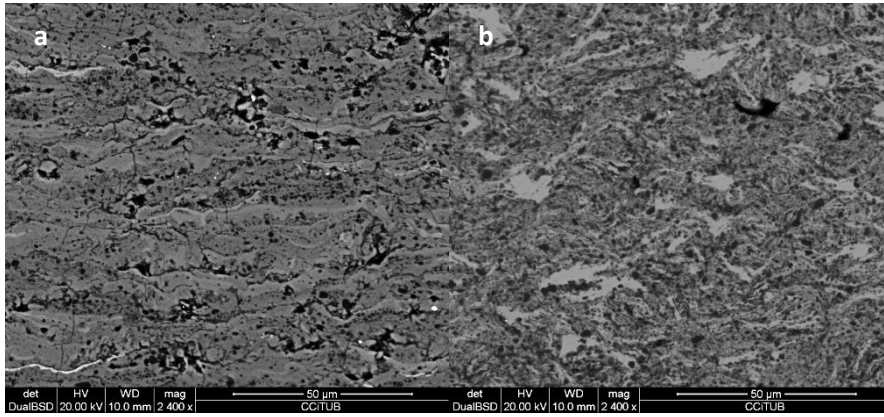


Figure 66: Microstructural comparison of Ti-SiC coating by a) HVOF b) CGS

HVOF coating shows dissolution of Ti matrix originated during the spraying process while the CGS coating shows an intact microstructure. The dark gray area can be seen spread out throughout (Figure 66a) the bands of dissolution of the SiC into the Ti matrix. This means there are few free carbides in the final coating resulting in a decrease in some mechanical properties, for example, fracture toughness which has been explained in further paragraphs, as a direct consequence of the formation of brittle hard SiO<sub>2</sub> phase. Initially in HVOF process, a partial dissolution of SiC grains in the liquid Ti matrix happens and this decomposition leads to a hardened matrix holding the submicronic partially dissolved SiC particles in place surrounded by TiC. This sub-carbide formation is due to the carbon diffusion toward the outside of the grains. During CGS there is no dissolution of the carbides into the matrix therefore allowing the coating to enhance the powder's initial properties. (Figure 66b)

### 2.2.2. Adhesion test

For the optimum coating obtained from Ti-SiC, three cylindrical samples were prepared and adhesion strength test was applied. The tensile strength values were shown at below table:

Table 17: Tensile strength values of produced coating from Ti-SiC by HVOF and using Propylene as fuel gas

Powder, Sub., fuel Gas	Adhesion value (MPa)
(Ti-SiC, C St., Propylene)	68±3



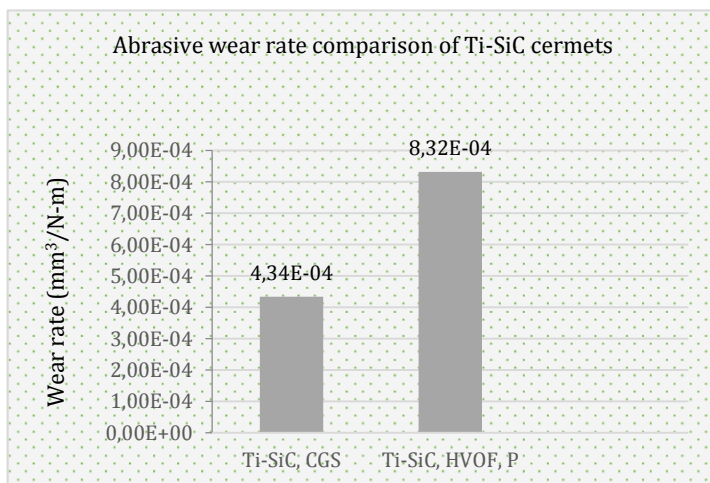
For all three samples, the failure has been happened in the glue.

### 2.2.3. Fracture toughness

The fracture toughness of optimum coating by each technique was calculated, its value for Ti-SiC by CGS (before HT) was  $2,5 \pm 0,7 \text{ MPa}\cdot\sqrt{\text{m}}$  and by HVOF was  $2,1 \pm 0,8 \text{ MPa}\cdot\sqrt{\text{m}}$ . The lower value of fracture toughness of Ti-SiC coating by HVOF can be attributed to the fact that during CGS the powder is not subjected to phase changes and no draining of the ductile free metallic matrix in the microstructure happens. The Ti present in the coating is kept and acts as a ductile element hence improving the fracture toughness of the CGS coating.

### 2.2.4. Wear test

BOD test was also done under ASTM G99-03 onto the obtained coating from Ti-SiC powder onto C St. substrate and using Propylene as fuel gas because of showing better microstructural properties than produced coating using  $\text{H}_2$  as the fuel gas in order to evaluate the coefficient friction and the lost volume. For this test, three trials were done and the average was obtained. Table 18 shows the coefficient friction and the lost volume which has been evaluated using the confocal microscope.



Powder	Wear rate (mm <sup>3</sup> /N.m)
Ti-SiC, CGS	4,3E-04±1,3E-05
Ti-SiC, HVOF, P	8,3E-04±2,7E-05

Figure 67: Abrasive wear rate comparison of optimum obtained coatings of Ti-SiC by different spraying techniques

Table 18: Lost volume and coefficient friction of obtained coating from Ti-SiC by HVOF and using Propylene as fuel gas

Powder, technique, gas	Lost volume (mm <sup>3</sup> )	Coefficient friction
Ti-SiC, HVOF, Propylene	2,9E-03±2,0E-04	0,63±0,01

Abrasive wear test was also done for the optimum coating by each technique, the abrasive wear comparison of coatings related to Ti-SiC are shown at graph 58:

Wear rate comparison of formed coatings related to Ti-SiC by CGS and HVOF using Propylene was shown in above graph, significantly lower wear rate of cold sprayed coating of Ti-SiC than HVOF can be explained by higher fracture toughness value of obtained coatings by CGS despite the higher hardness value of obtained coating by HVOF. Again because of low temperature of CGS, there is no melting happening in powder therefore the phase composition of coating will be kept the same as initial powder which means there is no SiO<sub>2</sub> phase in coating and the phase composition will be included of Ti and SiC but in contrast in formed coating by HVOF because of high working temperature, SiO<sub>2</sub> phase was formed in coating. SiO<sub>2</sub> has significantly less fracture toughness than SiC phase. Moreover laminar microstructure of HVOF coating could stimulate the crack propagation in the coating during the wear test.

### 3. Characterization of WC based-green matrix coatings

As it was explained in chapter 3 there were 4 different Ti-WC cermets with different hardness and Carbide phase content. These powders are designed to spray by three different techniques CGS, HVOF and APS in order to meet the expected properties.

#### 3.1. By CGS

The first powder Ti-WC (400 HV) was prepared for spraying by CGS onto the Al and C St. substrates considering the previous trials done for carbides at two different SOD of 20 and 40 and dense coatings were produced.

### 3.1.1. Microstructural properties

After characterization of produced coatings by CGS the optimum coating were selected at SOD 40 which the properties are shown at below table:

Table 19: Microstructural properties of optimum coatings by CGS for Ti-WC (400 HV) system

Powder	Ti-WC, 400	Ti-WC, 400
Substrate	Al	C St.
Fuel gas	N <sub>2</sub>	N <sub>2</sub>
Distance (mm)	40	40
Hardness (HV)	662±92	695±72
Thickness (um)	266±30	252±26
Porosity (%)	0,24±0,01	0,25±0,02

Later SEM cross section micrograph of optimum coatings from Ti-WC 400 onto Al and Steel substrates were taken which have been shown at below figure.

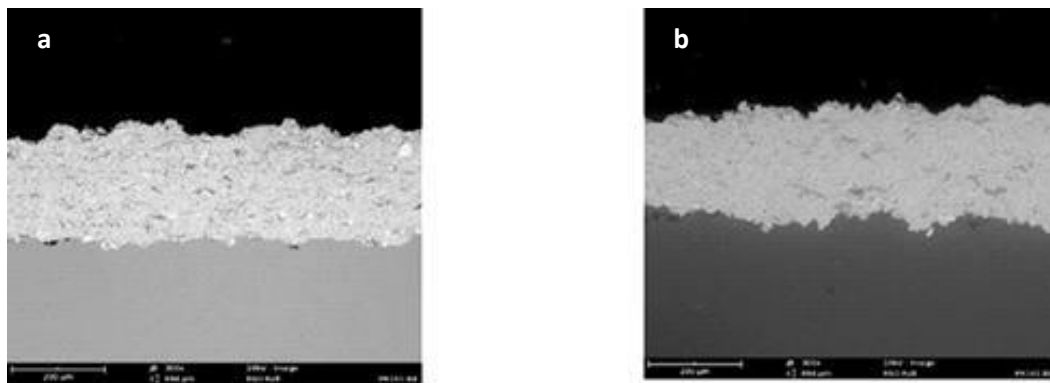


Figure 68: SEM cross section micrograph of Ti-WC obtained coatings by CGS on a) Steel substrate b) Al substrate

As it can be found from the above results, obtained coating onto C St. substrate shows higher hardness than Al substrate because of producing the higher strain hardening in carbon steel substrate.

### 3.1.2. Fracture toughness

The fracture toughness of Ti-WC (400 HV) by CGS onto the carbon steel substrate was calculated and its value was  $6,9 \pm 0,1 \text{ MPa}\cdot\sqrt{m}$ .

### 3.1.3. Wear test

The abrasive wear test was done onto the optimum coating related to Ti-WC (400 HV) and the wear rate was evaluated. The wear rate value comparison of coating related to T-WC and Ti-SiC by CGS was shown at below graph:

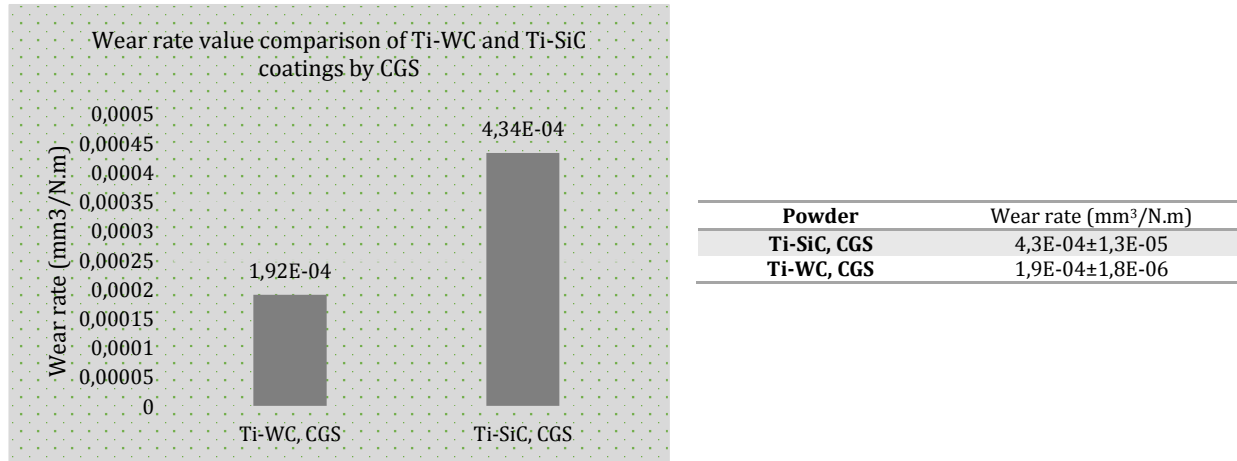


Figure 69: Abrasive wear comparison of coatings related to Ti-WC (400 HV) and Ti-SiC by CGS technique

From the above graph can be found that coating related to Ti-WC by CGS had better resistance to abrasive wear than the coating related to Ti-SiC by CGS. Once again in CGS process no melting and no phase decomposition are happening therefore the microstructure of produced coating is remained as the same as the initial powder. In nature SiC is harder than WC but more brittle and fragile and has lower fracture toughness which makes SiC less resistant to the abrasive wear.

In order to improve the microstructural properties of obtained coating related to Ti-WC (400 HV) by CGS, like Ti-SiC the powder was sprayed onto Carbon steel substrate with micro layer of Ti bond coat in order to improve the adhesion strength of coating and substrate and after obtaining the coating, it went through the post heat treatment in order to disappear the interfaces between the deposited powder particles and form a stronger metallurgical bond. Below table shows the microstructural properties of coating before and after HT:

Table 20: Microstructural properties of coating related to Ti-WC (400 HV) before and after HT

HT*	Powder	Substrate	Hardness	Thickness
Before	Ti-WC	C Steel+Ti bond coat	742±65 HV	313±18 um
After	Ti-WC	C Steel+Ti bond coat	1198±287 HV	313±18 um

\*(HT Temperature: 650°C, HT Isotherm: 60 mins, Ramp: 5 (°C/min), Atmosphere: Vacuum)

Below figure shows the SEM cross section of produced coating onto Carbon steel substrate with thin layer of Ti bond coat.

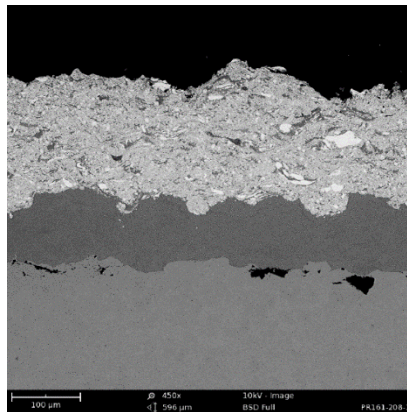


Figure 70: SEM cross section of obtained coating related to Ti-WC (400 HV) onto C steel + Ti bond coat by CGS.

As it can be observed after post heat treatment on coating the hardness of coating has been increased significantly. It reached a value of 1200 HV from 750 which was considerable. Increasing the hardness after annealing like Ti-SiC can be explained because of healing the interfaces and also because annealing led to the recrystallization of the deformed grains, remarkable grain growth accompanied by the disappearance of particle interfaces. Post thermal treatment on Ti-WC coating by cold gas led to dissolution of WC in Ti matrix and precipitation of new carbides (TiC) which is harder than Ti metal and as a result the hardness was increased [61–63].

In order to discuss the increment in hardness after HT, XRD study of coating after HT was done, the below graph shows the XRD graph to observe the phase composition of coating after HT.

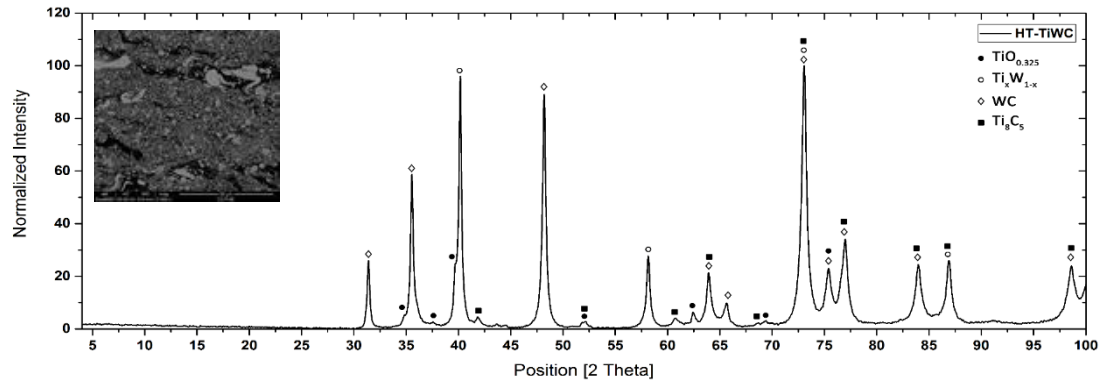


Figure 71: XRD study of produced coating related to Ti-WC (400 HV) after HT

SEM elemental mapping before and after HT was done in order to understand how annealing has affected the microstructure of coating, phase distribution and also how it has led to the improving the hardness.

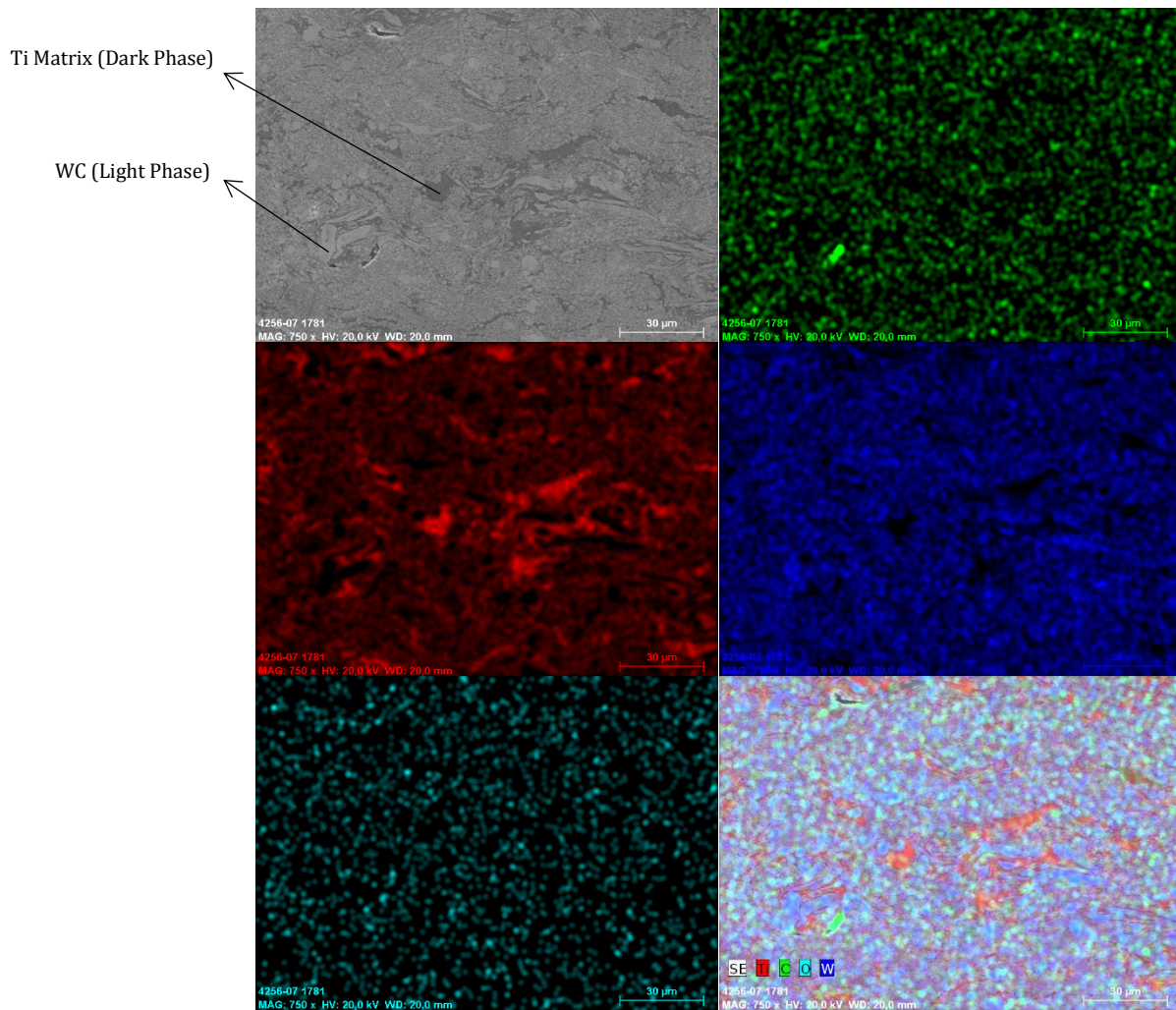


Figure 72: Elemental Mapping of Ti-WC coating by CGS before HT

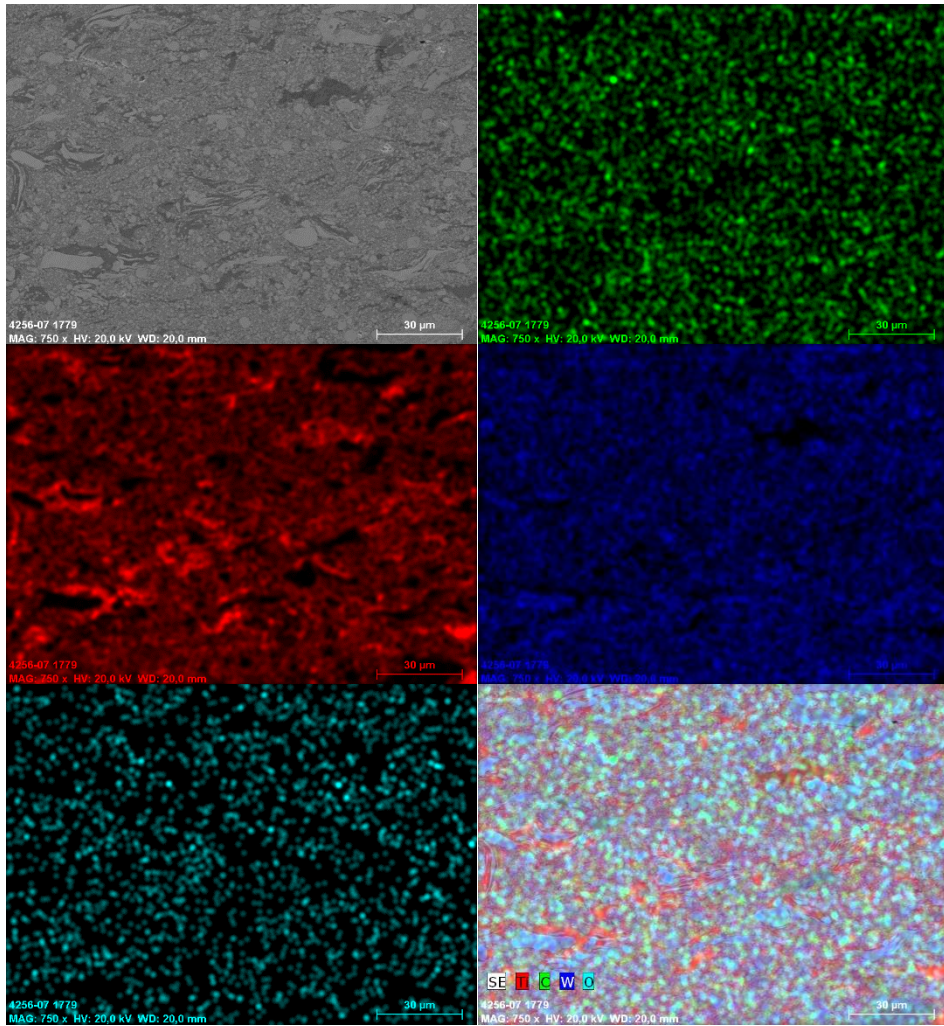


Figure 73: Elemental Mapping of Ti-WC coating by CGS after HT

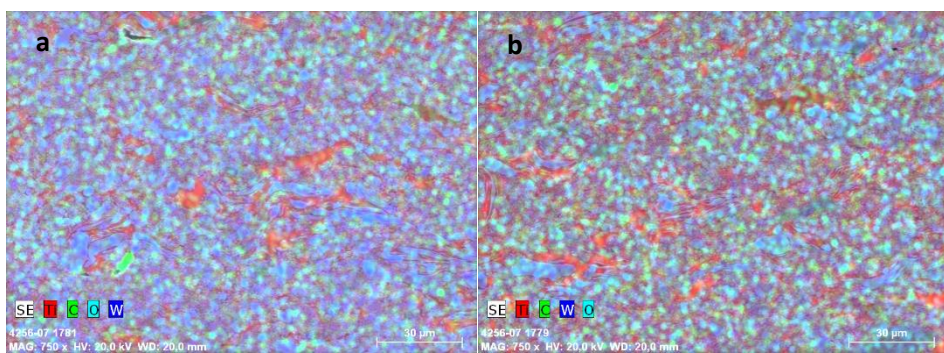


Figure 74: Elemental Mapping comparison of Ti-WC coating by CGS a) before and b) after HT

As it can be observed from the above results after HT distribution of Ti and C elements in coating has been increased and there are more carbide phases in coating. This microstructural changing means that new carbides (TiC) have

been formed in coating because annealing has led to dissolution of WC in Ti matrix and precipitation of TiC; therefore the higher hardness after post HT is because of decomposition of Ti-WC powder during the annealing process and hardening effect of Titanium carbide. Also the sample annealing has led to the formation of intermetallic phases ( $Ti_xW_{1-x}$ ) and produces more homogeneous coating structure which can promote less porosity and higher mechanical properties.

### 3.2. By HVOF

In order to compare the microstructural properties of obtained coatings from Ti-WC system by CGS technique, the powders were prepared for spraying by HVOF and using both  $H_2$  and Propylene as fuel gases. First trial for Ti-WC 400 HV was done by HVOF technique and using Hydrogen as the fuel gas. The standard parameters of the cermet carbides was implemented for this trial and the powder was sprayed onto the carbon steel and Aluminum substrates at 3 different distance 200, 225 and 250 mm, considering the ratio of  $O_2/H_2=0,44$  and spraying temperature less than the max flame temperature. For first trial there was no deposition on the substrate, therefore the second trial was done with changing the ratio of the fuel gases by decreasing the ratio of  $O_2/H_2$  to 0,42 and increasing the air volume in order to increase the velocity. The powder was sprayed onto the carbon steel and Al substrates but there was no deposition again. For the third trial, the ratio of  $O_2/H_2$  was kept constant and the air volume was decreased in order to decrease the velocity, so the powder was sprayed onto the carbon steel and Al changing the fuel gases mixture. There was no deposition on Aluminum substrate but the coating onto the carbon steel substrate was produced. For the fourth trial, the fuel gas was changed from Hydrogen to propylene and the powder was sprayed onto the carbon steel and Aluminum substrates considering the standard parameters of cermet carbides considering the ratio of fuel gases  $O_2/Prop= 4,08$  and the temperature less than the flame temperature. With these parameters, there was no deposition. For the fifth spraying trial, the powder was sprayed onto the carbon steel with decreasing the ratio of  $O_2/Prop$  to 3,7 and keeping the air volume and velocity as constant as before



and reaching max flame Temperature. There was again no deposition with this condition. For the sixth spraying trial using Propylene as the fuel gas, Ti-WC was sprayed onto the carbon steel substrate. For this trial the ratio of O<sub>2</sub>/Prop was kept constant and equal to 3,7 but the air volume and subsequently the velocity was decreased with reaching the max flame temperature. The powder was deposited onto the C St. substrate and the coating was obtained.

Ti-WC (thermally pre-heated, 650 HV) powder which is the harder version of previous Ti-WC (400 HV) was also provided by MBN for spraying trials by HVOF technique. The spraying trial for Ti-WC (650HV) powder was done by HVOF and using Hydrogen as the fuel gas. The optimal parameters of the previous Ti-WC (400HV) were implemented for this trial and the powder was sprayed onto the carbon steel substrate and the coating was obtained.

Ti-WC (1500 HV) thermally pre-heated powder is the harder version of previous Ti-WC (650HV) provided for spraying trials by HVOF technique. The first spraying trial for Ti-WC (1500HV) powder was done by HVOF technique and using Hydrogen as the fuel gas. The optimal parameters of the previous Ti-WC (650HV), was implemented and the powder was sprayed onto the carbon steel substrate but there was no deposition.

The last Ti-WC (richer in WC) was also provided for spraying trials by HVOF technique. With the standard condition of carbides and using Propylene as the fuel gas, even for this powder there was no deposition. At cermets with higher amount of carbide phase, there was no deformation because of hardness of carbide phase and just a very thin layer was formed onto the substrate and there was no bonding between the substrate and powder particle neither particles which could cause erosion on the surface.

### 3.2.1. Microstructural properties

After producing the coatings from Ti-WC system by HVOF method and using H<sub>2</sub> as fuel gas the samples went through the microstructural characterization. Below images show the SEM cross section micrograph of optimum obtained

coatings (SOD: 225 mm) from each individual Ti-WC powder (400 HV and 650 HV) using H<sub>2</sub> as fuel gas:

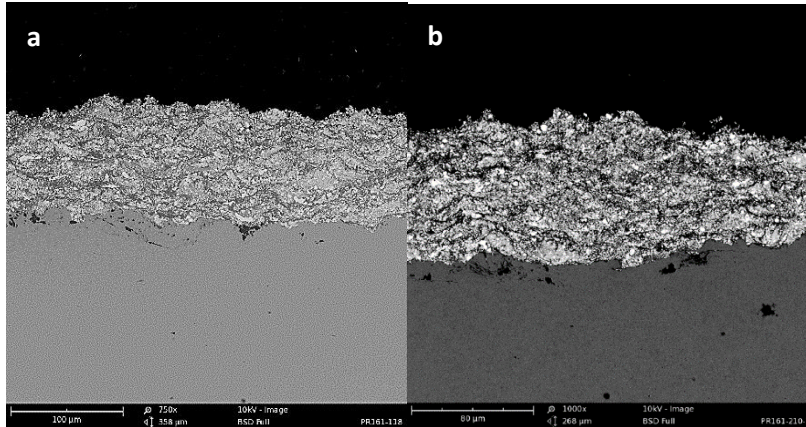


Figure 75: SEM cross section study of produced coatings related to Ti-WC system by HVOF and using H<sub>2</sub> as fuel gas a) Ti-WC (400 HV) (3<sup>rd</sup> trial) b) Ti-WC (650 HV) (1<sup>st</sup> trial)

Below table also shows the microstructural properties of obtained coatings related to Ti-WC system:

Table 21: microstructural properties of Ti-WC coatings by HVOF and using H<sub>2</sub>

Powder	Ti-WC 400 (3 <sup>rd</sup> trial)	Ti-WC 650 (1 <sup>st</sup> trial)
Substrate	C St.	C St.
Fuel gases	Hydrogen	Hydrogen
Distance (mm)	225	225
Hardness (HV)	836±9	714±77
Thickness (um)	90±9	84±10
Porosity (%)	0,1	0,9

Below figure also shows SEM cross section micrograph of samples related to Ti-WC (1500 HV), as it can be observed there was no deposition on substrate.

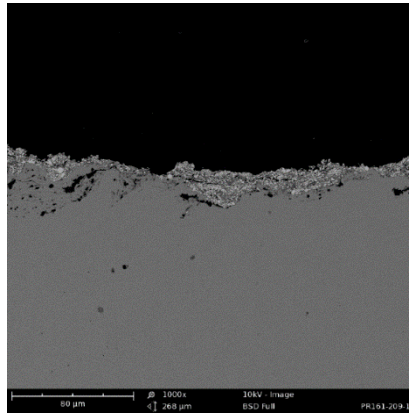


Figure 76: SEM cross section micrograph of sample related to Ti-WC (1500 HV) by HVOF and H<sub>2</sub> as fuel gas

Later produced coatings related to Ti-WC (400 HV) by HVOF and using Propylene as fuel gas were characterized and the SEM micrograph and microstructural properties of optimal coating were done. Below image show the SEM cross section of produced coating:

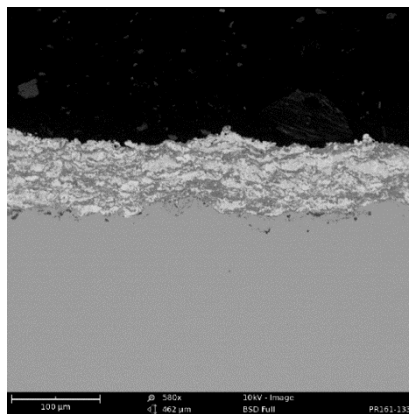


Figure 77: SEM cross section study of produced coatings related to Ti-WC (400 HV) system by HVOF and using Propylene as fuel gas (6<sup>th</sup> trial)

Below table exposes the microstructural properties of obtained coating related to Ti-WC (400 HV) by HVOF and using Propylene as fuel gas:

Table 22: microstructural properties of produced coating from Ti-WC (400 HV) by HVOF and using Propylene

Powder	Ti-WC 400 (6 <sup>th</sup> trial)
Substrate	C St.
Fuel gases	Propylene
Distance (mm)	225
Hardness (HV)	879±10

Thickness (um)	85±6
Porosity (%)	0,15

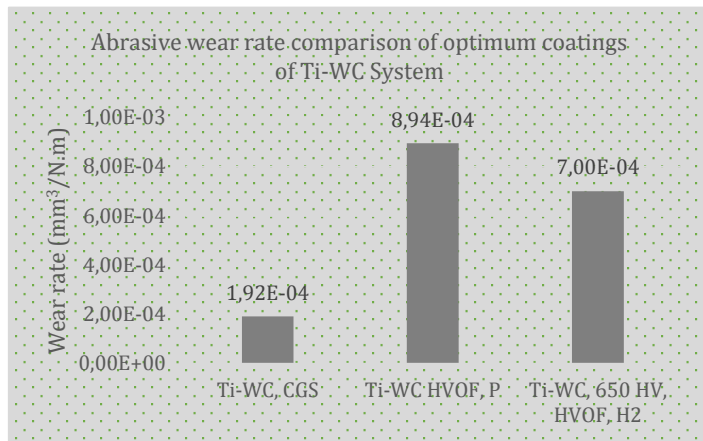
From the above microstructural properties can be found that produced coating related to Ti-WC (400 HV) by HVOF and using Propylene has slightly more hardness than the one produced by using H<sub>2</sub> as fuel gas which the reason has been explained for previous trials (Powders). HVOF is a high temperature process (up to ≈3000°C) and due to its high temperatures, decarburization and formation of brittle phases happen. In this system also HVOF coatings presented higher hardness values than CGS mainly because of decomposition of the WC-Ti powder during the spray process, dissolution of WC into the Ti matrix, depletion of ductile Ti and forming hard and brittle compositions. In HVOF particles are exposed to hot and usually Oxygen rich environment, therefore reaction between WC particles and Ti metal matrix and formation of W<sub>2</sub>C, and depending on the processing conditions even W as well as volatile CO and CO<sub>2</sub> can lead to form the harder coating. If the mainly Ti binder is melted, W and C dissolve in it and form depending on the cooling conditions after impact on the substrate surface either an amorphous phase, a solid solution Ti crystal or mixed carbide phases. In addition to the higher hardness, these coatings are also more brittle than those by CGS due to the lower content in elemental ductile Ti matrix and the presence of fragile and hard phases formed during the HVOF spraying process. [65].

### 3.2.2. Fracture toughness

In order to better understanding the results of rubber wheel test, the fracture toughness of coating from Ti-WC system was measured. For Ti-WC (400 HV) by CGS the value of  $6,9 \pm 0,1 \text{ MPa} \cdot \sqrt{m}$  was obtained. For coating related to this powder by HVOF, because of low thickness of coating, the fracture toughness couldn't be measured.

### 3.2.3. Wear test

The abrasive wear rate of optimum coating of Ti-WC system by different spraying systems was studied which the comparison graph was shown as following:



Powder	Wear rate (mm <sup>3</sup> /N.m)
Ti-WC, CGS	1,9E-04±1,8E-06
Ti-WC, HVOF, P	8,9E-04±6,8E-06
Ti-WC (650), HVOF, H <sub>2</sub>	7,0E-04±6,4E-06

Figure 78: Abrasive wear comparison of optimum coatings related to Ti-WC (400 HV) and Ti-WC (650 HV) by different techniques

As it can be understood from the above information, the produced coating related to Ti-WC (400 HV) by CGS showed better resistance to abrasive wear than the one produced by HVOF. Again, because of the low temperature of CGS, there is no melting in powder happening; therefore, the microstructure of the coating will be the same as the initial powder. It means there are no formed fragile and brittle compositions in the coating; but in contrast, HVOF coating presents lower resistance to abrasive wear because of high working temperature, hardening effect due to the presence of fragile and hard  $\eta$  phases (compositions between Ti-W-C) and lower content in elemental ductile Ti matrix.

### 3.3. By APS

Thermally pre-heated Ti-WC cermets, which are the harder version of Ti-WC 400 HV with hardness of 650 and 1500 HV, have been also designed for spraying trials by APS technique. The trial was done by spraying the powder onto the carbon steel substrate by APS technique. The parameters were between 30-35 l/min Argon (Primary gas) and 10-15 l/min Hydrogen (Secondary gas) with current intensity of 550-600 A. At 1<sup>st</sup> coating trial, with considering the mentioned parameters, the coating was produced. However, in order to improve the properties of the coating, another trial was done. At 2<sup>nd</sup> trial, we decreased the current intensity while keeping the rest of the parameters constant, and again the coating was deposited onto the substrate successfully. Again, for further improvement in properties of the coating, 3<sup>rd</sup>

spraying trial with increasing the current intensity and using only Argon as plasma gas was done.

### 3.3.1. Microstructural properties

After producing the coatings, microstructural properties were evaluated and the SEM micrograph of each coating was obtained. Below images show SEM micrograph of obtained coatings related to Ti-WC (650 HV) and Ti-WC (1500 HV) by APS under different spraying conditions:

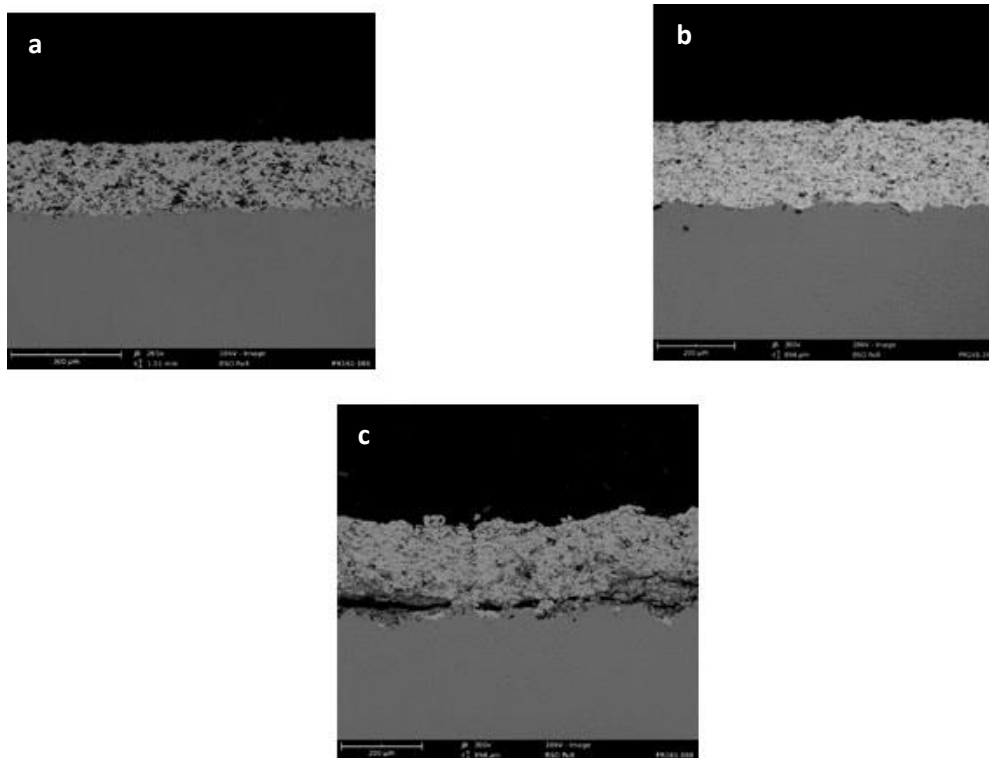


Figure 79: SEM cross section study of produced coatings related to Ti-WC (650 HV) by APS a) 1<sup>st</sup> trial b) 2<sup>nd</sup> trial c) 3<sup>rd</sup> trial

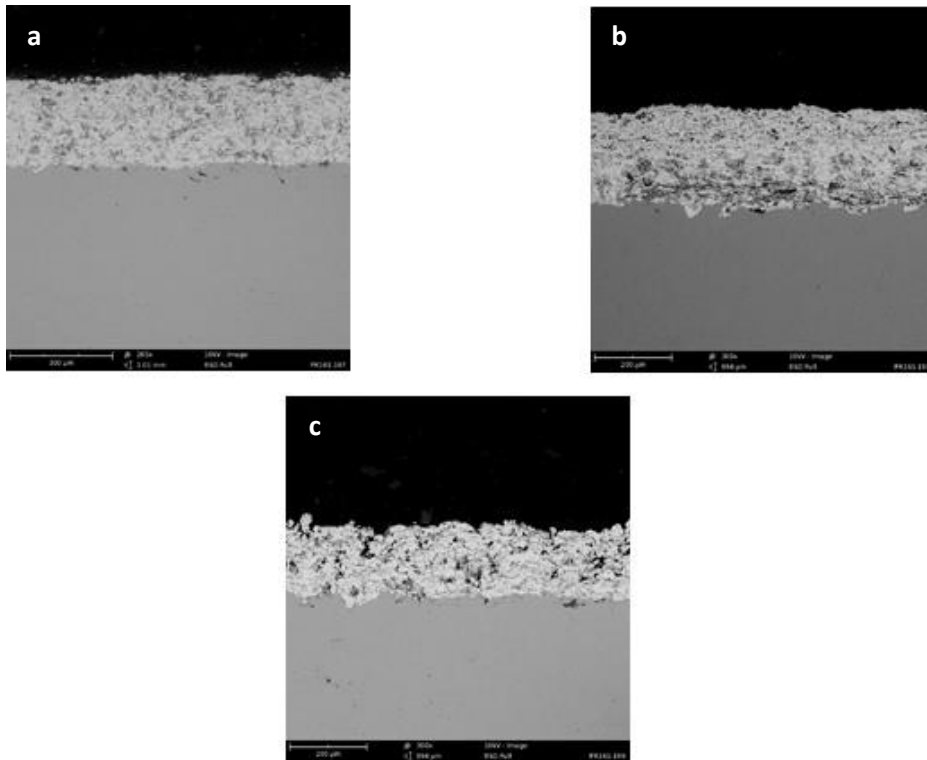


Figure 80: SEM cross section study of produced coatings related to Ti-WC (1500 HV) by APS a) 1<sup>st</sup> trial b) 2<sup>nd</sup> trial c) 3<sup>rd</sup> trial

The microstructural properties of coatings were shown at below table:

Table 23: Microstructural properties of produced coatings of Ti-WC system by APS

Powder	Ti-WC 650	Ti-WC 650	Ti-WC 650	Ti-WC 1500	Ti-WC 1500	Ti-WC 1500
Substrate	C St.	C St.	C St.	C St.	C St.	C St.
Spraying Condition	1 <sup>st</sup>	2 <sup>nd</sup>	3 <sup>rd</sup>	1 <sup>st</sup>	2 <sup>nd</sup>	3 <sup>rd</sup>
Hardness (HV)	340±27	598±28	602±42	447±36	611±63	779±76
Thickness (um)	183±5	203±14	244±18	232±7	239±12	175±15

Despite of a slight increase in hardness and thickness of produced coating from Ti-WC (650 HV), there was an almost complete decohesion of coating from the C St. substrate (Figure 80c). Moreover, a considerable number of cracks were also observed. Thermal expansion coefficient mismatch between coating and substrate may result in considerable accumulation of residual stress, which develops either cracks or delamination of the coating. However Ti-WC (650 HV) coating almost reached its maximum hardness ( $\approx 600$  HV) at 2<sup>nd</sup> trial and this coating was considered as the optimal of this powder by APS. For obtained coatings related to Ti-WC (1500 HV) under 3<sup>rd</sup> spraying

condition higher hardness was achieved though the thickness was decreased and porosity was increased; Therefore we considered the produced coating from the 2<sup>nd</sup> trial as the optimal coating for this system by APS. Despite of improving the properties of obtained coatings from both Ti-WC powders, the coatings had high porosity which is because of high temperature of APS method and quick decomposition of WC and consequently quick formation of CO and CO<sub>2</sub> phases in the coating which can provoke creation of porosity. XRD study of phase composition of coating related to Ti-WC (650 HV) and Ti-WC (1500 HV) by APS has been done and shown as below graphs respectively:

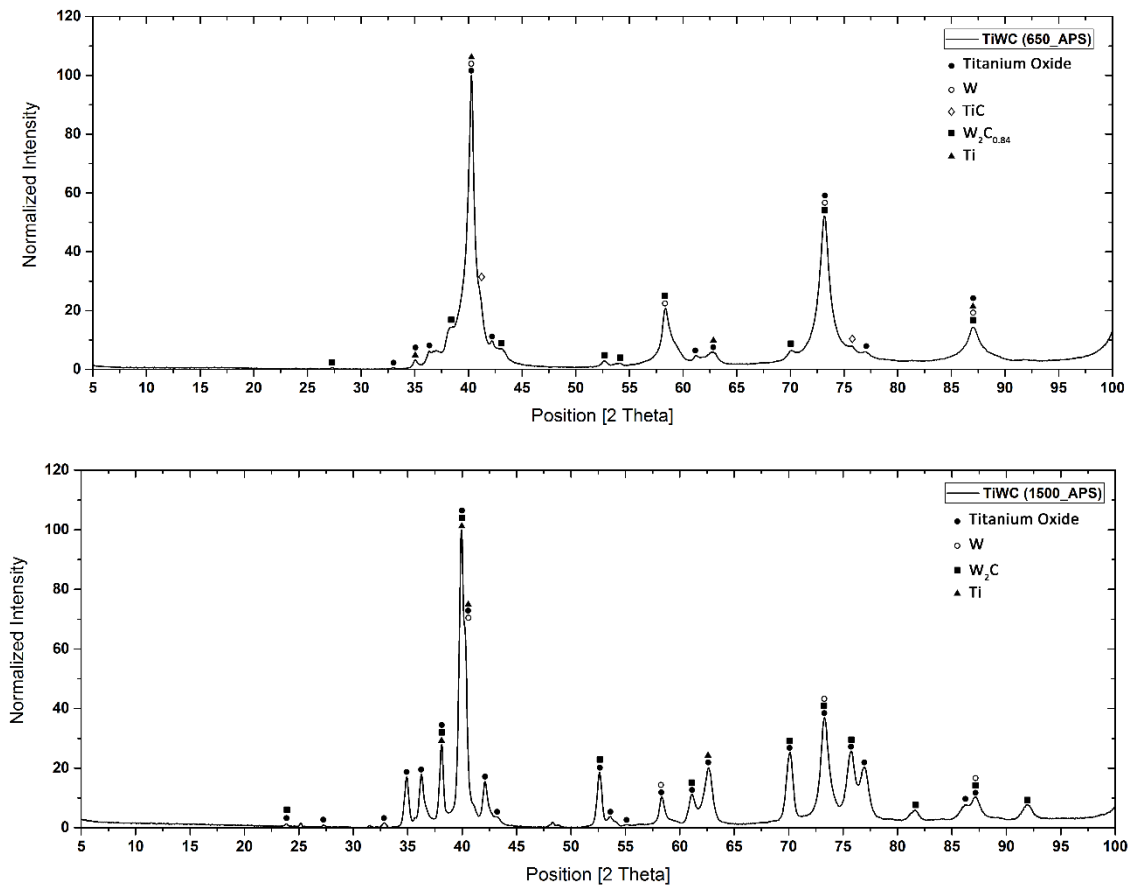


Figure 81: XRD phase composition of produced coatings by APS a) Ti-WC (650 HV)  
b) Ti-WC (1500 HV)

High hardness of produced coatings by APS from both powders can be related to the formation of brittle Tungsten carbide (W<sub>2</sub>C) and Titanium oxide phases and hardening effect of W<sub>2</sub>C during APS process but whereas



the coatings were so porous and cracked, further characterization was not done for APS technique.

## 4.2. GLOBAL COMPARISON BETWEEN COATINGS

As it has been explained before, in this thesis different carbides with different metal matrix have been provided for spraying by different thermal spraying techniques. In this section global comparison of optimum coating for each powder by different techniques from microstructural properties point of view till mechanical properties has been studied and the optimum coating of each system has been selected. For this reason in below table hardness and thickness of all produced coatings onto the carbon steel substrate have been shown and compared.

Table 24: microstructural comparison of optimum coating of each powder by different thermal spraying techniques

System	Powder	CGS		HVOF				APS	
		Nitrogen		Propylene		Hydrogen		Hydrogen-Argon	
		Hardness HV	Thickness um	Hardness HV	Thickness um	Hardness HV	Thickness um	Hardness HV	Thickness um
TiC	Ti-20%TiC	408±68	605±26						
	Ti-50%TiC	470±55	453±19						
	Ti-65%TiC #3	546±38	192±15						
	TiC-FeCrAlTi			962±95	359±6	954±54	353±11		
SiC	Ti-SiC	477±25 817±82 (After HT)	195±8	978±60	302±14	681±58	305±10		
WC	Ti-WC, 400	695±72 1198±287 (After HT)	252±26	879±10	85±6	836±9	90±9		
	Ti-WC, 650					714±77	84±10	602±42	244±18
	Ti-WC, 1500							779±76	175±15

As it can be observed from the above table, the optimum coating of each system has been highlighted and further comparison has been done. Below table shows mechanical comparison of optimum coatings including sliding wear resistance and fracture toughness.

Table 25: Abrasive wear resistance and fracture toughness comparison of optimums

Powder	Substrate	Technique	Gas	Hardness (HV)	Wear rate (mm <sup>3</sup> /N.m)	Fracture toughness MPa. $\sqrt{m}$
Ti-WC (400HV)	C St.	CGS	Nitrogen	695±72	1,9E-04±1,8E-06	6,9±0,1
TiC-FeCrAlTi	C St.	HVOF	Propylene	962±45	2,6E-04±1,4E-05	4,1±0,5
Ti-SiC	C St.	CGS	Nitrogen	477±25	4,3E-04±1,3E-05	2,5±0,7
Ti-65%TiC #3	C St.	CGS	Nitrogen	546±38	3,7E-04±6,2E-06	2,4±0,3
Ti-SiC	C St.	HVOF	Propylene	978±60	8,3E-04±2,7E-05	2,1±0,8

As it can be understood from the above table, Ti-WC coating by CGS (before HT) had the lowest wear rate and the highest fracture toughness and Ti-SiC coating by HVOF presented the highest wear rate and the lowest fracture toughness. However produced coating from Ti-SiC by HVOF had the highest hardness value in compare to the other coatings which it was because of formation of brittle oxide and carbide phases during HVOF process. Higher amount of brittle compositions decreases the cohesion between the splats which can result a decrease in coating's toughness, therefore Ti-SiC by HVOF showed the lowest value of fracture toughness among all the coatings which further explanation has been studied in previous chapter. The high value of hardness and consequently wear resistance of deposited coating from TiC-FeCrAlTi by HVOF was also related to the decomposition of carbide and formation of hard oxide phases and intermetallic phases. The lower wear rate of Ti-WC by CGS in compare to the obtained coating from Ti-SiC as it has been explained in previous chapters was because, in nature SiC is harder than WC but more brittle and fragile and has lower fracture toughness which makes SiC less resistant to the abrasive wear. Regarding the hardness Ti-WC coating by CGS after HT had the highest amount of hardness as a result of annealing and precipitation of hard carbides. However formation of hard phases during the annealing process might have decreased the fracture toughness value but we expect lower abrasive wear rate for this coating which lack of enough samples for further study didn't let us to measure those values although we have definitely considered it as the future work.

#### 4.2.1. Global trend for TiC system

For all three Ti-TiC powders by increasing the SOD from 20 to 40, hardness has been increased which could be related to the decreasing the porosity of

produced coatings by increasing the carbide phase which could be observed at SEM micrograph images in previous chapter. The Higher adhesion strength of coating related to Ti-65%TiC could be explained by higher amount of hard carbide phase. When powder impacted the substrate, powder with higher amount of hard phase deformed the substrate more and immersed into the substrate deeper and as a result stronger mechanical bonding between the coating and substrate happened. From the wear rate comparison of obtained coatings regarding different Ti-TiC cermets could be resulted that Ti-65%TiC showed better wear resistance properties because of higher hardness and lower porosity. The optimal coating for Ti-TiC system was obtained at medium pressure and medium-high temperature related to Ti-65%TiC and by increasing the temperature, there was erosion and the coating was brittle and fully cracked. At high pressure and high temperature there was no deposition at all. Obtained coating related to TiC-FeCrAlTi by HVOF and propylene as fuel gas presented relatively good microstructural and mechanical properties because of formation of oxides and intermetallic phases during the HVOF process.

#### 4.2.2. Global trend for SiC system

For this system SiC coating by CGS method had the hardness of about 500 HV. Though in order to improve the microstructural properties of coating especially the hardness, coating went through the thermal treatment (annealing at 750°C). The microstructure of the coating was significantly changed because of several reasons which were: disappearing the interfaces between the deposited powder particles, formation of stronger metallurgical bond [61–63], decomposition of Si, formation of intermetallic alloys (Ti-Si), dissolution of SiC in Ti matrix and precipitation of new carbides (TiC). HVOF coating of Ti-SiC presented higher hardness value than CGS mainly because of decomposition of Ti-SiC powder during the process and therefore hardening effect of SiO<sub>2</sub> phase. Despite of higher hardness, HVOF coating was more brittle (less fracture toughness value) than CGS coating due to the lower content in elemental ductile Ti matrix and the presence of fragile and hard SiO<sub>2</sub> phase which was formed during the HVOF process. The higher value of

fracture toughness in CGS coating can be attributed to the fact that during CGS the powder was not subjected to phase changes decomposition and no draining of the ductile free metallic matrix in the microstructure was happened. In CGS, Ti ductile metal in the coating was kept and acted as a ductile element hence improved the fracture toughness of the CGS coating and as a result coating showed better resistance to abrasive wear. Also produced coating by HVOF and using propylene had higher hardness than the one with H<sub>2</sub> which mainly was because of different amount of formed SiO<sub>2</sub> phase in produced coatings which in previous chapter it has been explained effectively.

#### 4.2.3. Global trend for WC system

Ti-WC (400HV) was deposited onto the carbon steel substrate by HVOF and a coating with hardness of almost 900 HV was obtained. The produced coating by using Propylene had higher hardness than the one produced by using H<sub>2</sub> though the thickness of coating for both coatings was not thick enough for further characterization. This powder was sprayed by CGS and reached the hardness of almost 750 HV though to improve the microstructural properties, further trial was applied on this coating. Ti-WC was sprayed onto the carbon steel substrate with a bond coat layer of Titanium in order to increase the adhesion between the powder particles and the substrate surface and after obtaining the coating the sample went through the post thermal treatment (HT Temperature: 650°C, HT isotherm: 60 mins, Ramp: 5 (°C/min), Atmosphere: Vacuum) in order to improve the hardness. After HT, hardness of coating reached a value of 1200 HV from 750 which was considerable. The higher hardness was the result of annealing procedure which has been explained in previous system (Ti-SiC). Mostly the higher hardness was because of dissolution of WC in Ti matrix and precipitation of TiC which is harder than Ti metal and also formation of intermetallic alloy phases (Ti-W) has led to the microstructural properties enhancement. The higher hardness of HVOF Ti-WC than CGS like previous system (Ti-SiC) was the result of decarburization of WC particles during HVOF, explosion of particles to hot and usually Oxygen rich environment and formation of oxides

and hard and brittle  $W_2C$  phase. From Ti-WC (650HV) and (1500 HV) powders the coatings were produced by APS technique. For both powders Better microstructural properties like hardness was happened at the condition of using only Argon as plasma gas and eliminating  $H_2$ . The produced coatings were so porous and fully cracked and we didn't consider any further characterization.

## CHAPTER 5. CONCLUSION



From this study following findings can be resulted:

1. Green cermets coatings with different metallic matrix (Ti, FeCrAlTi) and different carbide types (TiC, SiC, WC) have been produced successfully by different thermal spray techniques and can be used as alternative to WC-Co or Cr<sub>3</sub>C<sub>2</sub>-NiCr for anti-wear applications. Because of the high density of WC-Co and Cr<sub>3</sub>C<sub>2</sub>-NiCr coatings in applications where command reduction in weight is needed and its high relative cost as compared to TiC based hard metals and hazardous nature of Cobalt and Nickel matrix, green cermet coatings can be reliable alternatives in the bench market.
2. In CGS method has been observed a trend which by increasing the temperature to the max and increasing the pressure, visible cracks in deposited particles, weak bonding in central area of splats-substrate interface, less penetration and less plastic deformation have been observed. This trend can be explained by impact velocity of the particles which has been increased by increasing the spraying temperature and pressure till the critical value (the optimal condition) and afterward the excessive particle velocities has been resulted erosion and avoiding a proper deposition process. Spraying pressure and temperature both had the direct relation with the impact velocity of particles though increasing the pressure affected the impact velocity of particles more than the temperature. This phenomenon has led to a decrease in hardness value and fracture toughness of produced coatings. The optimal parameters have been set at intermediate temperatures and pressures.
3. In HVOF coatings there was a slight difference between microstructural and mechanical properties of the coatings by using hydrogen and propylene as fuel gases. Produced coatings by propylene had better microstructural properties mostly because of higher temperature of Hydrogen flame and higher probability of Carbides decomposition. This means more carbide phase (hard phase) was decomposed and the amount of hard carbide phase in coating became less and as a result the hardness was decreased.

4. In general HVOF has produced coatings with presence of continuous oxide phases network and lower content in elemental ductile metal matrix which has led to the higher hardness and lower fracture toughness. In contrast CGS has produced coatings with absence of fragile oxide phases which has led to the higher fracture toughness but lower hardness value. In CGS hard carbide phase was not melted and was not distributed in metallic matrix and no hard and fragile oxide phase was formed which all above reasons have led to the lower hardness value of CGS coatings against HVOF.
  
5. The optimum coatings of this study which can be considered as the alternative to WC-Co or Cr<sub>3</sub>C<sub>2</sub>-NiCr for anti-wear applications were Ti-WC by CGS and TiC-FeCrAlTi by HVOF and using propylene. Both produced coatings showed superior resistance to abrasive wear and owned high fracture toughness. Even though Ti-WC coating after HT reached the significantly enhanced microstructural properties and hardness value of 1200 HV due to the release of residual stress during the thermal treatment, dissolution of WC in Ti matrix and precipitation of TiC, but we couldn't consider further characterization (Abrasive wear rate and Fracture toughness) because of sample limitation, although it has been taken into the account for further research on green carbides coatings.

## CHAPTER 6. BIBLIOGRAPHY

[1]. The science and engineering of thermal spray coatings, second edition, Lech Pawlowski, John Wiley & Sons, 2008.

[2]. Metallic coatings deposited by cold gas spray onto light alloys, Maria Villa Vidaller, 2013, Universitat de Barcelona. Departament de Ciència dels Materials i Enginyeria Metal·lúrgica, Copyright deposit: B. 2148-2014.

[3]. Thermal Spray Fundamentals: From Powder to Part by Pierre L. Fauchais, Joachim V.R. Heberlein, Maher I. Boulos, New York, 2014.

[4]. An introduction to thermal spray, issue 4, Sulzer Metco, 2013.

[5]. Handbook of Thermal Spray Technology, ASM International, Edited by J.R.Davis & Associates, 2004.

[6]. Bonding mechanism in cold gas spraying, Assadi, F. Gartner, T. Stoltenhoff, H. Kreye, Department of Materials Engineering, Tarbiat Modarres University, Tehran, Iran; Department of Mechanical Engineering, University of the Federal Armed Forces Hamburg, Hamburg, Germany, Acta materialia. 51, 2003, pp 4379-4394.

[7]. Titanium Powder Metallurgy: Science, Technology and Applications, G. Bae, S. Kumar, S. Yoon, K. Kang, H. Na, H-J. Kim, C. Lee, Acta materialia. 57, 2009, pp 5654-5666.

[8]. Cold Spray Technology by Anatolii Papyrin, Vladimir Kosarev, Sergey Klinkov, Anatolii Alkhimov, Vasily M. Fomin, First edition, Russian Academy of Science, 2007.

[9]. <http://www.cptub.com/index.php/en/sub-technologies/cgs-ing>

[10]. Cold Spraying of Titanium: A Review of Bonding Mechanisms, Microstructure and Properties, T. Hussain, key engineering materials Vol. 533, 2013, pp 53-90.

[11]. Cold Spray Process Revised by Jeganathan Karthikeyan, ASM Handbook, Volume 5A, Thermal Spray Technology R.C. Tucker, Jr., editor, 2013.

[12]. The cold spray process and its potential for industrial applications, F. Gartner, T. Stoltenhoff, T. Schmidt, H. Kreye, Journal of Thermal Spray Technology, Volume 15, Issue 2, June 2006, pp 223-232.

[13]. Adiabatic shear instability based mechanism for particle/substrate bonding in cold gas dynamic spray process, M. Grujicic, C.L. Zhao, W.S. Derosset, D. Helfritsch, Mater. Design.25, 2004, pp 681-688.

[14]. Analysis of the impact velocity of powder particles in the cold-gas dynamic-spray process, M. Grujicic, C.L. Zhao, W.S. Derosset, D. Helfritsch, Department of Mechanical Engineering, Clemson University, Materials Science and Engineering A368, 2004, pp 222-230.

[15]. S. Vladimirovich Klinkova, V. Fedorovich Kosarev, M. Rein, Aerospace Science and Technology 9, 2005, pp 582-591.

[16]. J. Pattison, S. Celotto, A. Khan, W. O'Neill, Surf. Coat. Tech. 202, 2008, pp 1443-1454.

[17]. Cold Spray Deposition of WC-Co Cermets, Miguel Pereira de Magalhaes e Couto, 2014, Universitat de Barcelona. Facultat de Química, copyright deposit: B. 3583-2015.

[18]. From Particle Acceleration to Impact and Bonding in Cold Spraying, Tobias Schmidt, Hamid Assadi, Frank Gartner, Horst Richter, Thorsten Stoltenhoff, Heinrich Kreye, and Thomas Klassen, 2009.

[19]. Particles impact conditions and corresponding coating properties in cold spraying, T. Schmidt, F. Gaertner, H. Kreye, T. Klassen., Helmut Schmidt University, Cold Spray Conference, Ohio, USA, 2007.

[20]. A Model Study of Powder Particle Size Effects in Cold Spray Deposition, D. Helfritsch and V. Champagne, December 2008.

[21]. Particle Loading Effect in Cold Spray, K. Taylor, B. Jodoin, J. Karov And P. Richer, Journal of thermal spray technology, volume 15, issue 2, 2006.

[22]. Effect of standoff distance on coating deposition characteristics in cold spraying, W.Y. Li, C. Zhang, X.P. Guo, G. Zhang, H.L. Liao, C.-J. Li, C. Coddet, School of Materials Science and Engineering, Materials and Design 29, 2008, pp 297–304.

[23]. Substrate Roughness and Thickness Effects on Cold Spray Nanocrystalline Al-Mg Coatings, P. Richer, B. Jodoin, L. Ajdelsztajn, and E.J. Lavernia, Volume 15(2), 2006.

[24]. Global Coating Solutions, by Basil R. Marple, Margaret M. Hyland, Yuk-Chiu Lau, Chang-Jiu Li, Rogerio S. Lima, Ghislain Montavon, 2007.

[25]. Optimization and Characterization of High Velocity Oxy-fuel Sprayed Coatings, Maria Oksa, Erja Turunen, Tomi Suhonen, Tommi Varis and Simo-Pekka Hannula, Technical Research Center of Finland, 2011.

[26]. Experimental study of high velocity oxy-fuel sprayed WC-17Co coatings applied on complex geometries, Vasileios Katranidis, Sai Gu, Bryan Allcock, Spyros Kamnis, Surface and Coatings Technology, Volume 328, 2017, pp 499-512.

[27]. Influence of Process Parameters on High Velocity Oxy-Fuel Sprayed Cr<sub>3</sub>C<sub>2</sub>-25%NiCr Coatings, Mingxiang Xie, Yue Lin, Peng Ke , Shuoyu Wang, Shihong Zhang, Zhicheng Zhen and Liangshui Ge, Maanshan Ma, Steel Surface Engineering Technology Co. Ltd., China, 2017.

[28]. <http://www.gordonengland.co.uk/>

[29]. Introduction to Coating Design and Processing, ASM Handbook, Volume 5A, Thermal Spray Technology R.C. Tucker, Jr., editor, 2013.

[30]. Influences of atmospheric plasma spraying parameters on the porosity level of alumina coating on AZ31B magnesium alloy using response surface methodology, D. Thirumalaikumarasamy, K. Shanmugama, V. Balasubramanianb, Annamalai University, Volume 22, Issue 5, 2012, pp 568-479.

[31]. The Effect of V/Ti Ratio on the Partitioning of Mo in (V, Ti)C + (Ni,Mo) Cemented Carbides, R.K. Viswanadham, B. Sprissler, W. Precht, and J.D. Venables, Metall. Trans. A, Vol 10 (No. 5), 1979, pp 599-602.

[32]. J.L. Elhs and C.G. Goetzel, Cermets, ASM Handbook, Vol 2, ASM International, 1990, pp 978-1007.

[33]. Cemented Carbides, A.T. Santhanam, P. Tiernen, and J.L. Hunt, ASM Handbook, Vol 2, ASM International, 1990, pp 950-977.

[34]. Friction and Wear of Cemented Carbides, H.J. Scussel, ASM Handbook, Vol 18, ASM International, 1992, pp 795-800.

[35]. Cemented Carbides, R.W. Stevenson, ASM Handbook, Vol 7. ASM International, 1992, pp 773-783.

[36]. Cemented Carbides, E Swarzkopf and R. Kieffer, MacMillan, 1960, pp 7-9.

[37]. Cemented Titanium Carbide Cutting Tools, D. Moskowitz and M. Humenik, Jr., Modern Developments in Powder Metallurgy, Vol 3, 1966, pp 83-93.

[38]. Light weight TiC/Ti Wear-Resistant Coatings for Lightweight Structural Applications, M. Mohanty and R.W. Smith. Volume 4, Issue 4, 1995, pp 384-394.

[39]. Physical and Chemical Nature of Cemented Carbides, H.E. Exner, *Int. Met. Rev.*, Vo124 (No. 4), 1979, pp 149-173.

[40]. The Effect of Eta Phase on the Properties of CVD TiC-Coated Cemented Carbide Cutting Tools, V.K. Satin and J.N. Lindstorm, *J. Electrochem. Soc.*, Vo1126 (No. 4), 1979, pp 1281-1287.

[41]. Metallurgical Characterization of Plasma Sprayed WC-Co Coatings, S. Rangaswamy and H. Herman, *Advances in Thermal Spraying*, Pergamon Press, 1986, pp 101-107.

[42]. Vacuum Plasma Spray Deposition of WC-Co, Z.Z. Mutaslm, R.W. Smith, and L. Sokol, *ASM International*, 1996, pp 165-169.

[43]. Thermally Sprayed Coating Systems for Surface Protection and Clearance Control Applications in Aero Engines, T.N. Rhys-Jones, *Surface and Coatings Technology*, Vo143-44 (No. 1-3), 1990, pp 402-415.

[44]. The Effects of Plasma Spraying Parameters and Atmosphere on the Properties and Microstructure of WC-Co Coatings, D. Ghosh, D. Lamy, T. Sopkow, and I. Smugga-Otto, *Society for the Advancement of Material and Process Engineering*, 1992, pp 28-42.

[45]. Plasma Spraying for Wear Applications, E. Lugscheider, *ASM International*, 1988, pp 105-122.

[46]. Reactive Plasma Spray Forming for Advanced Materials Synthesis, R.W. Smith, *Powder Metall. Int.*, Vo125 (No. 1), 1993, pp 9-16.

[47]. The Structure and Properties of Thermally Sprayed TiC Particulate Reinforced Steel and Nickel-Chromium Alloy Powders, R.W. Smith, D. Genmer, E. Harzenski, and T. Robisch, *Thermal Spraying*, Vol 1, 1989, pp 95.1-95.3.



[48]. High Velocity Oxy-Fuel Spray Wear Resistant Coating of TiC Composite Powders, R.W. Smith, E. Harzenski, and T. Robisch, ASM International, 1991, pp 617-623.

[49]. Cermet coatings with Fe-based matrix as alternative to WC-CoCr, Giovanni Bolelli, Tim Börner, Francesco Bozza, Valeria Cannillo, Gennaro Cirillo, Luca Lusvarghi, Mechanical and tribological behaviours, University of Modena, 2012.

[50]. Standard test method for microindentation hardness of materials. ASTM E384-07, Book of standard 03.01, ASTM International, 2007.

[51]. <http://www.gordonengland.co.uk/hardness/microhardness.htm>

[52]. Effect of ultra-fine powders on the microstructure of Ti (CN)-xWC-Ni cermets, J. Jung, S. Kang, Acta Mater. 52 (6), 2004, pp 1379-1386.

[53]. Chemical composition, microstructure and sintering temperature modifications on mechanical properties of TiC-based cermet—a review, A. Rajabi, M.J. Ghazali, A.R. Daud, Mater. Des. 67, 2015, pp 95-106.

[54]. High temperature transformations in a steel-TiCN cermet, P. Alvaredo, D. Mari, E. Gordo, Int. J. Refract. Met. Hard Mater. 41, 2013, pp 115-120.

[55]. Preparation of Al-SBA-15 pellets with low amount of additives: effect of binder content on texture and mechanical properties, P. Topka, J. Karban, K. Soukup, K. Jirátová, O. Šolcová, Application to Friedel-Crafts alkylation, Chem. Eng. J. 168 (1), 2011, pp 433-440.

[56]. Milling performance of TiC-Ni cermet tools toughened by TiN nanoparticles, C. Han, C. Den, D. Zhao, K. Hu, Int. J. Refract. Met. Hard Mater. 30 (1), 2012, pp 12-15.

[57]. High energy ball milling a promising route for production of tailored thermal spray consumables, A. Wank, B. Wielage, Chemnitz university of technology, 2003.

[58]. Fabrication of Functionally Graded TiC/Ti Composites by Laser Engineered Net Shaping, Liu, W., and DuPont, J.N., Scripta Materialia, 48, 2003, pp 1337-1342.

[59]. TiC-based cermet prepared by high-energy ball-milling and reactive spark plasma sintering, Alireza Jam, Leila Nikzad , Mansour Razavi, Materials and Energy Research Center, Karaj, Iran, 2016.

[60]. “MBN Nanomaterialia SpA”, <http://www.mbn.it/eng/>

[61]. Thermal Spray: Practical Solutions for Engineering Problems, R.C. McCune, W.T. Donlon, E.L. Cartwright, A.N. Papyrin, E.F. Rybicki, J.R. Shadley, in: C.C. Berndt (Ed.), ASM International, Materials Park, OH, 1996, pp 397–403.

[62]. F. Gärtner, T. Stoltenhoff, J. Voyer, H. Kreye, S. Riekehr, M. Koçak, Surface and Coatings Technology 200, 2006, pp 6770–6782.

[63]. Effect of standoff distance on coating deposition characteristics in cold spraying, W.Y. Li, C.J. Li, H.L. Liao, J. Volume 29, Issue 2, 2008, Pages 297-304.

[64]. Improvement of microstructure and property of cold-sprayed Cu–4 at.%Cr–2 at.%Nb alloy by heat treatment, W.-Y. Li, X.P. Guo, C. Verdy, L. Dembinski, H.L. Liao and C. Coddet LERMPS, 2006.

[65]. Influence of thermal spraying method on the properties of tungsten carbide coatings, B. Wielage, H. Pokhmurska, A. Wank, G. Reisel, S. Steinhäuser, M. Woezel, Chemnitz University of Technology, 2003.



"Deposición de los recubrimientos de los cermets de respetuoso con el medio ambiente por las proyecciones térmicas".

## 1. Objetivos

En primer lugar, el objetivo principal de este trabajo de investigación fue producir recubrimientos cermets de respetuosos del medio ambiente, matriz libre de Ni y Co, alternativa a WC-Co convencional, por la proyecciones térmicas. WC-Co cermets siempre ha sido uno de los recubrimientos más demandados en aplicaciones anti desgaste y anticorrosión en la industria, pero los problemas ambientales de la matriz de metales (Co y Ni) se han debido a cambios en los procesos convencionales. Estos elementos no son dañinos en su estado fundamental, pero el procesamiento genera cambios en los estados de oxidación que los hacen cancerígenos. Por eso, esta tesis se ha centrado en reemplazar los procesos existentes o utilizar materias primas que son menos nocivas. Por lo tanto, depositar los nuevos cermets en los diferentes sustratos por proyecciones térmicas convencionales o novedosas (CGS) son los principales puntos de motivación de esta tesis. Nadie ha depositado previamente con éxito dicho material por el método CGS o HVOF con las mismas propiedades que el WC-Co convencional, que también fue uno de los principales puntos de motivación. En este trabajo podríamos producir recubrimientos de Ti-TiC con diferentes porcentajes de fase de Carburo por CGS, TiC con aleación metálica de FeCrAlTi por método HVOF, SiC con matrice metálica de Ti por ambas técnicas CGS y HVOF y WC cermet con matriz de metal Ti por técnicas CGS, HVOF y APS. Por eso, los objetivos principales de esta Tesis se titulan "Deposición de respetuoso con el medio ambiente recubrimientos de los cermets por el proyecciones térmicas".

## 2. Introducción

### 2.1. Consideración general

La protección de la superficie de los materiales contra cualquier factor dañino externo se ha estudiado en ingeniería de superficies. Una de las tecnologías más comunes para lograr este objetivo son los procesos de proyecciones térmicas de alta calidad.

Las técnicas de la proyección térmica son procesos de recubrimientos en los que los materiales fundidos (o calentados) se proyectan sobre una superficie

[1]. La "materia prima" se calienta por medios eléctricos (plasma o arco) o químicos (llama de combustión). Las propiedades y la microestructura de los recubrimientos dependen de los fenómenos que ocurren durante el vuelo de partículas [2].

La proyección térmica puede proporcionar recubrimientos gruesos (el intervalo de espesor aproximado es de 20 micrómetros a varios mm, dependiendo del proceso y de la materia prima), en un área grande a una velocidad de deposición elevada en comparación con otros procesos de recubrimiento. Los materiales disponibles para la proyección térmica incluyen metales, aleaciones, cerámicas, plásticos y materiales compuestos. Ellos son alimentados en forma de polvo o alambre, se calienta a un fundido o semi-estado fundido y acelerados hacia sustratos en forma de partículas de tamaño micrométrico. La descarga de combustión o de arco eléctrico se usa generalmente como fuente de energía para proyección térmica. Los recubrimientos resultantes se fabrican mediante la acumulación de numerosas partículas proyectadas. Se distinguen varias técnicas de proyección térmica que en esta tesis las más utilizadas fueron:

- Proyección por Plasma (APS)
- Proyección por alta velocidad (HVOF)
- Proyección fría (CGS)

A pesar de las ventajas de las técnicas de proyección térmica, existen algunos inconvenientes que limitan el uso de esas técnicas convencionales. Los principales son [2]:

- Oxidación de materia prima metálica
- Modificación química en el vuelo de partículas rociadas, como descarburación, oxidación o reducción.
- Las partículas en estado líquido pueden evaporarse y reducir su tamaño.
- Aumento de tensiones de tracción.
- Modificación de la microestructura del sustrato debido al calor y al impacto.

## 2.2. Métodos de producción de recubrimientos

### 2.2.1. Por proyección fría (CGS)

La proyección de gas frío (CGS) es una técnica de proyección en estado sólido que produce un recubrimiento al exponer un polvo, con una cierta distribución de tamaños, a una corriente de gas a alta presión (nitrógeno o helio). Estas partículas adquieren una alta energía cinética, lo que permite que la proyección en frío sea un proceso de deposición de estado sólido en el que partículas de polvo pequeñas (en el rango de 5 a 50)  $\mu\text{m}$ ) se aceleran a velocidades del orden de 500 a 1200 m / s en un chorro supersónico de gas comprimido sobre un sustrato donde las partículas de polvo se deforman y se unen rápidamente formando una pequeña capa de materiales depositados [31].

#### 2.2.2. Por alta velocidad

El recubrimiento de combustible de alta velocidad (HVOF) es un proceso de recubrimiento por proyección térmica utilizado para mejorar o restaurar las propiedades o dimensiones de la superficie de un componente, extendiendo así la vida útil del equipo al aumentar significativamente la erosión y la resistencia al desgaste y la protección contra la corrosión. Los materiales fundidos o semi-fundidos se proyectan sobre la superficie por medio de la corriente de gas a alta temperatura, produciendo un recubrimiento denso que se puede moler hasta un acabado superficial muy alto. La utilización de la técnica de recubrimiento por HVOF permite la aplicación de materiales como metales, aleaciones y cerámicas para producir un recubrimiento de dureza excepcional, una excelente adherencia con sustrato y una resistencia sustancial al desgaste y a la corrosión [22].

#### 2.2.3. Por plasma

El proceso de proyección por plasma es básicamente la proyección de material fundido o termo soldado sobre una superficie para proporcionar un recubrimiento. El material en forma de polvo se inyecta en una llama de plasma de muy alta temperatura, donde se calienta rápidamente y se acelera a una alta velocidad. El material caliente impacta en la superficie del sustrato y se enfría rápidamente formando un recubrimiento. Este proceso de proyección por plasma llevado a cabo correctamente se denomina "proceso en frío" (relativo al material del sustrato que se está recubriendo) ya que la temperatura del sustrato puede mantenerse baja durante el procesamiento evitando daños, cambios metalúrgicos y distorsión del material del sustrato.

### 2.3. Los cermets de respetuoso con el medio ambiente

Aunque recubrimientos de los WC-Co se han producido totalmente con éxito en muchos casos, como en materiales resistentes al desgaste, pero sus altas densidades prevenir su uso en aplicaciones que llaman la reducción de peso. En cambio, los carburos ligeros basados en Ti pueden usarse para mejorar y modificar las propiedades tribológicas de los materiales estructurales aeroespaciales [34].

Los cermets a base de carburo de titanio también muestran un acuerdo para aplicaciones de bajo peso y alta resistencia al desgaste a temperaturas bajas y altas. A pesar de su promesa, sin embargo, estos materiales base están restringidos por su baja resistencia al desgaste. Por lo tanto, se necesitan recubrimientos protectores de superficie. Los recubrimientos de WC-Co por proyecciones térmicas han sido ampliamente avanzados para aplicaciones tribológicas [44-47]. WC-Co se ha utilizado como el material de recubrimiento primario resistente al desgaste debido a su alta dureza, comportamiento aceptable de oxidación-corrosión y excelente compatibilidad con muchos materiales de sustrato a base de hierro. Su elección como recubrimiento del protector para estructuras livianas no se considera óptimo para muchos de los materiales livianos que se consideran en el sector aeroespacial y otros vehículos de transporte. La aplicación de tales recubrimientos en sustratos metálicos ligeros probablemente ha sido limitada en la industria de proyección térmica debido a los efectos de alta temperatura asociados con la mayoría de los procesos de proyección. Además, los carburos cermet convencionales recientemente basados en Co y Ni se han considerado como cermet alérgicos y se etiquetan como agentes carcinogénicos sospechosos que pueden causar problemas de toxicidad por inhalación. Por lo tanto la sustitución de Ti, y aleaciones de Ti (FeCrAlTi) son menos peligrosos y más ambientalmente amigable alternativa a Ni y Co que se presentan algunos problemas de seguridad y salud [29].

## 3. Procedimientos experimentales

### 3.1. Materias primas

En este tesis de doctoral trabajamos con diferentes polvos de alimentación de Ti-TiC con diferentes porcentajes de fase de carburo (20, 50 y 65), Ti-SiC, varios

tipos de Ti-WC (400HV, 650HV, 1500HV y el más rico en WC), y TiC-FeCrAlTi con diferentes morfologías fueron proporcionadas por MBN Co. de Italia y se proyectaron sobre los diferentes sustratos (Al y Acero) por diferentes técnicas de proyección térmica (CGS, HVOF y APS). Los polvos se proyectaron sobre los sustratos rectangulares (50x20x5 mm<sup>3</sup>) y cilíndricos (d = 25,4 mm, h = 35 mm) para diferentes propósitos.

## 3.2. Caracterización estructural

### 3.2.1. Morfología

La morfología del polvo es uno de los caracteres más importantes de cada polvo que debe obtenerse antes de la proyección. Por este propósito, los polvos pasaron por el microscopio electrónico de scanning (Phenom ProX desktop scanning electro microscope (SEM)) aunque para algunos polvos FEI QUANTA 200 SEM se ha usado para evaluar la morfología.

### 3.2.2. Distribución de tamaño de partícula

La distribución del tamaño de partícula del polvo se examinó usando la prueba de difracción láser (Beckman Coulter LS 13320). El rango de tamaño de partícula para el polvo se midió antes de la proyección.

### 3.2.3. Composición de fase

La composición de fase de los polvos se obtuvo por la técnica XRD. La prueba de difracción de rayos X se usó para analizar la composición de fase y la cuantificación de fase de cada polvo. El equipo usado fue un tipo de Bragg-Brentano de SIEMENS D500  $\theta/2\theta$  usando radiación  $\text{Cu K}\alpha_{1+2}$  ( $\alpha_1 = 1,54060$  y  $\alpha_2 = 1,54443$ ) a 40 Kv y una corriente de 30 mA. El difractograma obtenido se analizó por el software de análisis Xpert para identificar la composición de fase y la cantidad de cada fase en comparación con la base de datos del programa.

## 3.3. Equipo

### 3.3.1. Gas frío

En esta tesis se utilizaron tres técnicas diferentes, CGS, HVOF y APS para obtener los recubrimientos. El primer método fue la técnica de Cold Gas Spray. Se empleó el sistema de proyección de gas frío con una pistola de proyección comercial KINETICS® 4000 (CGT GmbH, Alemania) con una presión



de funcionamiento máxima de 4 MPa y una temperatura de 800 ° C, y utilizó nitrógeno como gas de proceso.

### 3.3.2. Alta velocidad

El segundo método en esta tesis fue proyección por alta velocidad. El equipo HVOF utilizado fue un Sulzer (Winterthur, Suiza) DJH con dos cabezas diferentes: DJH 2700 para propileno y DJH 2600 para hidrógeno.

### 3.3.3. Plasma

La tercera técnica utilizada en esta tesis para obtener recubrimientos fue APS convencional (Atmospheric Plasma Spray). El equipo de APS era Plasma technik A-3000 con F4 Torch.

### 3.3.4. Microdureza

Este parámetro ha sido evaluado por medio de un equipo Matsuzawa MTX- $\alpha$  Vickers de acuerdo con la norma ASTM E384-99. [30] La carga de 200 gf a 300 gf se aplicó para producir la huella de Vickers en forma de pirámide y se realizaron 10 mediciones a lo largo del recubrimiento y se midió un promedio.

### 3.3.5. Tenacidad a la fractura

La tenacidad a la fractura de los recubrimientos óptimos por técnicas CGS y HVOF se probó para medir el impacto de la formación de fases frágiles en HVOF y aumentar la ductilidad en recubrimientos por CGS. Para estudiar la tenacidad a la fractura en función de la microestructura del material, se utilizó la técnica de indentación de Vickers. El módulo de elasticidad se estimó usando una técnica de indentación de *Knoop* realizando 10 indentaciones de *Knoop* a una carga de 9.80N y para medir la tenacidad de la fractura se realizaron indentaciones de Vickers a 9,80 N en secciones transversales de recubrimiento pulido, y se midieron sus diagonales y longitudes de fisura usando un microscopio óptico.

### 3.3.6. Resistencia a la tracción

La adherencia se ha evaluado siguiendo el estándar ASTM C-633 con el equipo SERVOSIS ME-402/10. Esta prueba consiste en pegar una muestra recubierta cilíndrica con una resina a una muestra granallada sin recubrimiento.

### 3.3.7. Bola en el disco

Esta prueba según la norma ASTM G99-03 permite la evaluación del coeficiente de fricción del recubrimiento pulido y, además, después de realizar la prueba, se puede obtener el volumen perdido utilizando el microscopio confocal midiendo la pista de desgaste.

### 3.3.8. Rueda de goma

La prueba de desgaste abrasivo se evaluó usando un equipo de rueda de goma siguiendo la norma ASTM G65-00. La prueba de abrasión de la rueda de goma por arena seca es uno de los métodos de prueba de abrasión más ampliamente utilizados.

## 4. Materias primas

### 4.1. Sustratos

En esta tesis se dio especial atención a los recubrimientos obtenidos sobre sustratos de aceros y aleaciones de aluminio, Al7075-T6. Los sustratos rectangulares y sustratos cilíndricos para diferentes propósitos, se prepararon primero mediante el rectificado de la superficie para eliminar la oxidación de la superficie y posterior chorro de arena a crea aspereza en la superficie y aumenta la adhesión entre el sustrato y el recubrimiento.

### 4.2. Polvos de alimentación

#### 4.2.1. Cermet basado en TiC

Este carburo a base de TiC consistía en cermetos Ti-TiC y TiC-FeCrAlTi. El polvo de Ti-TiC se proporcionó en 3 tipos con diferente cantidad de fase de carburo (Ti-20% TiC, Ti-50% TiC, Ti-65% TiC) para proyección por CGS y TiC-FeCrAlTi. Para proyección por HVOF.

#### 4.2.2. Cermet basado en SiC

Este carburo a base de SiC se proporcionó en un tipo con fase metálica de Ti. Este polvo fuera diseñados para proyectar por técnicas CGS y HVOF.

#### 4.2.3. Cermet basado en WC

Este polvo se proporcionó en 4 tipos. Ti-WC (400HV), Ti-WC (65 0HV), Ti-WC (15 00HV) y Ti-WC más rico en fase WC. Estos cermets se diseñaron para proyectar por técnicas CGS, HVOF y APS.

## 5. Recubrimientos obtenidos

5.1. Los polvos Ti-TiC se proyectaron sobre los sustratos de acero y Al por la técnica CGS y los recubrimientos se produjeron sobre los sustratos con éxito. Se mejoraron las propiedades micro estructurales de los recubrimientos que incluyen microdureza y porosidad al aumentar la cantidad de fase de carburo. El recubrimiento óptimo obtenido en SOD 40. Al cambiar las condiciones iniciales de CGS, el recubrimiento obtenido a una presión y una temperatura de intermedia mostraron mejores propiedades micro estructurales que otras condiciones. TiC-FeCrAlTi también se depositó con éxito sobre el sustrato de acero mediante la técnica HVOF con propiedades micro estructurales significativamente buenas.

5.2. Polvo Ti-SiC se depositaró con éxito sobre el acero por ambas técnicas de CGS y HVOF aunque el recubrimiento obtenido por HVOF tenía mas dureza y menos tensidad de fractura que lo por CGS. Para mejorar las propiedades del recubrimiento obtenido relacionado con Ti-SiC por CGS, este recubrimiento pasó por los tratamientos térmicos posteriores y después de la caracterización del recubrimiento posterior a TT, se mejoraron significativamente las propiedades micro estructurales del recubrimiento que incluyen la dureza.

5.3. Los polvos Ti-WC se pulverizaron sobre el acero por técnicas CGS, HVOF y APS. Ti-WC (400HV) se produjo con éxito mediante la técnica CGS y HVOF. Aunque como Ti-SiC la dureza del recubrimiento producido por HVOF era mas que por CGS. Incluso para este sistema, el recubrimiento producido relacionado con Ti-WC por CGS pasó por el tratamiento térmico posterior y las propiedades micro estructurales del recubrimiento, especialmente la dureza, se mejoró significativamente. Ti-WC (650) fue depositado con éxito por HVOF y APS que las propiedades iniciales de uno producido por HVOF fueron mejores que APS. Para Ti-WC (1500) no hubo deposición por HVOF aunque por APS se depositó sobre el sustrato y finalmente no hubo deposición en absoluto para Ti-WC más rico en fase WC.

5.4. Comparación de las propiedades mecánicas de recubrimientos obtenidos

En esta tesis, se compararon las propiedades mecánicas de los recubrimientos producidos según la resistencia a la tracción y propiedades abrasivas.

5.4.1. TiC cermets

Para recubrimientos basados en Ti-TiC aumentando el porcentaje de fase de TiC, se mejoraron las propiedades mecánicas de los recubrimientos obtenidos. El valor de resistencia de adhesión con mayor cantidad de fase de TiC fue mayor y el volumen perdido según la prueba de bola sobre el disco fue menor. La tasa de desgaste abrasivo de los recubrimientos con un mayor porcentaje de fase de carburo fue menor, lo que puede explicarse por un mayor fenómeno de tenacidad a la fractura. TiC-FeCrAlTi mostró bastante buenas propiedades mecánicas con respecto a la mayor fuerza de adhesión, menor volumen perdido y coeficiente de fricción y, posteriormente, menor valor de tasa de desgaste abrasivo y significativamente tenacidad a la fractura mayor.

#### 5.4.2. SiC cermets

Para estos recubrimientos se observó que la fuerza de adhesión de recubrimiento Ti-SiC sobre el acero es mayor que el sustrato de Al y también produjo recubrimiento mediante el uso de propileno muestra mejor fuerza de adhesión con el sustrato que el uso de H<sub>2</sub>. El recubrimiento producido relacionado con Ti-SiC por CGS tenía una tasa de desgaste menor que la obtenida por HVOF que se puede explicar por el valor mas alto de la tenacidad a la fractura.

#### 5.4.3. WC cermets

El recubrimiento producido relacionado con Ti-WC (400HV) por CGS tenía una resistencia bastante superior al desgaste por abrasión que el recubrimiento relacionado con Ti-SiC por CGS. De los resultados obtenidos se dedujo que el recubrimiento producido relacionado con Ti-WC (400 HV) por CGS despues de TT, se ha mejorado significamente con respecto a las propiedades de microestructura.

#### 5.5. Comparación de la tenacidad a la fractura de los recubrimientos óptimos

Se ha calculado la tenacidad a la fractura de los recubrimientos óptimos relacionados con cada polvo y se ha discutido su relación con la dureza y la tasa de desgaste. El recubrimiento óptimo de cada polvo y sus propiedades se muestra en la siguiente tabla:

Polvo	Sustrato	Técnica	Gas	Dureza (HV)	Tasa de desgaste (mm <sup>3</sup> /Nm)	Tenacidad a la fractura (MPa)
Ti-WC(400HV)	C St.	CGS	Nitrógeno	742 ± 65	0,00019	6,95 ± 0,11
TiC-FeCrAlTi	C St.	HVOF	Propileno	962 ± 45	0,00026	4,08 ± 0,47
Ti-SiC	C St.	CGS	Nitrógeno	477 ± 25	0,00043	2,53 ± 0,69
Ti- 65% TiC	C St.	CGS	Nitrógeno	546 ± 38	0,00037	2,44 ± 0,28
Ti-SiC	C St.	HVOF	Propileno	978 ± 60	0,00089	2,13 ± 0,79

Como puede entenderse en la tabla anterior, el recubrimiento Ti-WC por CGS tiene la menor tasa de desgaste y la mayor tenacidad a la fractura y el recubrimiento Ti-SiC por HVOF tiene la mayor tasa de desgaste y la menor tenacidad a la fractura, aunque tiene un valor de dureza más alto compare con los otros recubrimientos que pueden explicarse debido a la formación de las fases frágiles en la técnica HVOF.

## 6. Discusión y conclusión

### 6.1. Sistema TiC

Para los tres polvos Ti-TiC aumentando el SOD de 20 a 40, se ha aumentado la dureza que puede relacionarse con la disminución de la porosidad de los recubrimientos producidos al aumentar la fase de carburo que se puede observar en las imágenes SEM. La mayor resistencia a la adherencia del recubrimiento en relación con Ti-65% TiC puede explicarse por una mayor cantidad de fase de carburo duro. Cuando el polvo impacta en el sustrato, el polvo con mayor cantidad de fase dura deforma más el sustrato y inmerge el sustrato más profundo y como resultado se producirá una unión mecánica más fuerte entre el recubrimiento y el sustrato. A partir de la comparación de la tasa de desgaste de los recubrimientos obtenidos con respecto a diferentes cermet de Ti-TiC, se puede obtener que el Ti-65%TiC mostró mejores propiedades de resistencia al desgaste debido a una mayor dureza y una menor porosidad. El recubrimiento óptimo se obtuvo a una presión y temperatura intermedia relacionada con Ti-65%TiC y al aumentar la temperatura por encima de 900°C hubo una deposición pero el recubrimiento era frágil y completamente craqueado. El recubrimiento obtenido relacionado con TiC-FeCrAlTi por HVOF y el uso de Propileno mostró mejores propiedades micro estructurales y mecánicas que H<sub>2</sub>.

## 6.2. Sistema SiC

el recubrimiento obtenido relacionado con Ti-SiC por el método CGS tenía una dureza de aproximadamente 500 HV. Para mejorar las propiedades microestructurales del recubrimiento, especialmente la dureza, el recubrimiento pasó por el tratamiento térmico (recocido a 750°C). La microestructura de los resfriados recó Ti-SiC se modificó significativamente debido a que las interfaces entre las partículas de polvo depositadas tendieron a desaparecer y se formó un enlace metalúrgico más fuerte [61-63]. Recubrimiento Ti-SiC por HVOF presentó mayor valor de la dureza que el de CGS principalmente debido a la descomposición del polvo de Ti-SiC durante el proceso y el efecto por lo tanto, el endurecimiento de SiO<sub>2</sub> fase. Además de una mayor dureza, el recubrimiento HVOF era más frágil (menos valor de tenacidad a la fractura) que el CGS debido al menor contenido en matriz Ti dúctil y y la presencia de la fase de SiO<sub>2</sub> formada frágil y dura durante el proceso de proyección HVOF. El menor valor de la tenacidad a la fractura en el recubrimiento por HVOF se puede atribuir al hecho de que durante el proceso del CGS el polvo no está sujeto a cambios de fase y no se produce el drenaje de la matriz metálica libre dúctil en la microestructura. El Ti presente en el recubrimiento se mantiene y actúa como un elemento dúctil, mejorando así la tenacidad a la fractura del recubrimiento de CGS. La tasa de desgaste significativamente menor del recubrimiento de Ti-SiC por CGS que HVOF puede explicarse por el mayor valor de la tenacidad a la fractura de los recubrimientos obtenidos por CGS a pesar del mayor valor de dureza del recubrimiento obtenido por HVOF.

## 6.3. Sistema de WC

Ti-WC (400 HV) se depositó sobre el sustrato de acero por HVOF y se obtuvo un con una dureza de casi 900HV. El recubrimiento producido mediante el uso de propileno tenía una dureza mayor que el producido mediante el uso de H<sub>2</sub> aunque el espesor de recubrimiento para ambos recubrimientos no era lo suficientemente gruesa. Este polvo se proyectó sobre el sustrato de acero con una capa de recubrimiento de titanio por CGS para aumentar la adhesión entre las partículas de polvo y la superficie del sustrato y después de obtener el recubrimiento, la muestra pasó por el tratamiento térmico posterior por parte de MBN (HT Temperatura: 650 ° C, isoterma HT: 60 minutos, Rampa: 5 (°C/min), Atmósfera: vacío) para aumentar la dureza del

recubrimiento. Después de TT, la dureza del recubrimiento alcanzó un valor de 1200HV que fue considerable. La mayor dureza de Ti-WC POR CGS que HVOF puede explicarse debido a la descarburación de partículas de WC durante la proyección, ya que las partículas están expuestas a un ambiente caliente y generalmente rico en oxígeno. Como resultado,  $W_2C$  y dependiendo de las condiciones de transformación se forma incluso W, así como CO y  $CO_2$  volátil. Desde recubrimientos Ti-WC (650 HV) y (1500 HV) producidos por la técnica APS, pero eran tan porosos.